

Astronomical X-ray Polarimetry as a diagnostic for questions of fundamental Physics. What we learned from the Imaging X-Ray Polarimetry Explorer (IXPE)

Paolo Soffitta, Enrico Costa
INAF-IAPS

Using materials from G. Galanti (INAF), F. Kislat (New Hampshire U.), G. Matt (Roma Tre U.), R. Taverna & R. Turolla (Padua U.)

ICHEP
17-24 July 2024
Prague (Czech Republic)

Polarization from celestial sources may derive from:

- **Emission processes themselves: cyclotron, synchrotron, non-thermal bremsstrahlung**

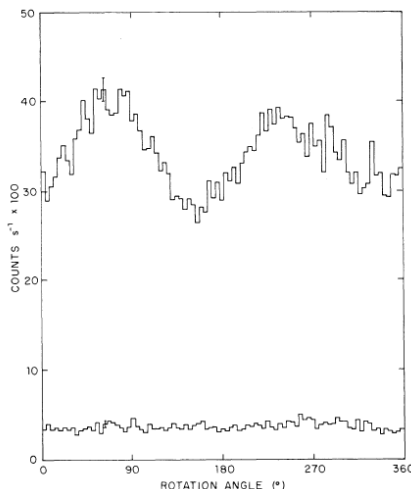
(Westfold, 1959; Gnedin & Sunyaev, 1974; Rees, 1975)

- **Scattering on aspherical accreting plasmas: disks, blobs, columns.**

(1975; Sunyaev & Titarchuk, 1985; Mészáros, P. et al. 1988)

- **Vacuum polarization and birefringence through extreme magnetic fields**

(Gnedin et al., 1978; Ventura, 1979; Mészáros & Ventura, 1979)



Notwithstanding the theoretical previsions the polarization of only one source was detected so-far by OSO-8 back in the '70:

Positive measurement: of X-ray polarization of the Crab Nebula without pulsar contamination (by lunar occultation, Weisskopf et al., 1978).

$$P = (19.2 \pm 1.0) \% ; \theta = 156^\circ.4 \pm 1^\circ.4 \text{ (2.6 keV)}$$

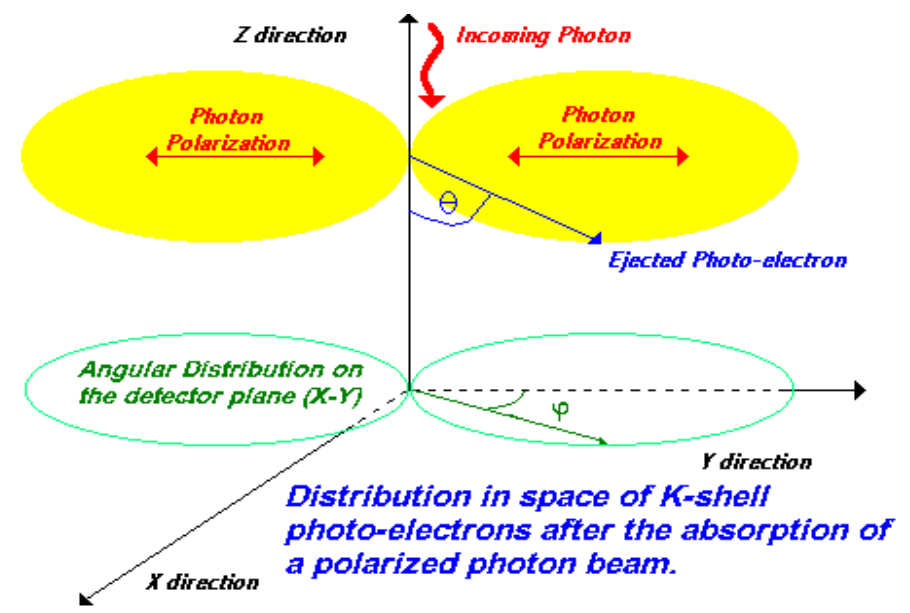
$$P = (19.5 \pm 2.8) \% ; \theta = 152^\circ.6 \pm 4^\circ.0 \text{ (5.2 keV)}$$

The technique was the limit !



MODERN TECHNIQUES: PHOTOELECTRIC EFFECT AT 2-10 KEV

Costa, Nature, 2001



Costa et al., Nature, 2001

Heitler W., The Quantum Theory of Radiation $\beta = v/c$

$$\frac{\partial \sigma}{\partial \Omega} = r_0^2 \frac{Z^5}{137^4} \left(\frac{mc^2}{h\nu} \right)^{3/2} \frac{4\sqrt{2} \sin^2(\theta) \cos^2(\varphi)}{(1 - \beta \cos(\theta))^4}$$

One-stage polarimeter → The analyzer and the detector are the same device.

↓

Border-effect polarimeter

→ **Subdivided Polarimeter**

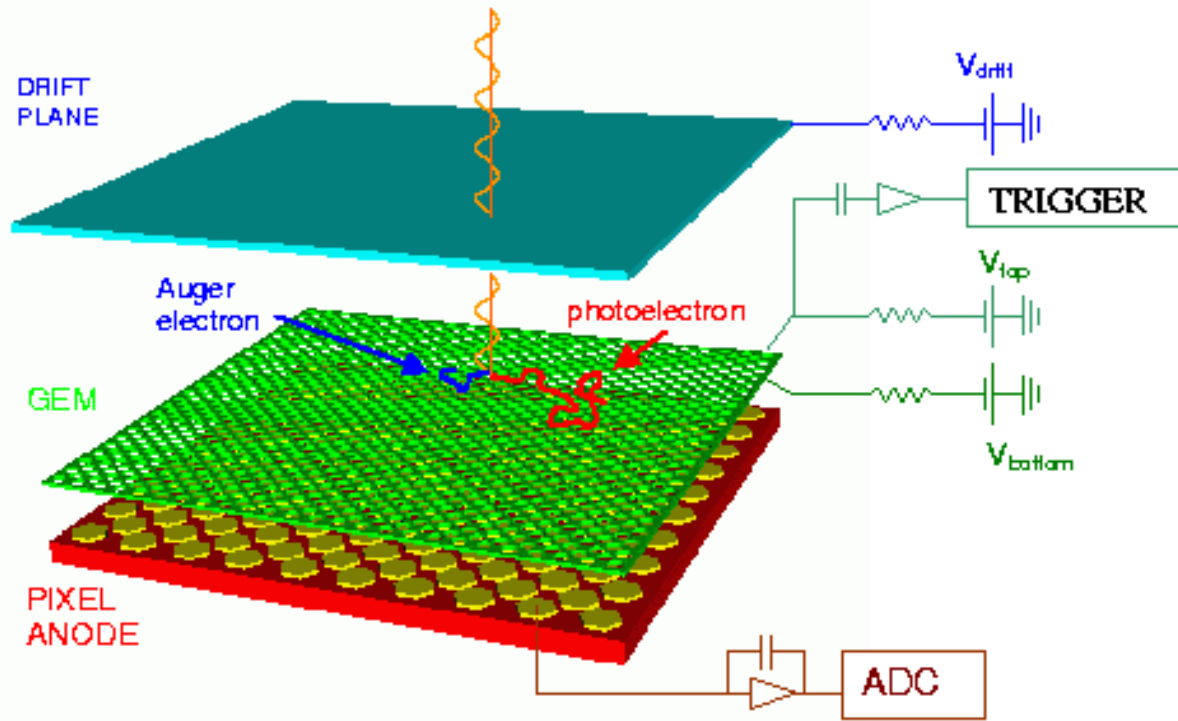
Polarimeter sensitive to a 'borderline' crossed by the carrier of the polarization information. The polarimetric response is sensitive to the interaction point (CCD, AC polarimeter) leading to large systematic effects.

The detection pixel is smaller than the path of the carrier of the polarization information (rise-time => *dispersive*, photoimager, charge-imager => *non dispersive*) The polarimetric response is much less sensitive to the interaction point (smaller systematic effects).

Focal-Plane Non Dispersive Imaging One-Stage Subdivided Wide-Band Photoelectric effect

By measuring the angular distribution of the ejected photoelectrons (the modulation curve) it is possible to derive the X-ray polarization.

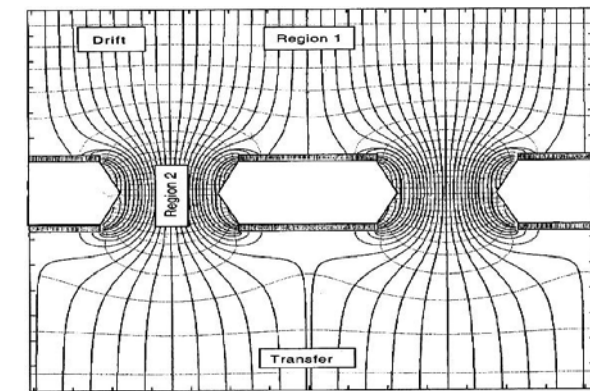
X-RAY POLARIMETRY WITH A GAS PIXEL DETECTOR



Costa et al., 2001, Bellazzini et al. 2006, 2007

- A Beryllium window
- A gas cell for photon conversion
- An electric field to drift the track
- A multiplication plane to get more charge
- An ASIC CMOS chip to make the image of the track

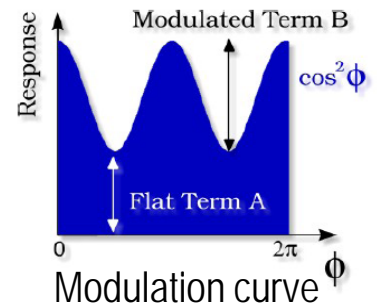
GEM electric field



The Gas Pixel Detector makes the charge image of the photoelectron track.

Fit function: $\mathcal{M}(\phi) = A + B \cos^2(\phi - \phi_0)$

Modulation: $\frac{\mathcal{M}_{\max} - \mathcal{M}_{\min}}{\mathcal{M}_{\max} + \mathcal{M}_{\min}} = \frac{B}{B + 2A}$



Polarization: $\frac{1}{\mu} \frac{B}{B + 2A}$ μ is the modulation factor, i.e. the modulation for 100% polarized radiation

Or by using Stokes Parameters

$$S(\varphi) = I + U \sin(2\varphi) + Q \cos(2\varphi)$$

$$I = \left(A + \frac{B}{2}\right) \quad U = \left(\frac{B}{2}\right) * \sin(2\varphi_0) \quad Q = \left(\frac{B}{2}\right) * \cos(2\varphi_0)$$

$$P = \frac{\sqrt{Q^2 + U^2}}{I} \quad \varphi = \frac{1}{2} \text{atan} \frac{U}{Q}$$

No V → no circular polarization with present techniques

Kislat et al. (2015) introduced the Stokes parameters from the direction of the single carrier of polarimetric observation

THE FIRST LIMIT: IN POLARIMETRY THE SENSITIVITY IS A MATTER OF PHOTONS

$$MDP = \frac{4.29}{\mu R_S} \sqrt{\frac{R_S + R_B}{T}} \quad \text{Minimum Detectable Polarization (MDP)}$$

R_S is the Source rate, R_B is the Background rate, T is the observing time
 μ is the modulation factor: the response of the polarimeter to a 100% polarized beam
 (spanning from 0 or no sensitivity, to 1 or maximum sensitivity)

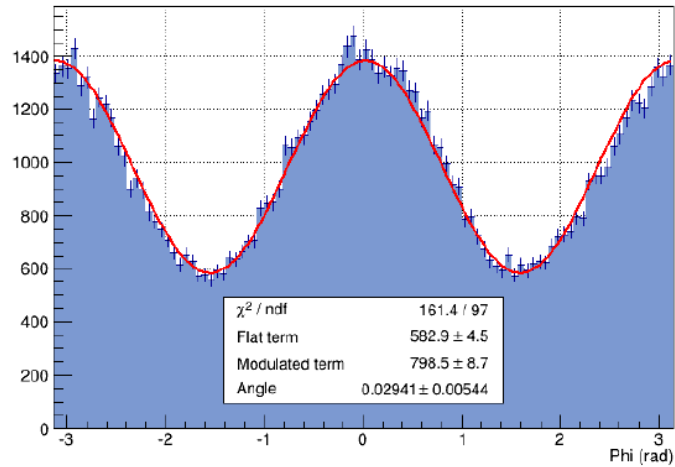
If background is negligible: $MDP = \frac{4.29}{\mu \sqrt{N_{ph}}}$

To reach MDP=1% with $\mu=0.5$: $N_{ph} = \left(\frac{4.29}{\mu MDP} \right)^2 = 736 \cdot 10^3 \text{ ph}$

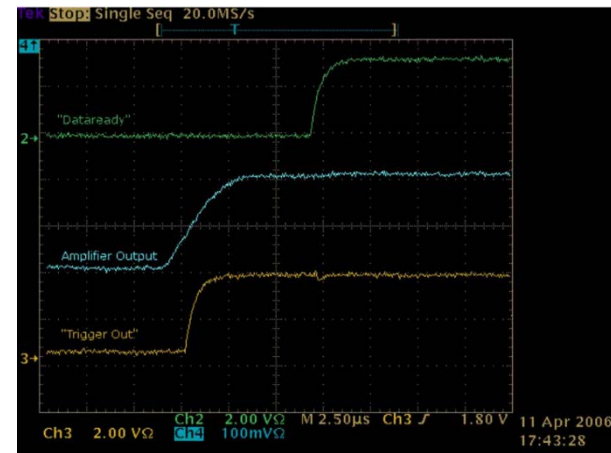
- Source detection > 10 counts
- Source spectral slope > 100 counts
- Source polarization > 100.000 counts

Caution: the MDP describes the capability of rejecting the null hypothesis (no polarization) at 99% confidence.

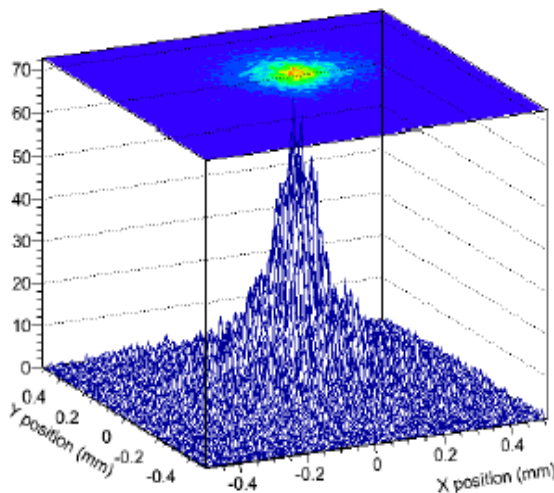
SIMULTANEOUS LINEAR POLARIZATION, IMAGE, ENERGY, TIME



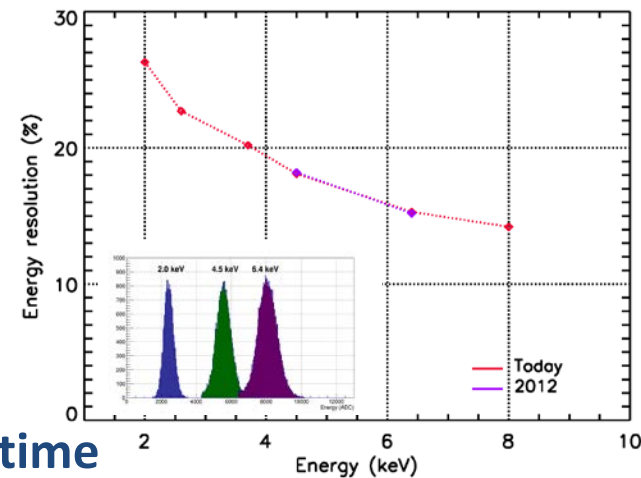
Real modulation curve derived from the measurement of the emission direction of the photoelectron.



Bellazzini et al. 2006



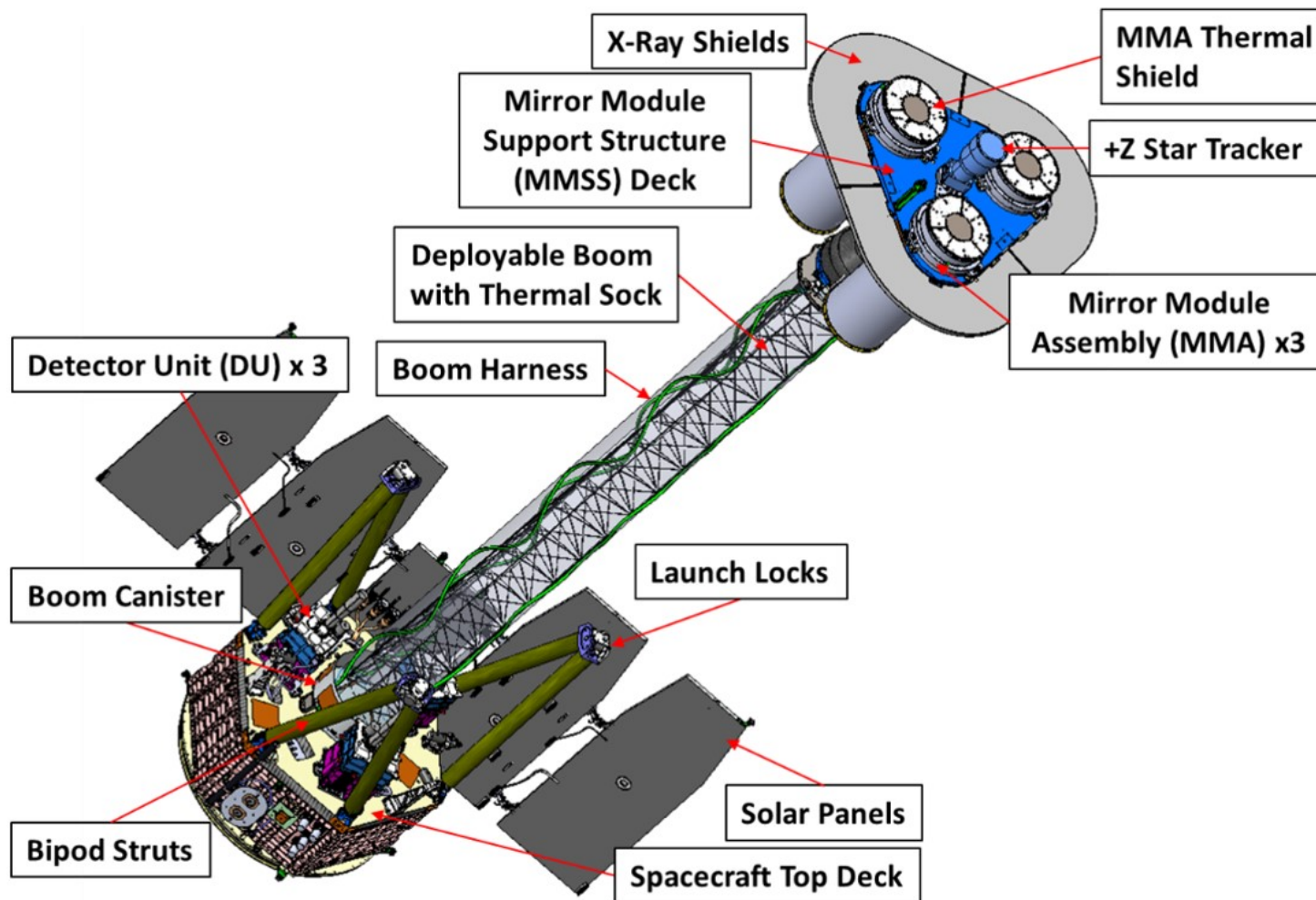
Fabiani et al 2012



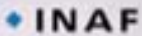












Mulieri et al. 2016

**Energy, space and time
 resolved X-ray polarimetry**

ICHEP 17-24 July 2024 Prague



 <p>Marshall Space Flight Center</p> <p>PI team, project management, SE and S&MA oversight, mirror module fabrication, X-ray calibration, science operations, and data analysis and archiving</p>	  <p>ISTITUTO NAZIONALE DI ASTROFISICA NATIONAL INSTITUTE FOR ASTROPHYSICS</p>    <p>Polarization-sensitive imaging detector systems</p>
 <p>Detector system funding, ground station</p>	 <p>Mission operations</p>
 <p>Spacecraft, payload structure, payload, observatory I&T</p>	  <p>Scientific theory</p>  <p>Thermal shields</p>  <p>Massachusetts Institute of Technology</p> <p>Co-Investigator</p>



PI Philip E. Kaaret (formerly Martin Weisskopf [Emeritus])



ABOUT 75 DIFFERENT SOURCES OBSERVED SO FAR

Classes.	Number of objects.	Sources observed.
PWNe	5 PWNe and isolated pulsars	Crab PWN, Vela PWN, MSH 15-52, PSR B0540-69, G21.5
SNRs	7 SNRs (8 pointings)	Cas A, Tycho's, NE SN 1006, RCW 86, RX J1713.7-3946, Vela Jr, RCW 86, SN1006SW
Black Hole binaries	14 Accreting stellar-BH	Cyg X-1, 4U 1630-472, Cyg X-3, LMC X-1, SS433, 4U 1957-115, SS 433 Lobes, LMC X-3, SWIFT J1727.8-1613, 4U 1957+115, Swift J0243.6+6124, Swift J1727.8-1613, GX 339-4, SWIFT J151857.0-572
Neutron Stars binaries	23 Accreting NS	Cen X-3, Her X-1, GS1826-67, Vela X-1, Cyg X-2, GX 301-2, Xpersei, GX 9-9, 4U 1820, GRO J1008-57, XTE 1701-46, EXO 2030+375, LS V+44 17, GX 5-1, 4U 1624-49, Sco X-1, Cir X1, GX13+1, SMC X-1, SRGA J144459.2-604207, 4U 1538-52, V395 CAR, PSR J1023+00
Magnetars	4 Magnetars	4U 0142+61, 1RXS J170849, SGR 1806-20, 1E 2259+586
RQ AGNs&Sgr A*	5 Radio-quiet AGN & 1 Sgr A*	MCG 5-23-16, Circinus Galaxy, NGC 4151, IC 4329 A, Sgr A* Complex, NGC 1068
Blazars	17 Blazars & radio galaxies	Cen A, S5-0716-714, 1ES 19-59-650, Mrk 421, BL Lac, 3C 454, 3C 273, 3C 279, Mrk 501, 1ES 1959-650, BL-Lac, 1ES 0229-200, PG 1553 -113, S4 0954+65, 1E 2259+586, RGB J0710+591, H 1426+428

Some sources have been revisited

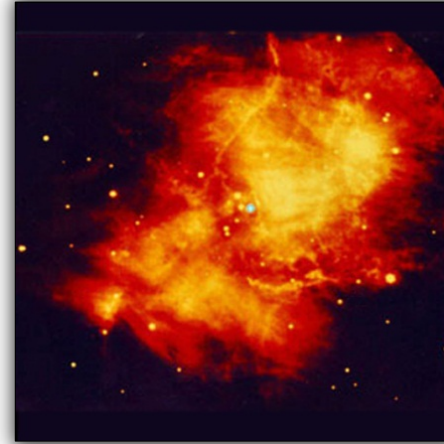
Mrk 421, Mrk 501, BL Lac, Vela X1, Her X-1, MCG 5-23-16, Crab, MSH 15-52, Cyg X-1, Sgr A (complex), NGC 4151 ...

About 50 % of the observed celestial sources displayed a polarization with at least 6σ significance in the Quick Look Analysis (Integrating in time, energy and position) . Resolved analysis showed polarization on a much larger number of sources.

THE CRAB NEBULA (BEFORE IXPE)



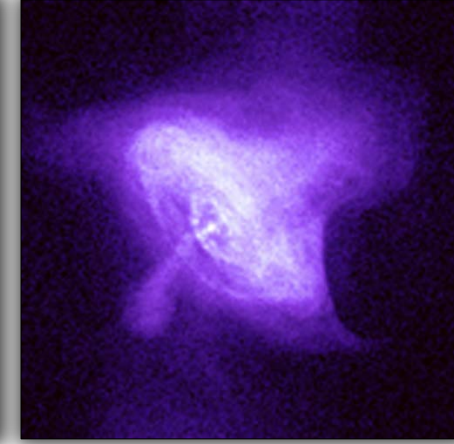
Radio (VLA)



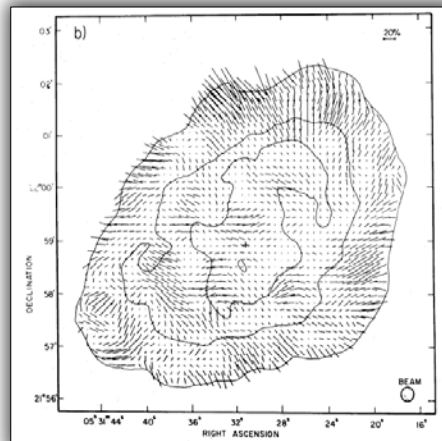
Infrared (Keck)



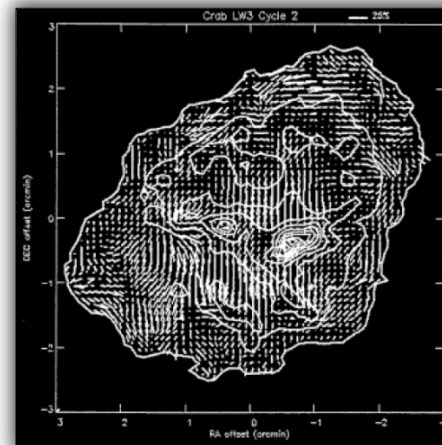
Optical (Palomar)



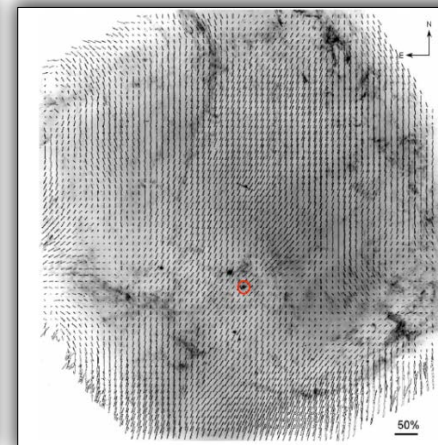
X-rays (Chandra)



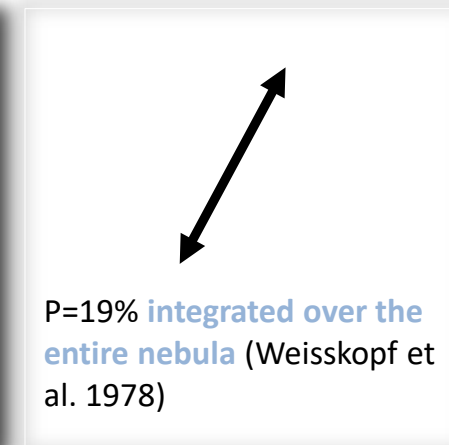
Radio polarisation



IR polarisation



Optical polarisation



P=19% **integrated over the entire nebula** (Weisskopf et al. 1978)

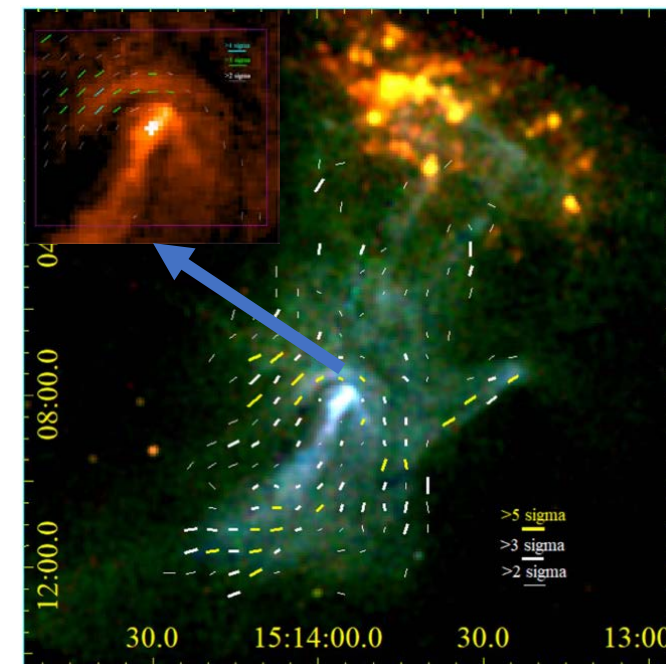
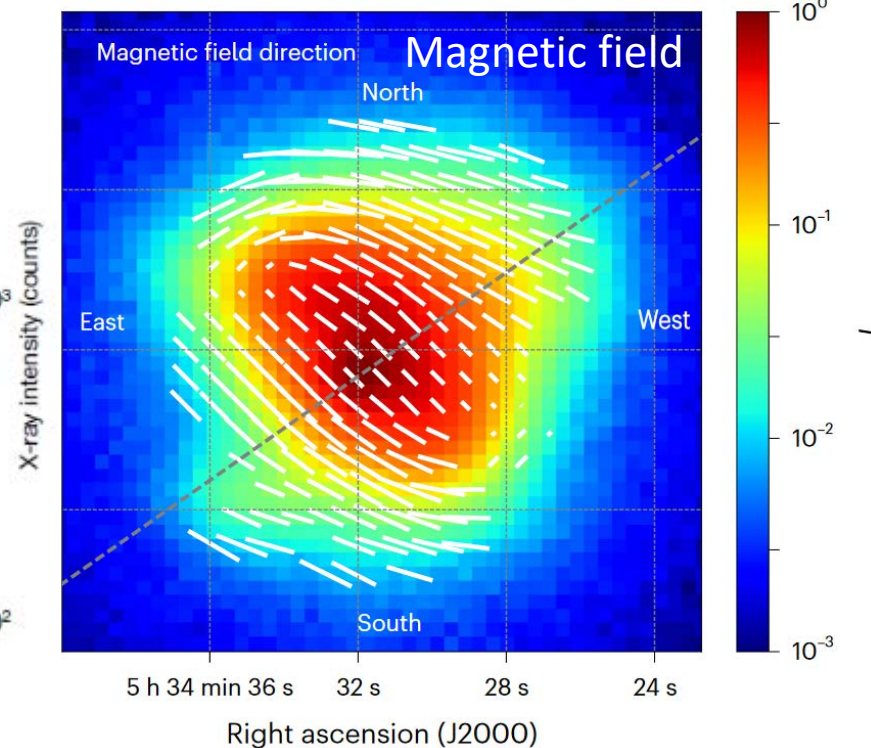
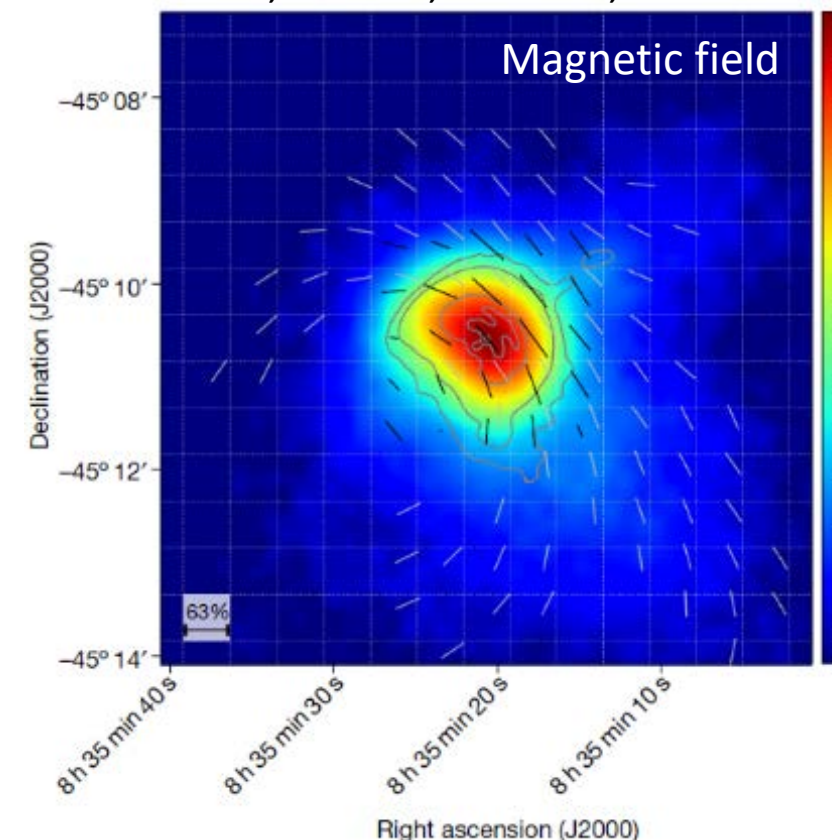
X-ray polarisation

X-rays probe **freshly accelerated** electrons and their acceleration site

Xie, F. et al., Nature, 2022

Bucciantini, N. et al., Nature Astronomy, 2023

Romani, R. et al., ApJ, 2023



- High level polarization (Vela up to 63 %, Crab up to 45-50 %, MSH 1552 up to 70 %)->Turbulence less effective than expected.
- Vela polarization structure symmetric with respect to the spin which is parallel to its proper motion.
- Crab IXPE polarization angle is rotated 12° counter-clockwise with respect to OSO-8.
- MSH 15-52 IXPE polarization reaches 70% at the base of the jet, in the arc and in the thumb.

Through years many papers suggested that some astrophysical measurement could be the evidence for some phenomenology of fundamental physics.

There is a certain number of publications suggesting that X-Ray Polarimetry could provide some of these evidences.

The point is that X-Ray polarimetry did not exist. Now it exist. IXPE is there.

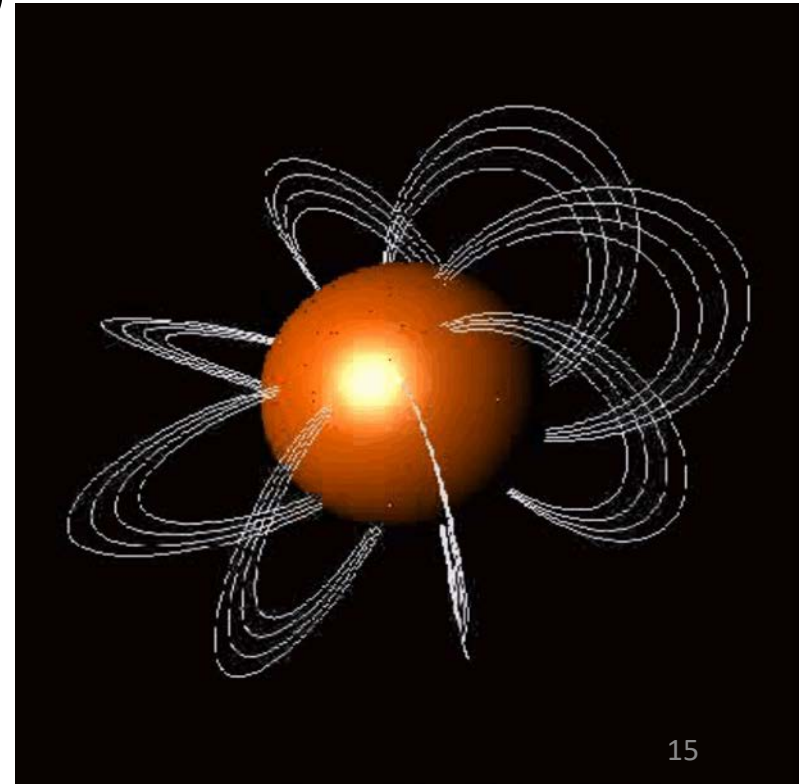
We know:

- How polarized are some sources of most of classes.
- What is the spread of polarization properties
- What we can do with IXPE

- **Vacuum Polarization and Birefringence.**
- General Relativity in Strong Fields.
- Equation of State of Neutron Stars.

- $P \approx 2 - 12 \text{ s}$ $\dot{P} \approx 10^{-14} - 10^{-10} \text{ s s}^{-1}$
- $B_{sd} \approx 10^{14} - 10^{15} \text{ G}$
- $L_{X,persist} \approx 10^{35} - 10^{36} \text{ erg s}^{-1}$ (typically $> \dot{E}_{rot} = 10^{33} - 10^{34}$)
- Bursting activity (short bursts – intermediate/giant flares)
- Enhanced activity in transient sources (outbursts)
- Two components (thermal and PL) spectra
- **Powered by their own magnetic energy**

A twisted magnetic field is coupled to flowing charged particles which up-scatters (power law) the radiation emitted from the neutron star surface (Thermal)



VACUUM POLARIZATION AND BIREFRINGENCE WITH MAGNETARS

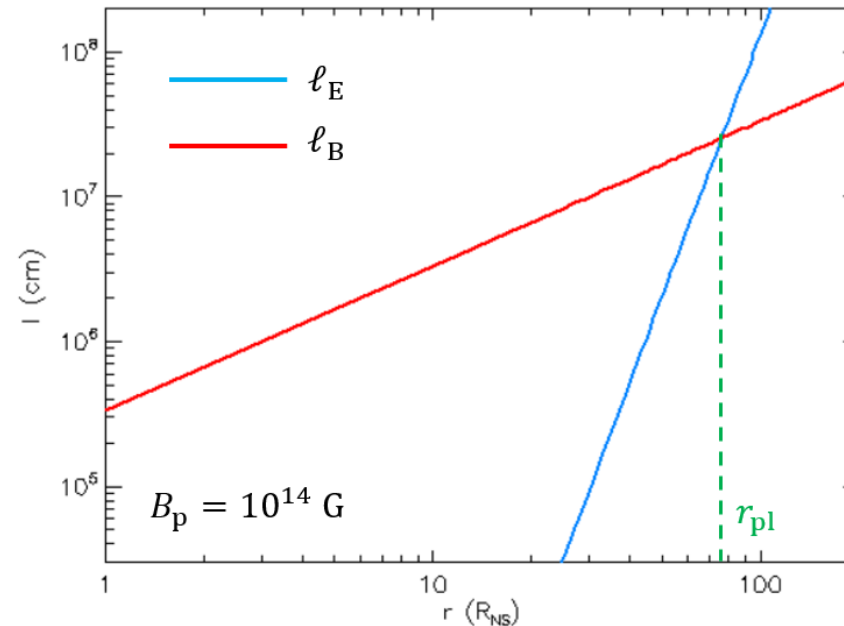
The large magnetic field of a magnetar is ideal to probe vacuum polarization.

The presence of virtual e^+/e^- pairs modify the vacuum dielectric and the magnetic permeability tensors so that the wave-form equation allows to define two characteristic lengths:

E-field evolution length:

$$\ell_E = \frac{2}{k_0 \delta} \approx 130 \left(\frac{B}{10^{11} \text{ G}} \right)^{-2} \left(\frac{\hbar \omega}{1 \text{ keV}} \right)^{-1} \text{ cm}$$

ℓ_E is the length scale at which the electric field changes direction in its trajectory



(Dipolar) *B*-field evolution length:

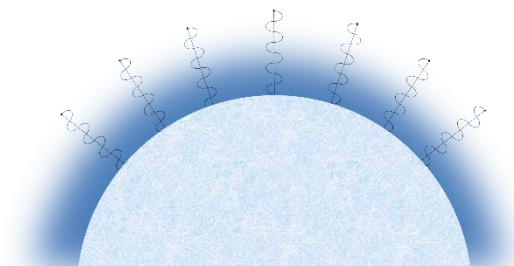
$$\ell_B = \frac{B}{|\mathbf{k} \cdot \nabla B|} \approx \frac{r}{3}$$

ℓ_B is the length-scale along which the star magnetic field B evolves (independently on E)

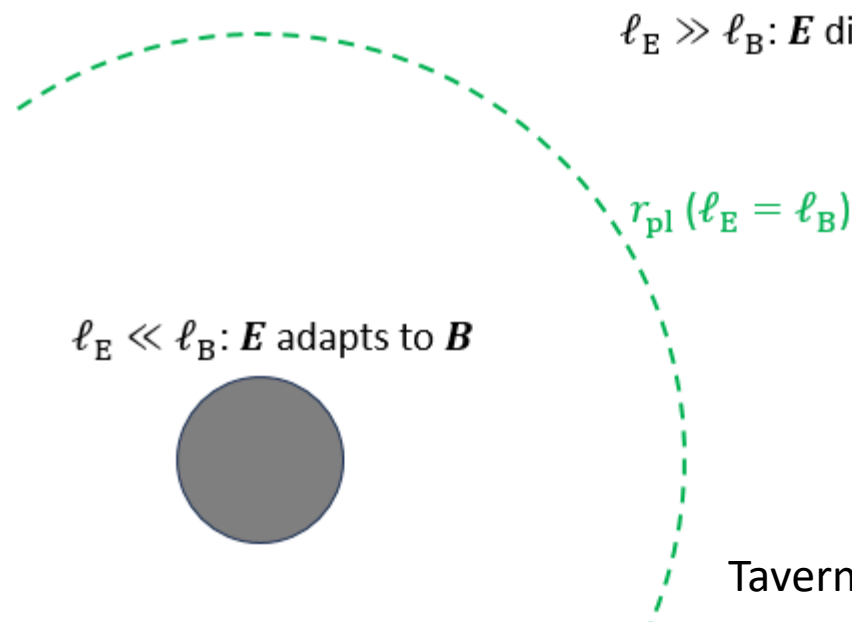
R. Taverna & R. Turolla 2024

The polarization limiting radius (r_{pl}) defines two regions for the propagation of photons:
 $R < r_{pl}$ a photon in extraordinary mode remain extraordinary a photon in ordinary mode remain ordinary.
 $R > r_{pl}$ the two polarization modes couple again to provide the observed polarization.

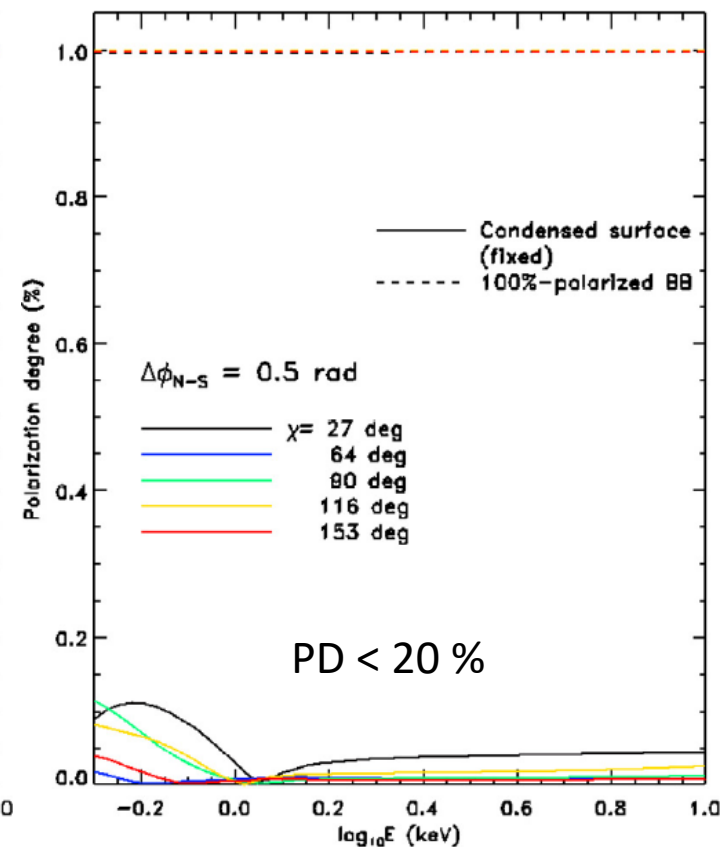
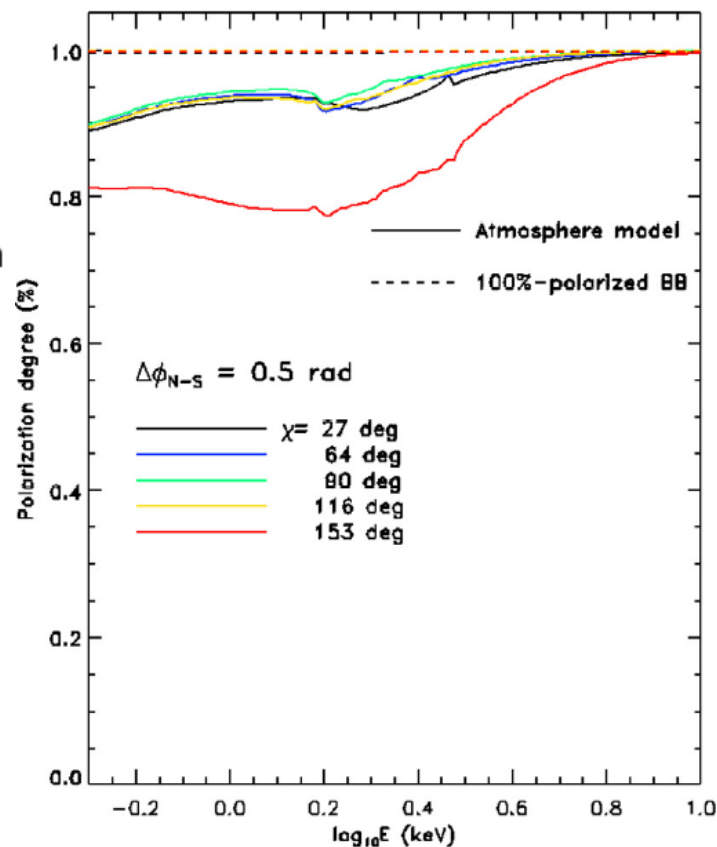
POLARIZATION DEGREE AT THE NS SURFACE DEPEND ON THE NATURE OF THE EMITTING REGION



No atmosphere but a condensed surface

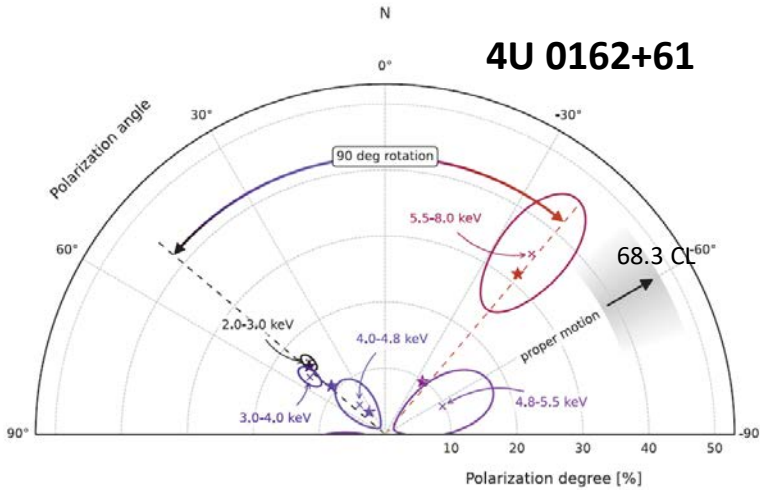


Taverna et al., 2022



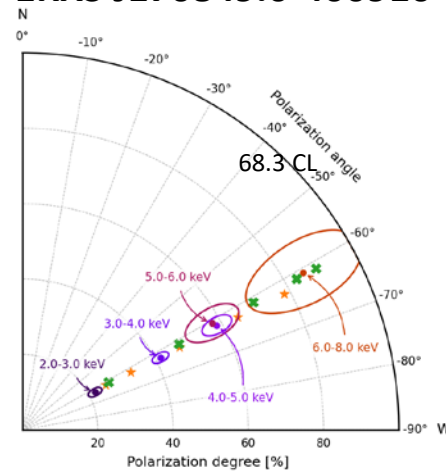
MAGNETARS: 1 MILLION SECOND NET-TIME EACH

Taverna et al., Science 2022



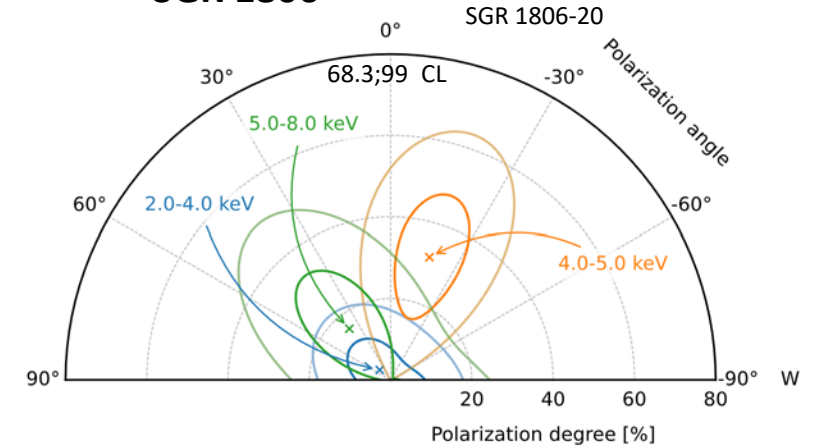
Equatorial belt condensed surface (low energy-O mode). Resonant Compton Scattering at high energy (X-model)

Zane et al. ApJL 2023
1RXS J170849.0-400910



Condensed surface region (low-P) plus hot regions with on-top an atmosphere (high P)

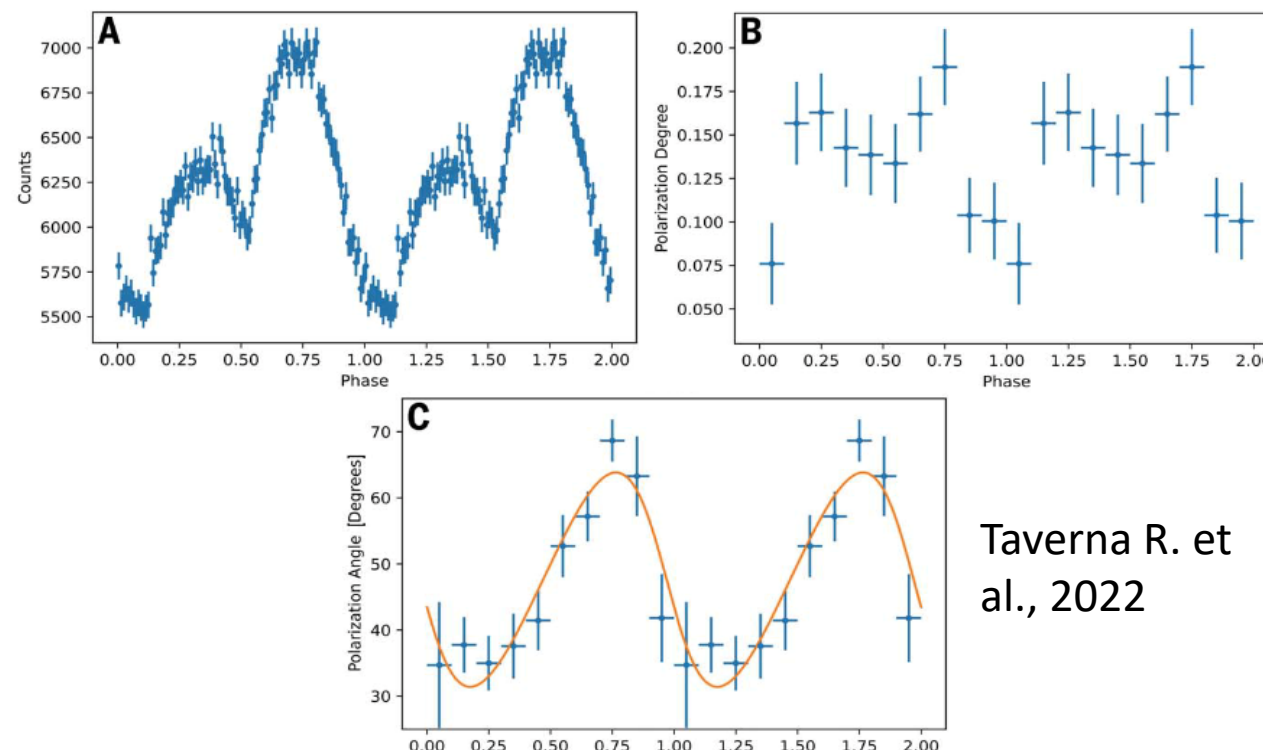
Turolla et al., ApJ 2023
SGR 1806



Only upper limits. Hint of behavior similar to 4U 0162+61

The magnetars observed by IXPE have very different polarization dependence with energy may be due to the fact that the emission pattern and physical properties are different for each one. 1E 2259+586 was also observed (Heyl et al., 2024) showing a polarization of about 20 % and an even different pattern of emission region by using the rotating vector model.

- Low phase-averaged PD ($< 40\%$) \Rightarrow Vacuum birefringence cannot be probed
- Phase dependent results
 - In the light-curve PD is in-phase with flux (determined at the surface)
 - PA is sinusoidal (Rotating Vector Model-RVM)



Taverna R. et al., 2022

The phase-dependent polarization degree is similar to the phase dependent light-curve (determined at the surface) where the field is twisted.

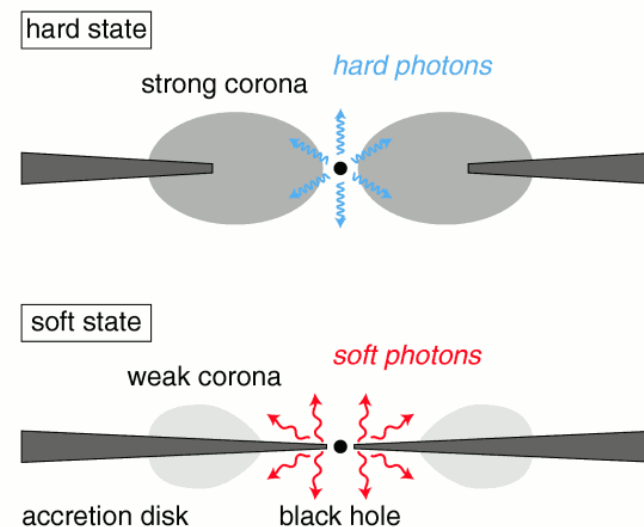
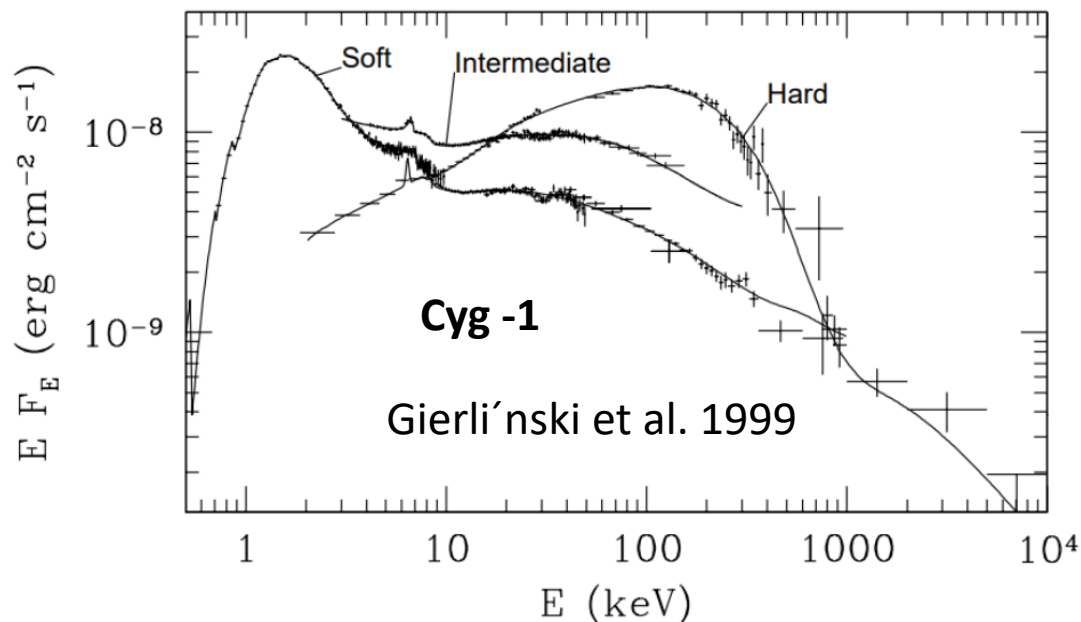
The polarization angle follows the rotating vector model that for an extended source implies that the field is dipolar therefore far-way from the surface

Not a smoking gun but a hint of QED effect

IXPE showed that the emission regions in magnetars are very different one respect to the other. Finding a smoking gun means finding a very low pulsed fraction and a very high polarization measured

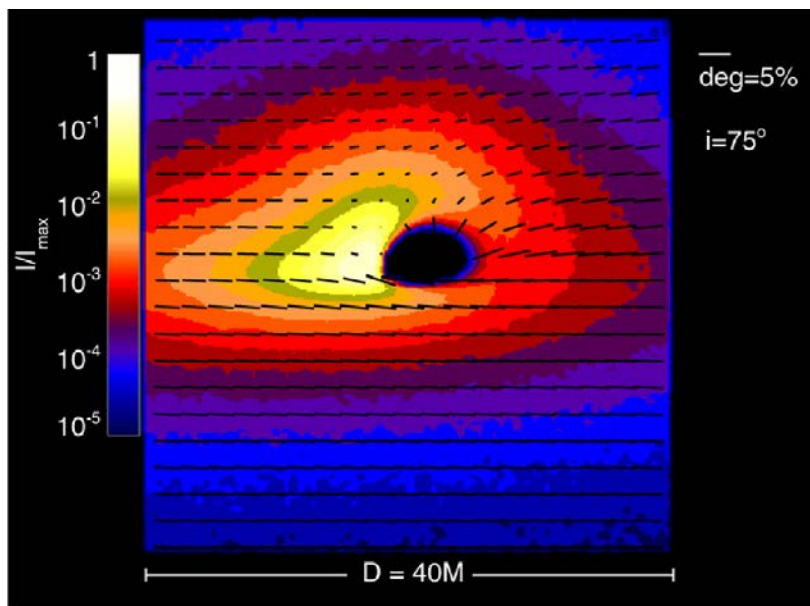
- Vacuum Polarization and Birefringence.
- **General Relativity in Strong Fields.**
- Equation of State of Neutron Stars.

Polarimetry cannot say much on Strong Gravity but contributes to understand the overall complexity of the system. In particular provides a direct measurement of the spin of the black-hole.

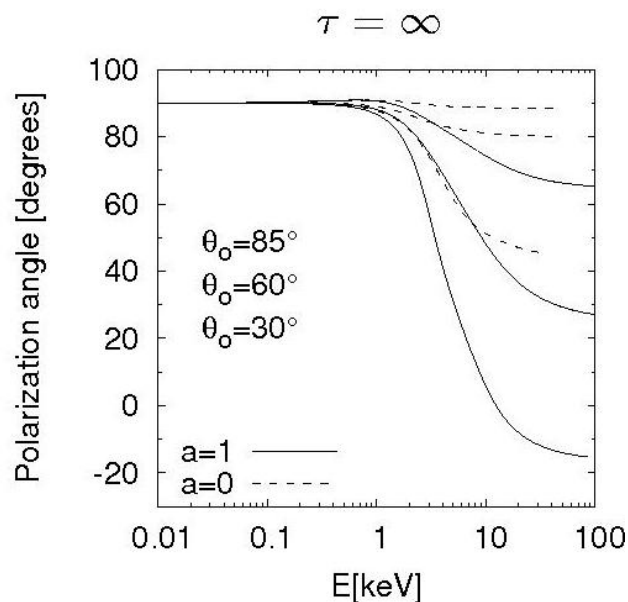


The two main states of a Black-Hole binaries are High-Soft where the X-ray emission is dominated by thermal emission of a disk around the Black-Hole (multi-temperature black-body) possibly extending down to the Innermost Circular Orbit (ISCO) and Low-Hard where the emission is due to Comptonized X-ray photons by a hot Corona. The transition between states is an intermediate state. The transition to soft-state can be anticipated by a jet emission.

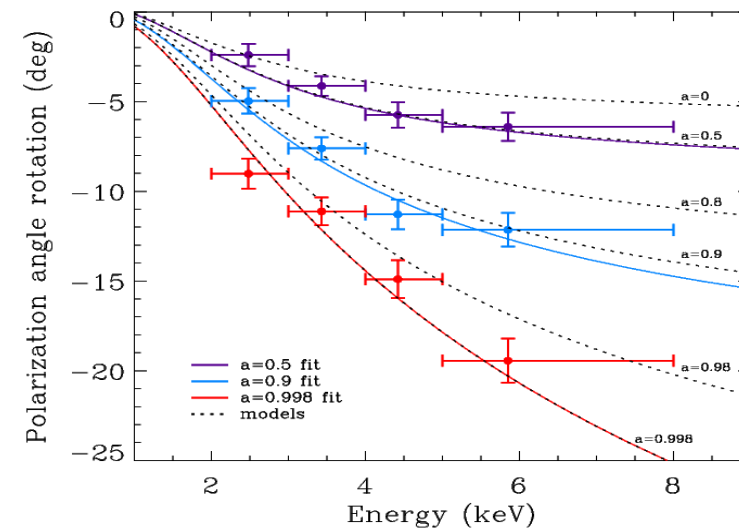
STRONG GRAVITY: THE ROTATION OF THE POLARIZATION ANGLE TO MEASURE THE BH SPIN



Schnittmann & Krolick 2009: Polarization from an accretion disk in thermal State



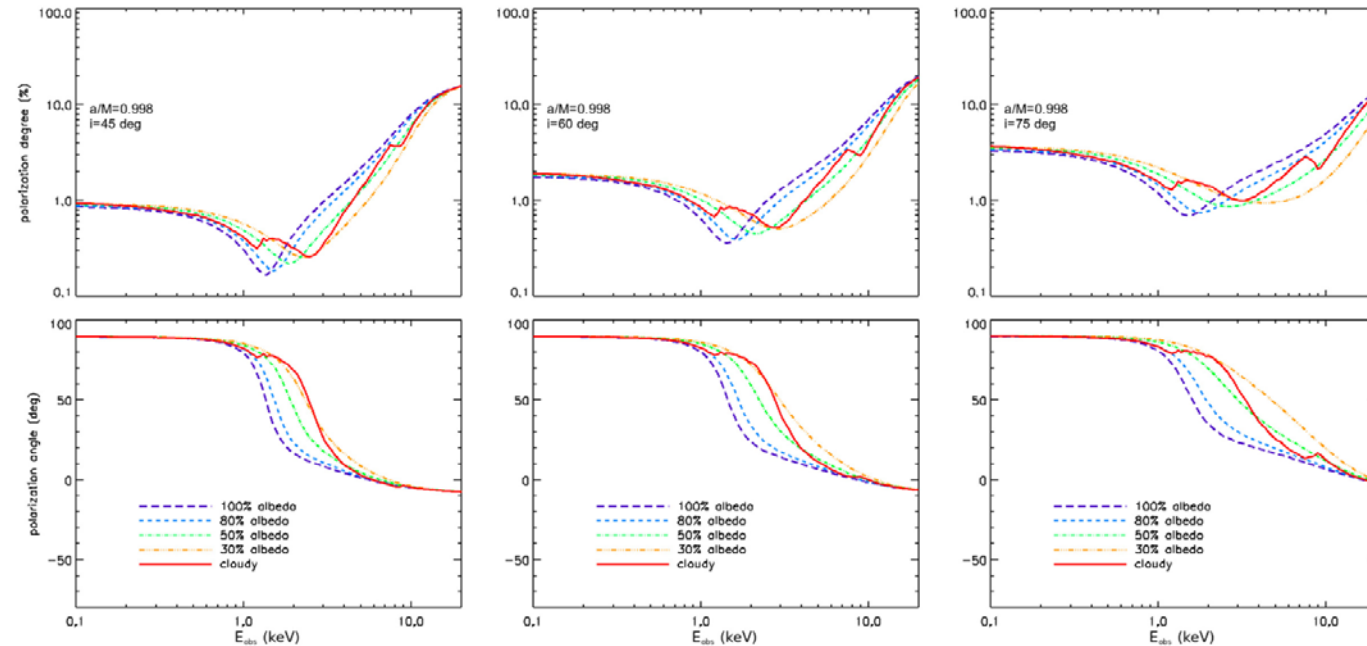
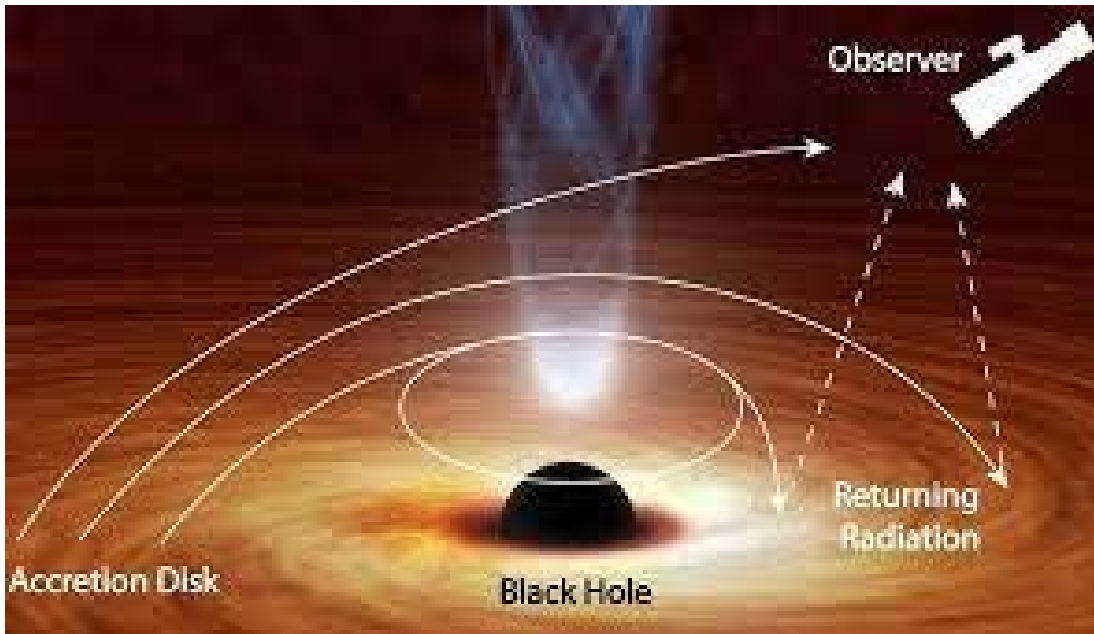
Courtesy: Michal Dovciak



200 ks IXPE observation of GRS1915+105

X-ray polarimetry has always thought as a method for determining the spin of the black hole (the larger is the spin the larger is the rotation of the X-ray polarization angle with energy) more than a way to test general relativity in Strong Field regime (Connors&Stark, Stark& Connors, Nature 1977. Different methods provide a different answer for the same source.

TWO ADDITIONAL COMPLICATIONS: RETURNING RADIATION (W. ALBEDO) & REAL ACCRETION DISK (W. ABSORPTION)



Taverna et al., 2020

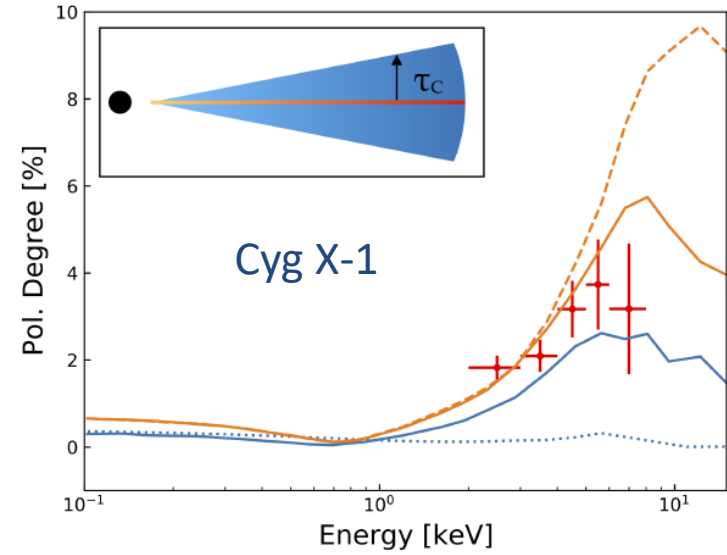
“Returning radiation” (Cunningham 1976), is disk radiation illuminating the disc itself do to geodetics close to the BH. The effect depends on the albedo (photoelectric absorption, Taverna et al., 2020) and on the spin.

The “standard disk model” assumed (Novikov-Thorne: pure scattering with GR effect) may be more complex due to the presence of absorption (Taverna et al., 2021).

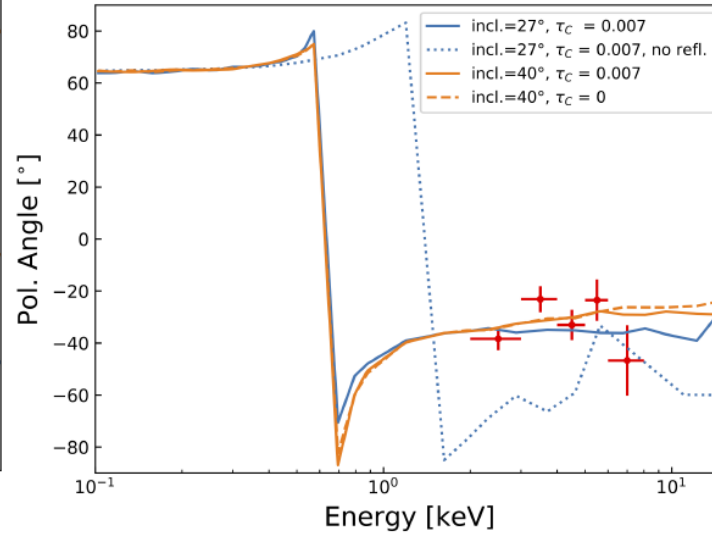


IXPE
Imaging
X-Ray
Polarimetry
Explorer

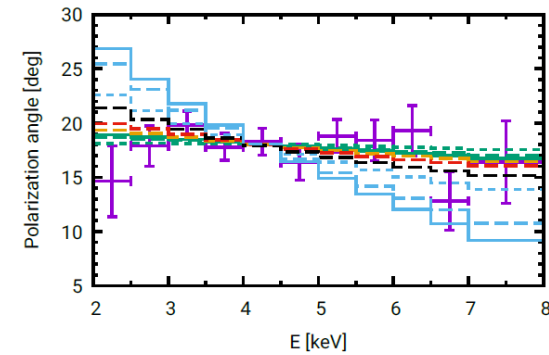
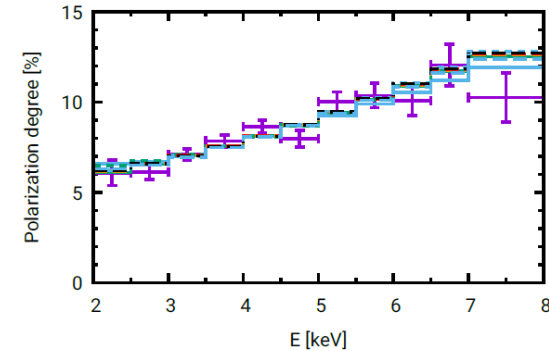
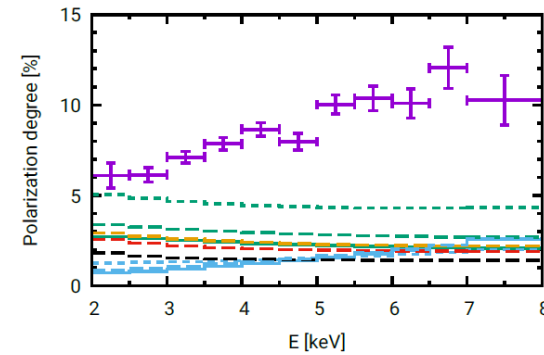
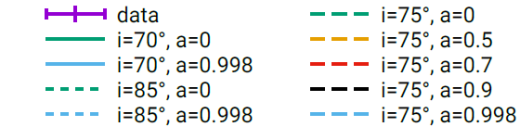
CYG X-1 AND 4U 1630 OBSERVED IN SOFT STATE:



Steiner et al., ApJ 2024 (accepted)



4U 1630 Ratheesh et al., ApJ 2023

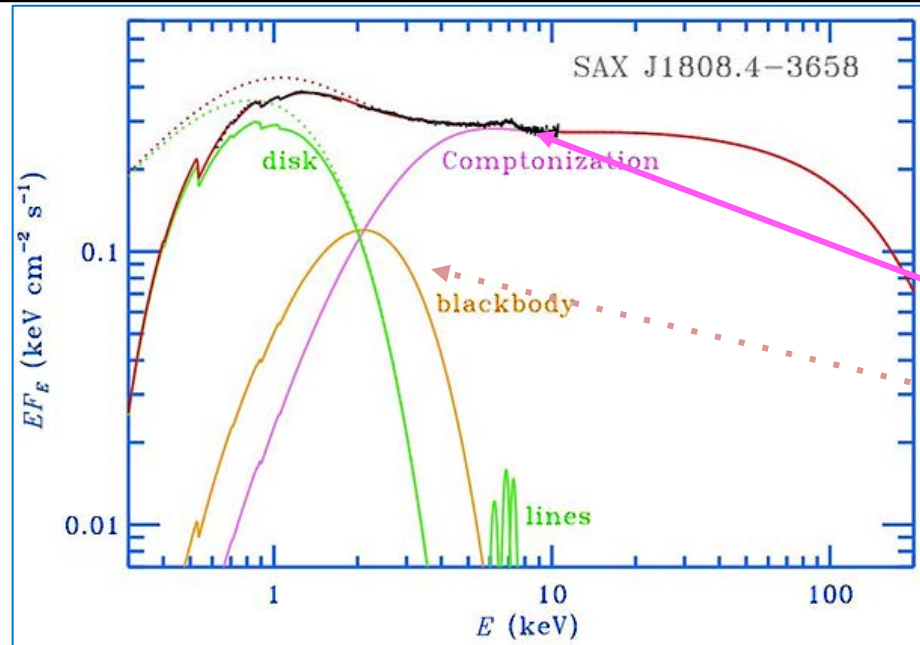


Cyg X-1 is modeled with a standard disk with returning radiation a wedge corona and high spin.

4U 1630 was observed in High Soft State during an Outburst by a ToO: No standard disk can model the data (high and increasing polarization degree with energy) A more complicate disk (including absorption and relativistic wind) has to be modeled (with low or intermediate-spin) . In the 2-8 keV energy range the coronal emission is < 2 %.

- Vacuum Polarization and Birefringence.
- General Relativity in Strong Fields.
- **Equation of State of Neutron Stars.**

BEST CANDIDATE: ACCRETING MILLISECOND PULSARS

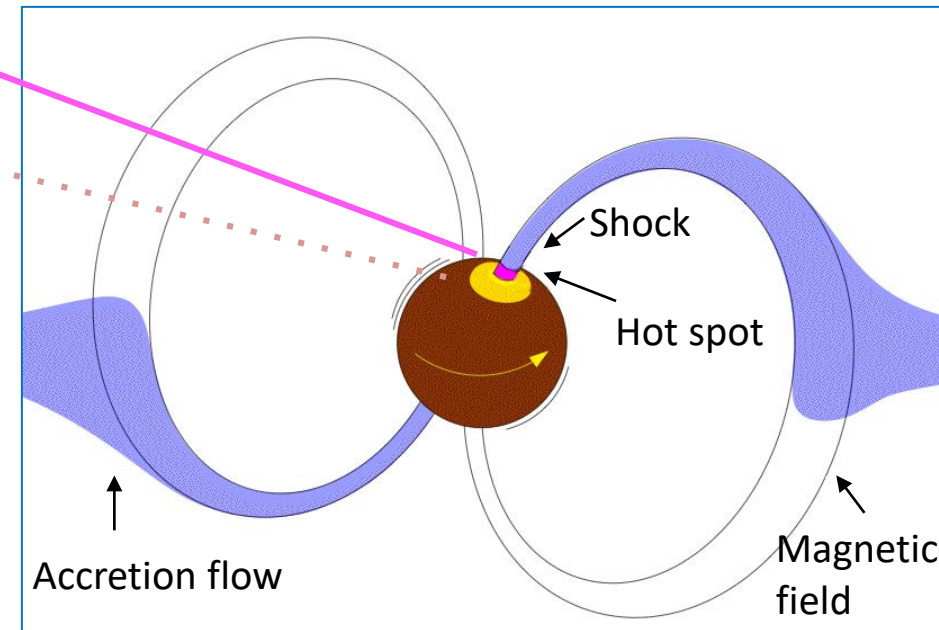


A pulsed blackbody component

- neutron star **surface hot spot**

Hard X-ray component pulsates

- produced probably at the **shock**

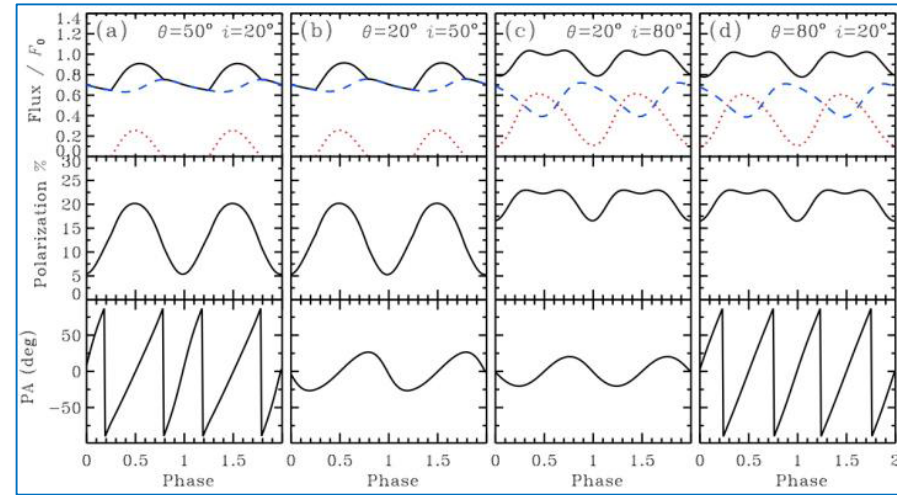
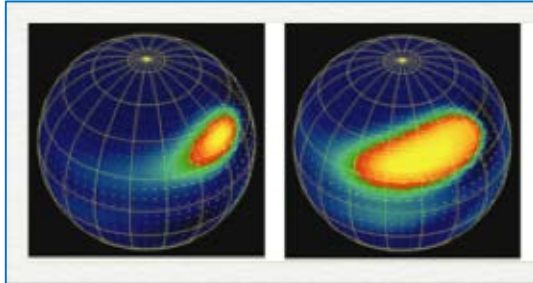


Expected polarization in 2-10 keV range: **P=5-20%**, strongly energy dependent.

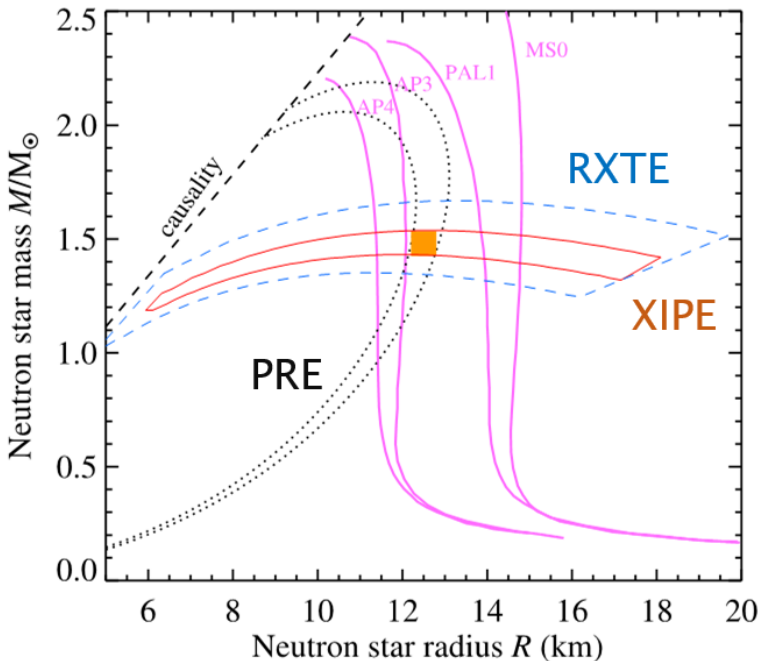
ACCRETING MILLISECOND PULSARS (AMPs): EQUATION OF STATE

Emission from hot spots

Phase-dependent linear polarization



Viironen & Poutanen 2004



XIPE Yellow Book (2017)

Polarization measurements **constrain** the **geometrical parameters** of the system. When combined with spectral measurements of photospheric radius expansion (PRE), **will give strong constraints on EoS** (Poutanen, 2020) (M-R within $\sim 5\%$)

The experiment of timing (e.g. eXTP/LAD (CAS) and Strobe-X (NASA) are more sensitive but they may not be launched in the near future. But polarimetry can tell more about geometry.

IXPE Observed a new accreting msec pr: SRGA J144459.2-604207. Analysis is underway. Proprietary data !



Quantum Gravity

Axions & Axion-like Particles

Lawrence Invariance Violation in Quantum Gravity Theories

$$E_P = \sqrt{\frac{hc^5}{G}} = 1.22 \cdot 10^{19} \text{ GeV}$$

Theories of quantum gravity suggest that Lorentz invariance may be violated at the Planck scale, but effects must be strongly suppressed at attainable energies. Photons propagating over astrophysical distances enable some of the strongest tests as tiny effects will accumulate during propagation of the photons.

Typically a tiny effect can become detectable due to a long baseline. Search of the effect as a function of distance could be a way. The main difficulty is the lack of knowledge of the polarization in the frame of the source.

Two approaches:

1. A rotation of polarization angle proportional to the distance. The problem is the knowledge of the angle in the frame of the source.
2. A “shuffling” namely one or many full rotations. If a distant source of known distance is polarized a limit to rotation and therefore to QG effect can be derived.

UPPER LIMITS BY USING X-RAY POLARIMETRY STARTED FROM A MISTAKE

In 2003 Coburn and Boggs claimed the detection of a very high polarization (consistent with 100%) in gamma rays of the Gamma Ray Burst GRB021206.

This is the starting point generating two different approaches:

The shuffling argument

Immediately after the claim, Igor G. Mitrofanov sent a letter to Nature (2003) stating that the predicted rotation of the polarization plane proportional to the square of the energy would have destroyed the polarization. Thence he derives a limit to the coupling constant of $X < 10^{-14}$. Or possibly the effect is not linear in the energy and a higher power must be assumed.

$$V_{\pm} = c (1 \pm \chi (E/E_{QG})^n) \quad \Delta\phi_1(E) \approx \chi (D/hc) E^2/E_{QG} \approx 10^4 \chi (E/0.1 \text{ MeV})^2 D \quad n=1$$

The measured rotation

Soon after Phil Kaaret submitted a short letter to Nature to remind that a much worse but much more robust upper limit of $X < 10^{-4}$ could be derived by comparing the measurements of OSO-8 at 2.6 and 5.2 keV of the Crab Nebula.

The paradox is that the measurement that started the quest has been criticized and substantially disclaimed by the team that built the instrument electronics.

Measures of GRB polarization in hard-X/soft-Gamma

Some missions (not-dedicated to polarimetry) declared to have detected high polarization in gamma-ray burst. Every time a new burst was found at a larger redshift a stricter upper limit was declared for the coupling constant.

The most stringent value is $X < 10^{-16}$ (GRB140206A, $z = 2.74$, Gotz et al., 2014).

McConnell (2017)

Table 1
GRB polarization measurements.

Pub Date	GRB	Instrument	Energy (keV)	Π	Refs.
2004	GRB 021206	RHESSI	150–2000	$80\% \pm 20\%$	Coburn and Boggs (2003)
2004	GRB 021206	RHESSI	150–2000	$< 4.1\%$	Rutledge and Fox (2004)
2004	GRB 021206	RHESSI	150–2000	$41^{+57}_{-44}\%$	Wigger et al. (2004)
2005	GRB 930131	CGRO/BATSE	20–1000	$(35–100\%)^a$	Willis et al. (2005)
2005	GRB 960924	CGRO/BATSE	20–1000	$(50–100\%)^a$	Willis et al. (2005)
2007	GRB 041219a	INTEGRAL/SPI	100–350	$98\% \pm 33\%$	Kalemci et al. (2007)
2007	GRB 041219a	INTEGRAL/SPI	100–350	$96\% \pm 40\%$	McGlynn et al. (2007)
2009	GRB 041219a	INTEGRAL/IBIS	200–800	$43\% \pm 25\%^b$	Götz et al. (2009)
2009	GRB 061122	INTEGRAL/SPI	100–1000	$< 60\%$	McGlynn et al. (2009)
2011	GRB 100826a	IKAROS/GAP	70–300	$27\% \pm 11\%^c$	Yonetoku et al. (2011b)
2012	GRB 110301a	IKAROS/GAP	70–300	$70\% \pm 22\%$	Yonetoku et al. (2012)
2012	GRB 110721a	IKAROS/GAP	70–300	$80\% \pm 22\%$	Yonetoku et al. (2012)
2013	GRB 061122	INTEGRAL/IBIS	250–800	$> 60\%$	Götz et al. (2013)
2014	GRB 140206a	INTEGRAL/IBIS	200–800	$> 48\%$	Götz et al. (2014)
2016	GRB 151006a	Astrosat/CZTI	100–300	–	Rao et al. (2016)

^a Albedo polarimetry.

^b Variable Π .

^c Variable position angle.

Kole et al., 2023 (POLAR)

Table 2. Length, fluence, location, and polarization properties of the 14 GRBs resulting from the analysis presented in this work.

GRB	T90 (s)	Fluence ^(*)	PD (%)	PA (deg)	θ	RA (deg)	Dec (deg)
161203A	$4.1 \pm +0.1$	$(7.84 \pm 1.05) \times 10^{-6}$	16^{+29}_{-15}	x	85°	13.5°	-146°
161217C	$6.3 \pm +0.3$	$(4.37 \pm 1.05) \times 10^{-6}$	21^{+30}_{-16}	x	35°	34.6°	-4.0°
161218A	$11.5 \pm +0.1$	$(8.72 \pm 1.44) \times 10^{-6}$	$7.0^{+10.7}_{-7.0}$	x	24.3°	245.3°	-4.1°
161218B	$25.1 \pm +0.2$	$(8.55 \pm 0.30) \times 10^{-5}$	13^{+28}_{-13}	68^{+36}_{-54}	80.5°	0.9°	-14.7°
161229A	$31.3 \pm +0.4$	$(4.21 \pm 0.22) \times 10^{-5}$	17^{+24}_{-13}	106^{+55}_{-22}	87.6°	78.9°	45.7°
170101A	$2.0 \pm +0.1$	$(6.8 \pm 1.4) \times 10^{-6}$	$6.3^{+10.8}_{-6.3}$	98^{+37}_{-34}	6.0°	276.1°	11.7°
170101B	$11.1 \pm +0.4$	$(1.2 \pm 0.12) \times 10^{-5}$	60^{+24}_{-36}	109^{+34}_{-21}	75.0°	69.6°	-1.0°
170114A	$10.4 \pm +0.2$	$(1.84 \pm 0.30) \times 10^{-5}$	$10.1^{+10.5}_{-7.4}$	166^{+25}_{-32}	26.4°	13.1°	-13.0°
170127C	$0.14 \pm +0.01$	$(5.4 \pm 2.4) \times 10^{-6}$	$9.9^{+19.3}_{-8.4}$	45^{+39}_{-36}	41.8°	339.3°	-63.9°
170206A	$1.26 \pm +0.01$	$(1.04 \pm 0.06) \times 10^{-5}$	$13.5^{+7.4}_{-8.6}$	x	19.5°	212.8°	14.5°
170207A	$38.8 \pm +0.3$	$(6.80 \pm 0.47) \times 10^{-5}$	$5.9^{+9.6}_{-5.9}$	x	67.2°	316.9°	59.1°
170210A	$47.6 \pm +2.5$	$(7.21 \pm 0.28) \times 10^{-5}$	$11.4^{+35.7}_{-9.7}$	13^{+24}_{-21}	80.6°	226.1°	-65.1°
170305A	$0.45 \pm +0.01$	$(1.08 \pm 0.12) \times 10^{-6}$	40^{+25}_{-25}	88^{+30}_{-20}	31.4°	39.7°	9.9°
170320A	$6.8 \pm +0.1$	$(9.6 \pm 4.8) \times 10^{-6}$	18^{+32}_{-18}	x	84.7°	320.1°	55.1°

Notes. The T_{90} parameter as calculated using POLAR data are provided along with the off-axis incoming angle (θ) and the RA (J2000) and Dec (J2000) positions used in the analysis. For the RA (J2000) and Dec (J2000) parameters we report those used to produce the instrument response in the analysis. In cases where the PA, which is given according to the IAU convention, is not constrained (meaning that the total 1σ error exceeds 180°) an x is added in this table. ^(*)in units of erg cm^{-2} in 10–1000 keV.

The polarimetry of GRBs of different instruments generally not specifically designed for polarimetry are at odds with the measurements of POLAR specifically designed and calibrated for GRBs. So all the upper limit on quantum gravity derived from INTEGRAL, for example, became questionable.

Lawrence Invariance Violation in Standard Model Extension

$$E_P = \sqrt{\frac{\hbar c^5}{G}} = 1.22 \cdot 10^{19} \text{ GeV}$$

The Standard-Model Extension (SME) describe the small-energy effect with respect to a more fundamental High-Energy theory:

$$E \simeq p \left(1 - \zeta^{(0)} \pm \sqrt{(\zeta^{(1)})^2 + (\zeta^{(2)})^2 + (\zeta^{(3)})^2} \right)$$

Modified Vacuum Dispersion relation in SME
Kostelecky & Mewes 2009

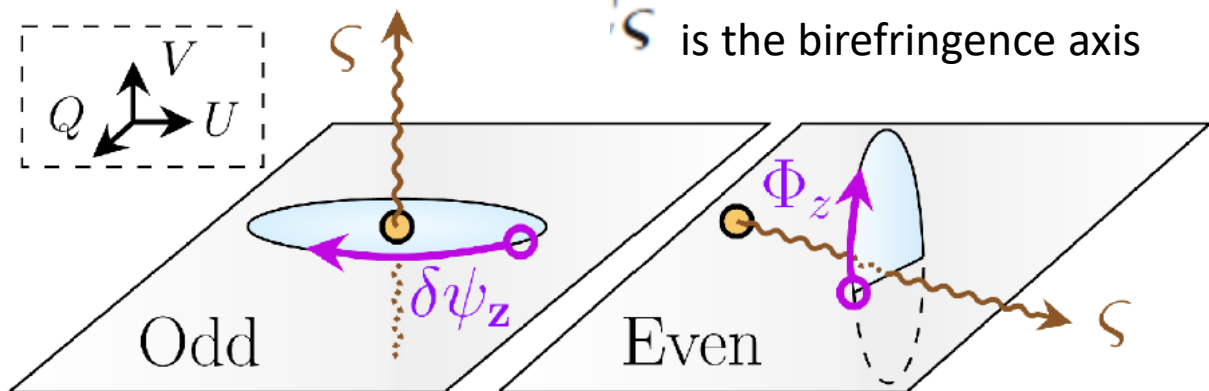
The coefficients can be expanded in spherical harmonics and in the mass dimension d .

The odd coefficient describe a rotation of the linear polarization. The even coefficient describe the appearance of a circular polarization at a constant linear polarization angle

$$\frac{ds}{dt} = 2E\zeta \times s,$$

(KISLAT, F, 2023)

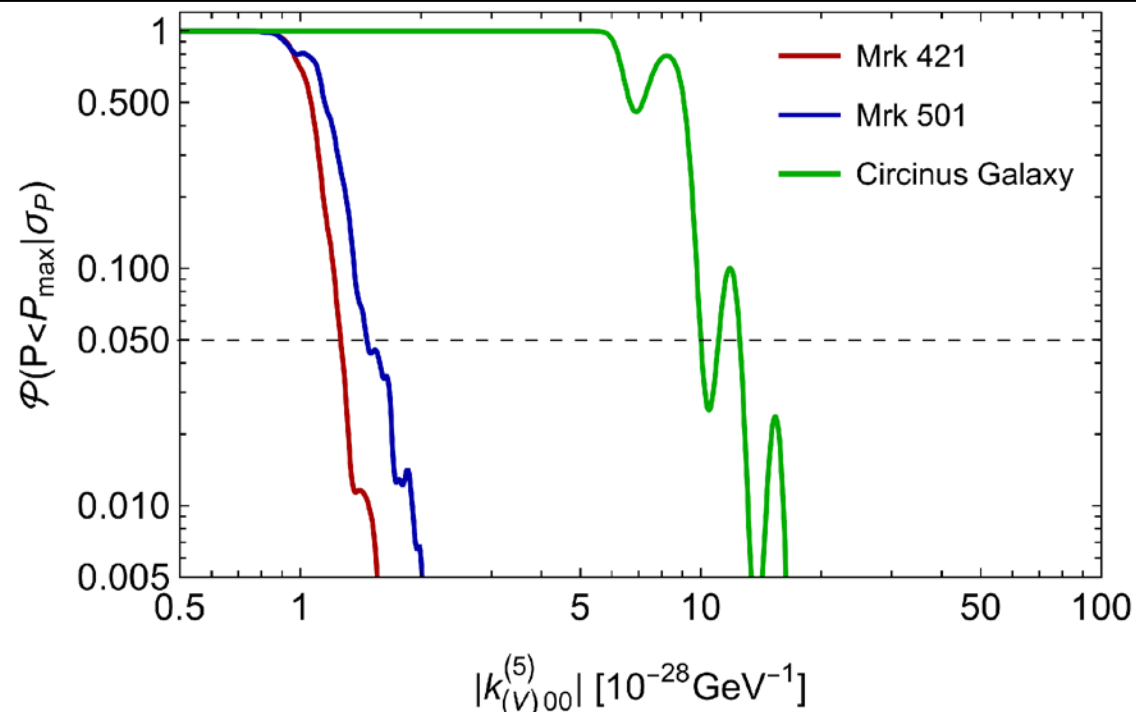
\mathbf{s} is the Stokes vector
 ζ is the birefringence axis



plane of linear polarization Friedman et al., 2020

$$|k_{(V)00}^{(5)}| < 3.5 \times 10^{-25} \text{ GeV}^{-1}$$

The Upper-Limit from optical polarimetry of high redshift galaxies are 10^3 larger than those obtained by IXPE



Isotropic Results

Source	z	IXPE Polarization result	Isotropic SME Limit (95% CL)
Mrk 421	0.030	$P = (15 \pm 2)\%$ (2 – 8 keV) [3]	$ k_{(V)00}^{(5)} < 1.26 \times 10^{-28} \text{ GeV}^{-1}$
Mrk 501	0.033	$P = (10 \pm 2)\%$ (2 – 8 keV) [4]	$ k_{(V)00}^{(5)} < 1.46 \times 10^{-28} \text{ GeV}^{-1}$
Circinus Galaxy	0.001449	$P = (20 \pm 3.8)\%$ (2 – 6 keV) [5]	$ k_{(V)00}^{(5)} < 12.5 \times 10^{-28} \text{ GeV}^{-1}$

For anisotropy much more sources are needed

Quantum Gravity

Axions & Axion-like Particles

Axions:

A Clean Solution to Strong CP and Dark Matter?

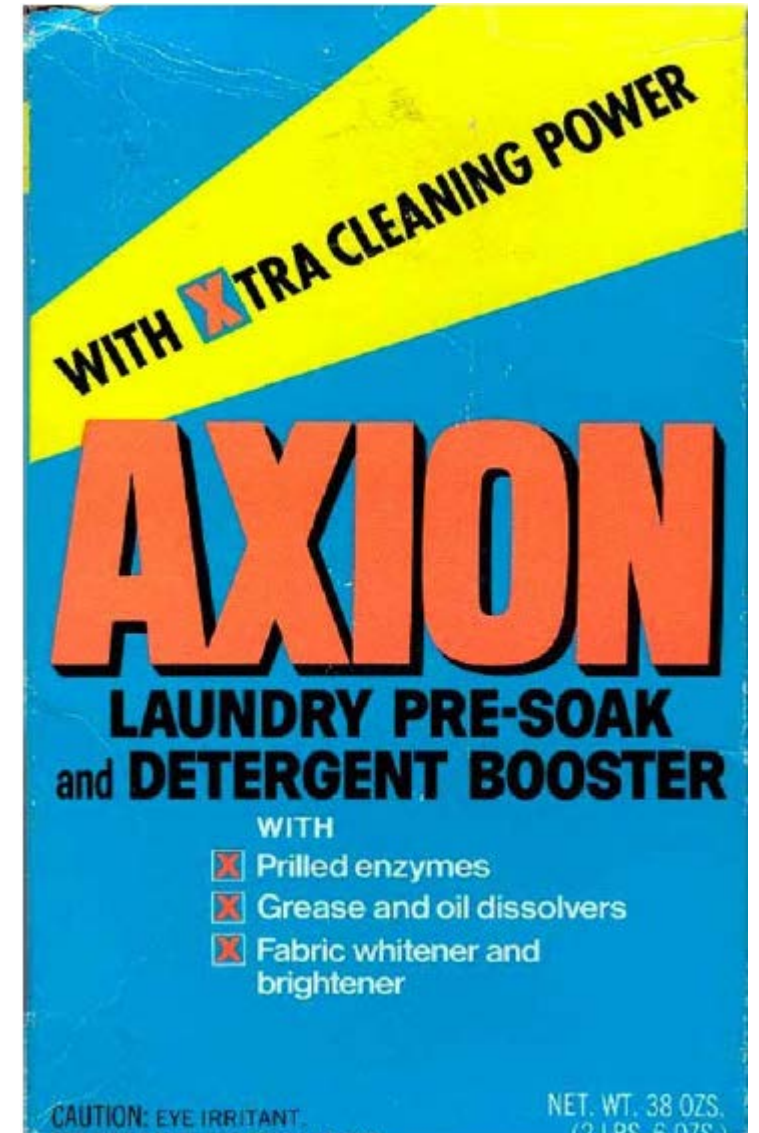
$$\mathcal{L}_{a\gamma} = g_{a\gamma} \mathbf{E} \cdot \mathbf{B}$$

$$g_{a\gamma} = 2 \times 10^{-10} \text{ GeV}^{-1} \zeta(m_a/1 \text{ eV})$$

Within the Standard Model
(Ayala Phys Rev. Lett. 2014)

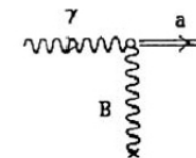
Axions-like Particles (ALPs):

- Predicted by String Theory
- Photon coupling but not with relation between mass and coupling constant.
- Very light particles ($m_a < 10^{-8}$ eV)
- Spin 0
- **Interaction with two photons** (coupling $g_{a\gamma\gamma}$)
- Interactions with other particles discarded
- Possible candidate for dark matter
- **Induce the *change of the polarization state* of photons**

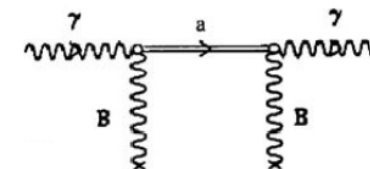


Linearly polarized X-rays passing through magnetic field reduce their parallel component while perpendicular component is unchanged.

(rotation of the plane of polarization)

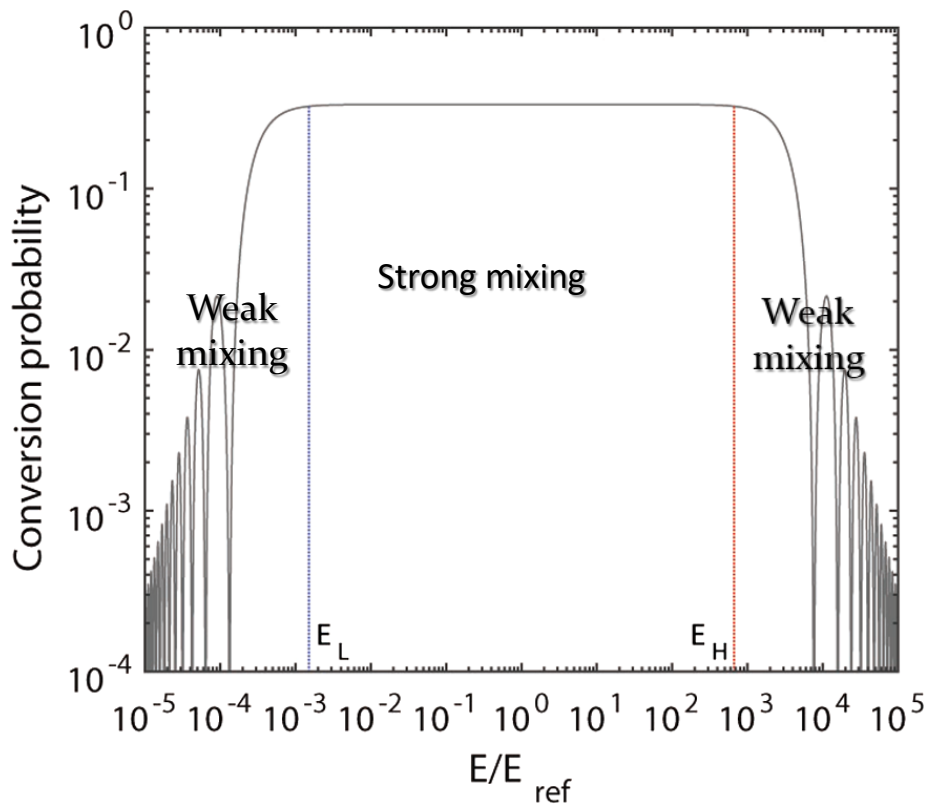


Further vacuum birefringence may change linear to elliptical polarization.



Bassan et al., 2010 deal with a long baseline astrophysical setup to study ALP effects on the polarization of X-ray and Gamma -ray photons from distant sources as a modification of the initial polarization distribution of GRB polarization who nobody knows !!

The role of the magnetic field is crucial in this respect and we have to contemplate all kinds of magnetic field configurations.



$$E_L \sim |m_a^2 - \omega_{pl}^2| / (g_{a\gamma} B_T)$$

$$E_H \sim g_{a\gamma} / B_T$$

Bassan et al., 2020 and reference therein

For energy between E_L and E_H Axions and photons oscillate in regime of strong mixing where the conversion is independent on the energy

For energy below E_L and above E_H the oscillation is in regime of weak mixing where the conversion probability depends on the energy so we have also a modification of the spectrum

Constraints on $g_{a\gamma\gamma}$ and m_a but the firmest is $g_{a\gamma\gamma} < 6.6 \times 10^{-11} \text{ GeV}^{-1}$ for $m_a < 0.02 \text{ eV}$ (CAST collaboration, 2017)

From Galanti G. presentation at Villa Mondragone 2022

In order to have strong mixing at X-ray energies (highest mixing probability and no spectral change) it is necessary that the mass of the axions be very small

THE CLUSTER OF GALAXIES ARE THE BEST CANDIDATE TO SEARCH FOR ALPS THROUGH X-RAY POLARIZATION

We should not consider the modification to the unknown GRB at-source polarization distribution (as in Bassan et al. 2020 which neglects the effects in the source and in Galaxy) but the modification to a zero-polarization distant source like X-ray galaxy cluster ($P < 0.1\%$ Komarov 2016) of the X-ray continuum. A significant detection of linear polarization from cluster may be interpreted as a due to photon-axion mixing.

GALAXY CLUSTER

- Diffuse emission in the cluster central region ($r_{\text{core}} \sim 100$ kpc)
 - X-ray: Bremsstrahlung, initial $\Pi_{L,0} = 0$ (Felten+1966)
 - High-energy (HE) range: e.g. Compton, initial $\Pi_{L,0} = 0$ (Timokhin+2004)
- Electron number density $n_{e,\text{clu}} \rightarrow$ (double) *beta model* (Hudson+2010)
- Magnetic field $B_{\text{clu}} = O(10)$ μG , Kolmogorov-type turbulence, profile
- $\propto (n_{e,\text{clu}}/n_{e,\text{clu},0})^{\eta_{\text{clu}}}$, where $n_{e,\text{clu},0}$ is the central $n_{e,\text{clu}}$ and $\eta_{\text{clu}} \sim 0.75$ (Meyer+2014)

EXTRAGALACTIC SPACE

- 10^{-7} nG $< B_{\text{ext}} < 1.7$ nG with coherence $O(1)$ Mpc (Pshirkov+2016)
- $B_{\text{ext}} \sim 1$ nG with coherence $O(1)$ Mpc favored (Rees & Setti, 1968; Kronberg+1999)
- Domain-like model (Galanti & Roncadelli, 2018)

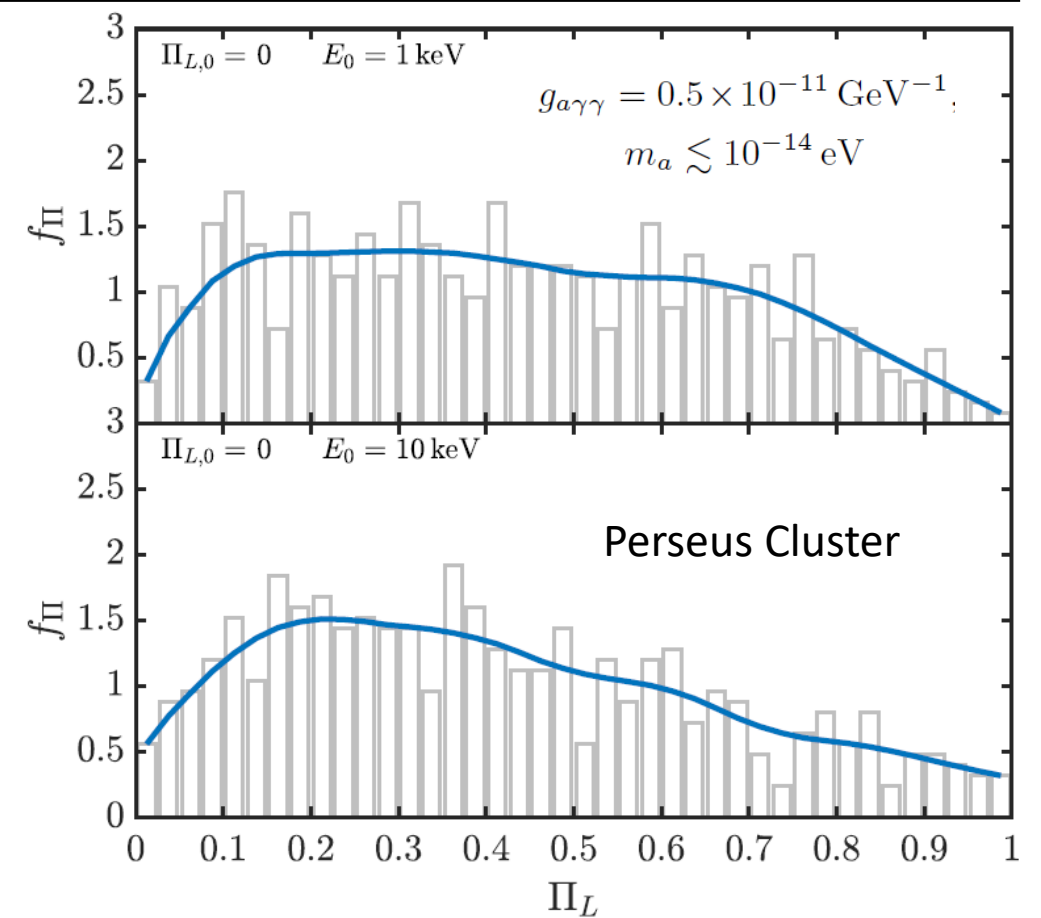
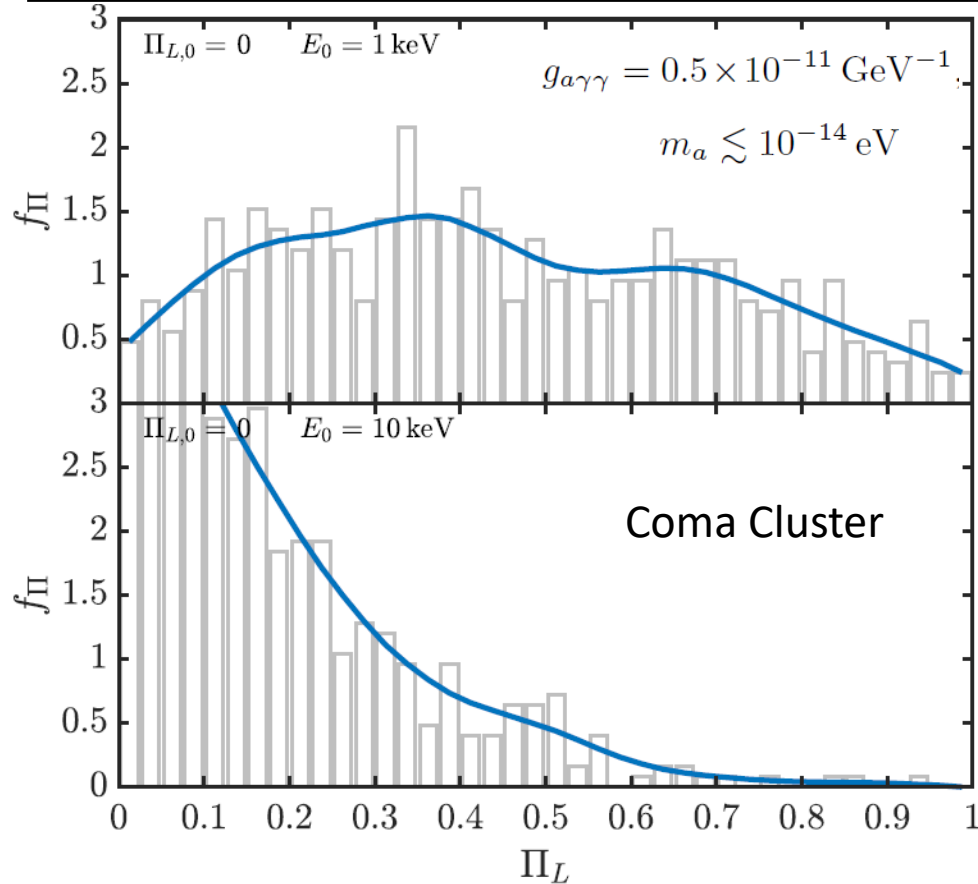
MILKY WAY

- B_{MW} map by Jansson & Farrar (Jansson & Farrar, 2012a,b)

PHOTON-ALP BEAM PROPAGATION

- **Stochastic process** \rightarrow exact expression of $B_{\text{clu}}, B_{\text{ext}}$ unknown
- \rightarrow Several realizations of the propagation process

MODIFICATION OF UNPOLARIZED PHOTONS FROM AN X-RAY CLUSTER WHILE TRAVELING TOWARD THE OBSERVER



Galanti et al., 2023

Coma Cluster ($z \sim 0.023$): 100 Mpc; Perseus Cluster ($z \sim 0.018$): 75 Mpc;
Bullet Cluster ($z \sim 0.296$): 1.2 Gpc; CL J1226.9+3332 ($z \sim 0.89$): 3.2 Gpc

With IXPE we are at the beginning of the story

Dark corners of known physics

More magnetars need to be observed by IXPE for QED effects

More Black Hole binaries should be observed possibly in a high energy band to separate the components: time resolved polarimetry (eXTP).

For equation of state polarimetry and timing of a large number of neutron stars (eXTP).

New physics

Quantum gravity: Large number of extragalactic objects (Seyfert-2 e Blazars) to see if there is a trend of rotation of the polarization angle with the distance

Error on polarization angle of 5° for 1ES0229+200, $z = 0.14$ (590 Mpc)

X-ray polarimetry cannot compete with gamma polarimetry for effects due E^2 . The best is to increase area and the band (up to 80 keV). Gamma polarimetry will be the way when reliable results will arrive. This could be already possible with COSI.

ALPs: Needed long pointings of X-ray clusters without a strong AGN (eg Coma).

Table 1. Contemporaneous multiwavelength polarization properties of HSPs.

Source	X-ray		Optical & IR ^a		Radio ^a	
	II(%)	$\psi(^{\circ})$	II(%)	$\psi(^{\circ})$	II(%)	$\psi(^{\circ})$
Mrk 501 I ¹	10 ± 2	134 ± 5	4 ± 1	119 ± 9	1.5 ± 0.5	152 ± 10
Mrk 501 II ¹	11 ± 2	115 ± 4	5 ± 1	117 ± 3	–	–
Mrk 421 I ²	15 ± 2	35 ± 4	2.9 ± 0.5	32 ± 5	3.4 ± 0.4	55 ± 2
Mrk 421 II ³	10 ± 1	Rotation	4.4 ± 0.4	140 ± 6	2.4 ± 0.1	139 ± 8
Mrk 421 III ³	10 ± 1	Rotation	5.4 ± 0.4	145 ± 1	–	–
Mrk 421 IV ⁴	14 ± 1	107 ± 3	4.6 ± 1.3	206 ± 9	1.8 ± 0.1	167 ± 4
1ES1959+650 I ⁵	8 ± 2	123 ± 8	4.5 ± 0.2	159 ± 1	–	–
1ES1959+650 II ⁵	<5	–	4.7 ± 0.6	151 ± 19	<1.6	–
PG1553+113 ⁶	10 ± 2	86 ± 8	4.2 ± 0.5	Rotation	2.6 ± 0.7	133 ± 7
1ES0229+200 ⁷	18 ± 3	25 ± 5	3.2 ± 0.7	–5 ± 9	<7	–

^{1–8} Results compiled from the following references: [57–63]; ^a median polarization properties during the IXPE observation. Especially for optical and IR polarization, only corrected polarization values, accounting for the dilution of polarization by unpolarized starlight from the host galaxy, were considered for calculation; ^b at the lowest radio frequency (4.85 GHz).

Kim et al., 2024

X-ray polarization of HBL are comparable higher than at longer wavelength

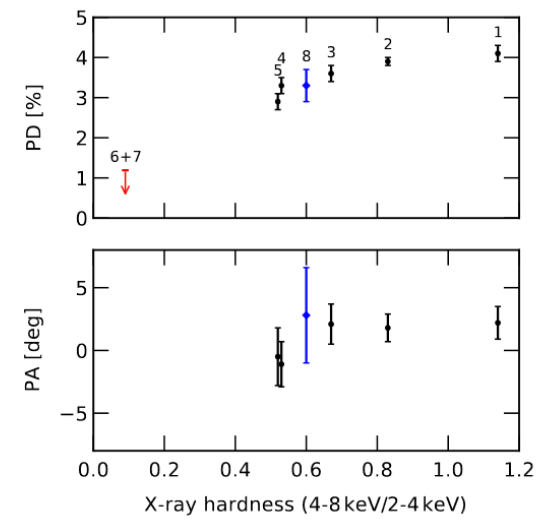
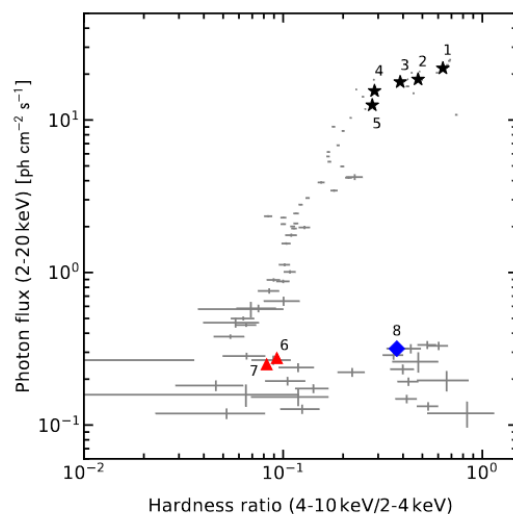
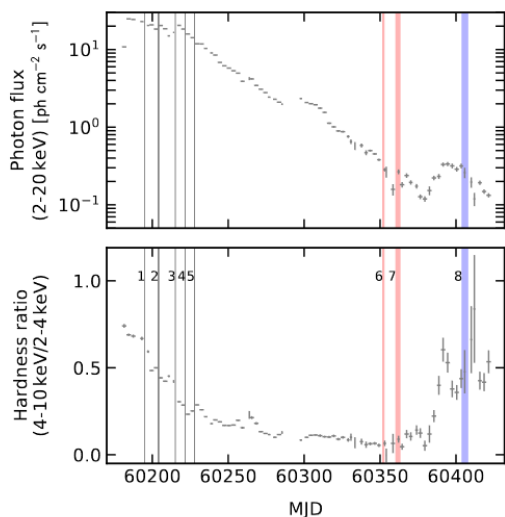
Notably Mrk 421 was found rotating in X-rays and not in longer wavelength while PG1553 was rotating in longer wavelength but not in X-rays

IXPE TRACES A STATE TRANSITION WITH SWIFT J1727.8-1613

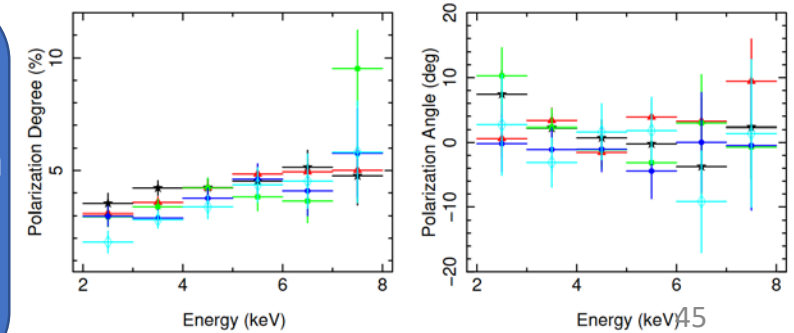
Discovered on 24th August 2023 (7 Crab in 2-20 keV band)

Most probably a BH-binary transient: (X-ray spectrum, QPO, flat-spectrum radio emission)

Ingram, A. et al., 2023ApJ accepted, Podgorny', A&A submitted



IXPE is covering the hard-to-soft-hard transition. X-ray PA is parallel to Radio-PA implying that corona is extended along the disk in all observations.
 PD decreases with time implying that disk emission with orthogonal or null polarization is coming into play.
 PD increases with energy as in others BH-Binaries
 PD drops in the soft state while recovers in the hard dim state at level of outburst

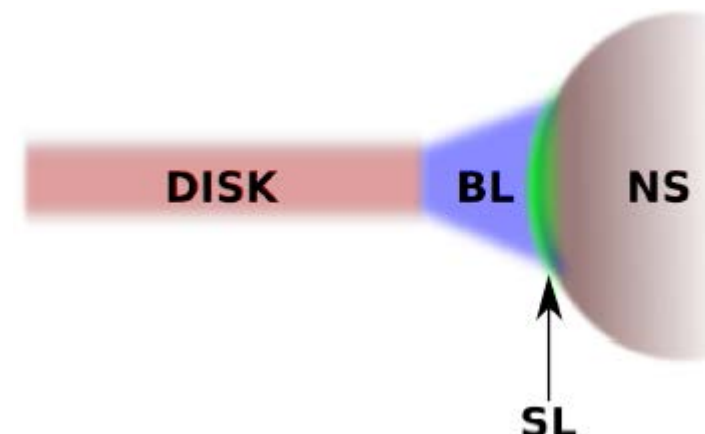
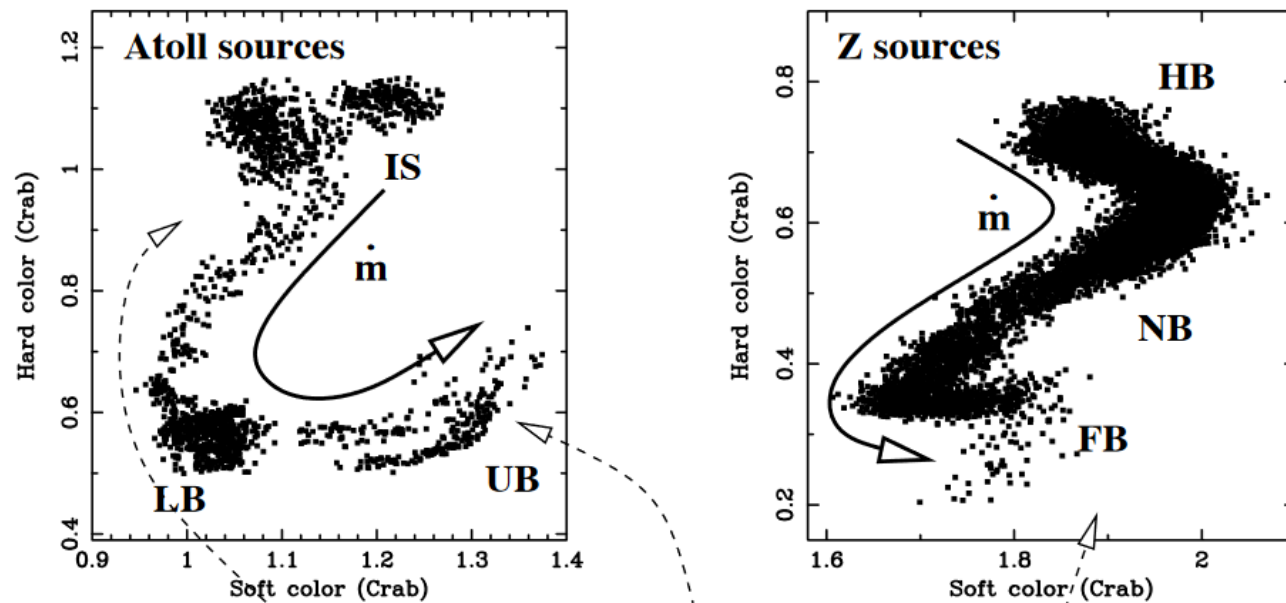


LOW MAGNETIZED NEUTRON STARS

IS = Island State, LB= Lower Banana, UB = Upper Banana

HB = Horizontal Branch, NB = Normal Branch, FB = Flaring Branch

BL = Broad Line Region; SL = Spreading Layer



NS: $B < 10^{10}$ G,
 $M_{\text{com}} \approx M_{\odot}$
 Accreting matter via Roche-lobe overflow

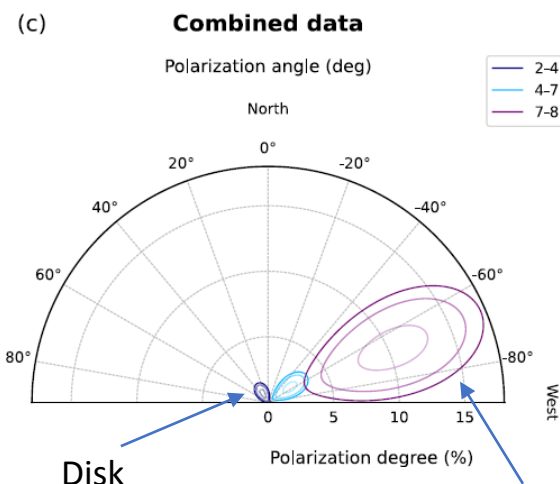
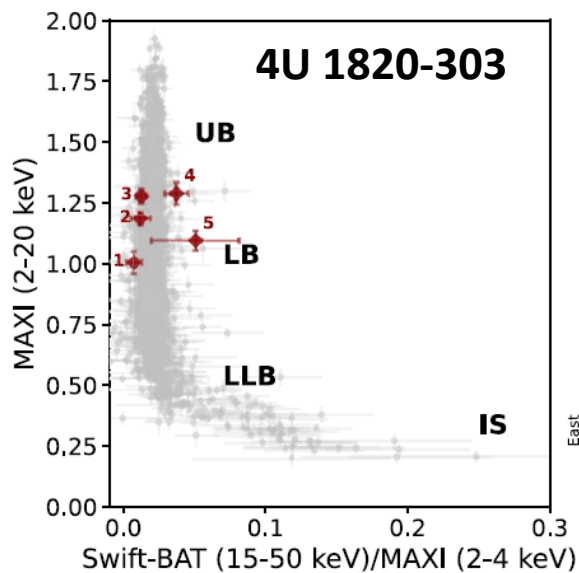
~0.01 ~0.1
 'Hard' atoll sources 'Soft' atoll sources 'Z' sources

Luminosity / Eddington

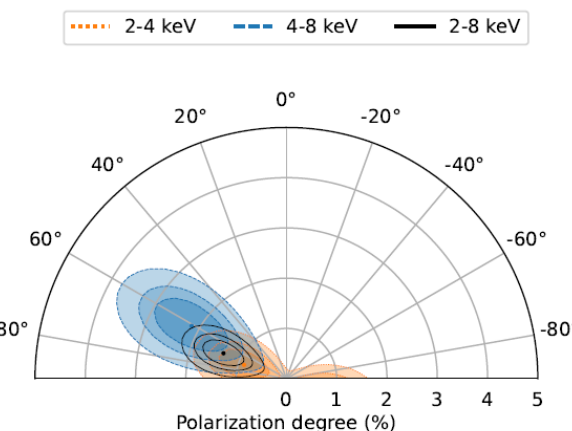
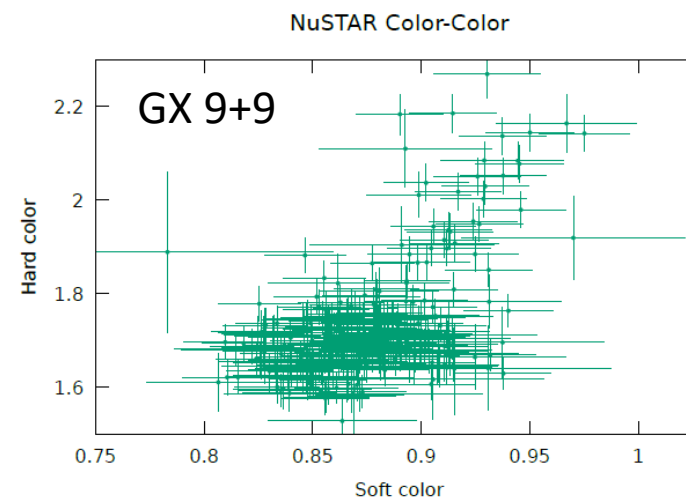
Di Salvo et al., 2023

Di Marco et al., 2023

Ursini et al. 2023



Spreading (boundary layer)



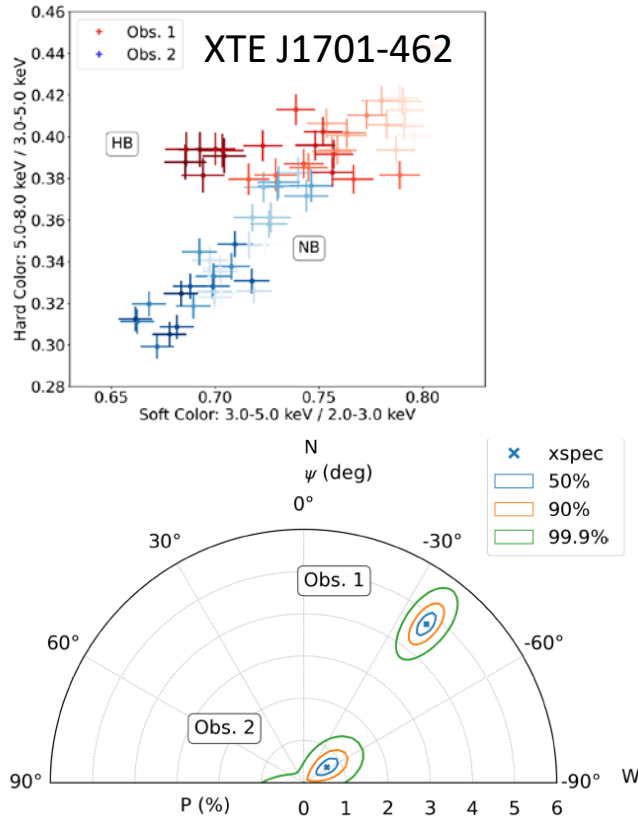
In 4U 1820 a rotation of the polarization angle of 90° with energy may indicate that the disk (low energy) is polarized orthogonal to the spreading/boundary layer. The reflection fraction is negligible $< 5\%$.

In GX 9+9 the 4-8 keV polarization is significant and may be a combination of reflection from the disk and a of Comptonization (boundary/spreading layer) and reflection from the disk.

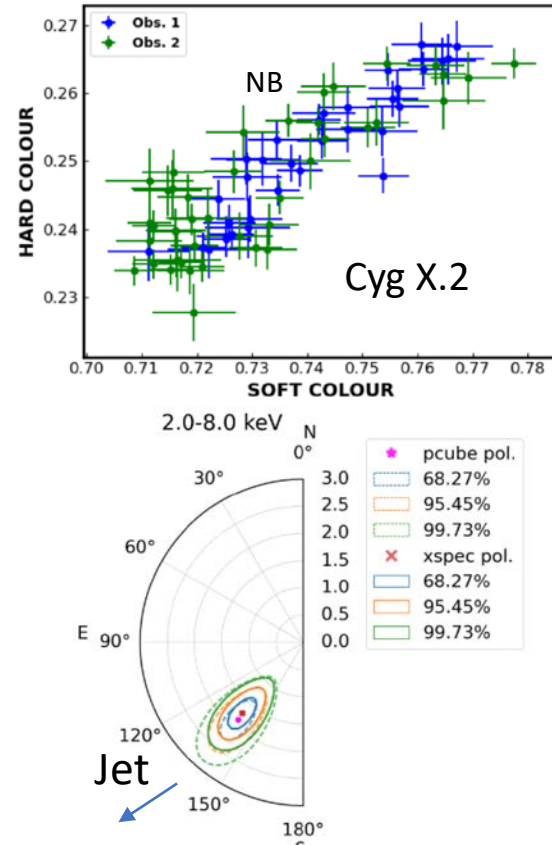
In GS1826-238 (Capitanio et al., 2023) only upper limit albeit significant were measured.

Z-SOURCE SOURCES: XTE J1701-462, CYG X-2 AND SCO X-1

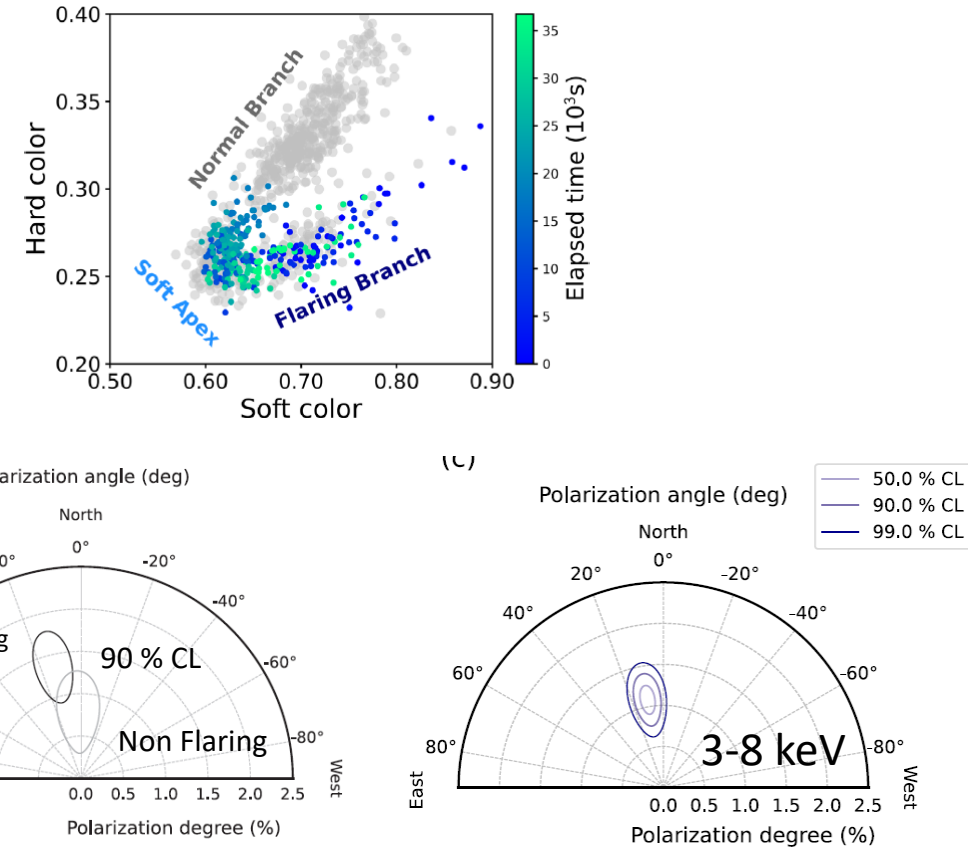
Cocchi et al., 2023



Farinelli et al. 2023



La Monaca et al 2024



The polarization on the Horizontal Branch seems larger with respect to the polarization of the Normal Branch (See also GX 5.1, Fabiani et al., 2023). In Sco X-1 flaring and non Flaring seems to have comparable PD and PA not aligned with the jet. I Data shows a larger polarization with energy may be connected to a larger contribution of scattering.

- High Mass X-ray binaries:

Source (no. obs)	Goal of the study
Cyg X-1 Hard State (2)	Corona
Cyg X-1 Soft State (5)	Corona + Disk
Cyg X-3 hard & Intermediate (2)	Reflection from cone
LMC X-1 High Soft State (1)	Disk
LMC X-3 High Soft State (1)	Disk

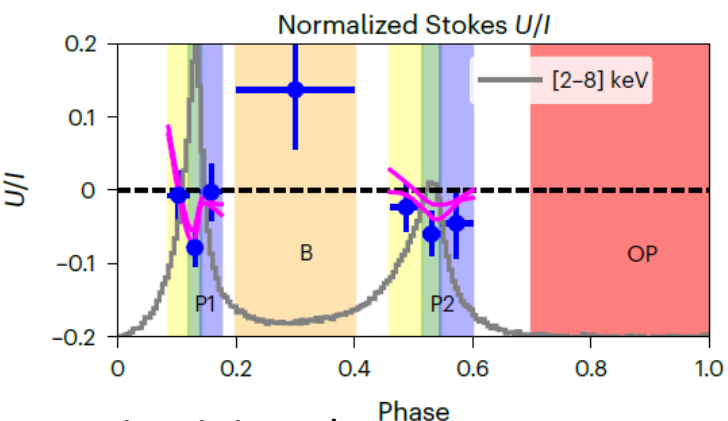
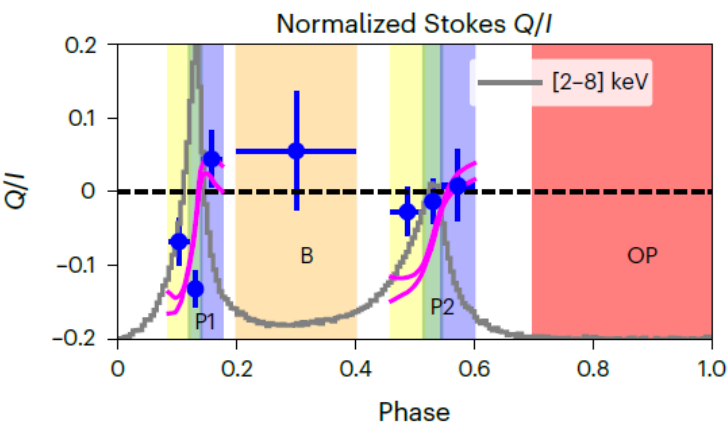
- Low Mass X-ray binaries:

Source (no. obs)	Goal of the study
4U 1630-47 High-Soft State (1)	Disk
4U 1630-47 Steep PL/Interm (1)	Disk + Corona
SWIFT J1727 Low Hard/Inter (5)	Disk + Corona
SS 433 Eastern Lobe (1)	Synchrotron emission

WHAT ABOUT THE PULSAR ?

- Vela pulsar is too weak in the IXPE energy band

PSR B0531+21 (Crab PSR)



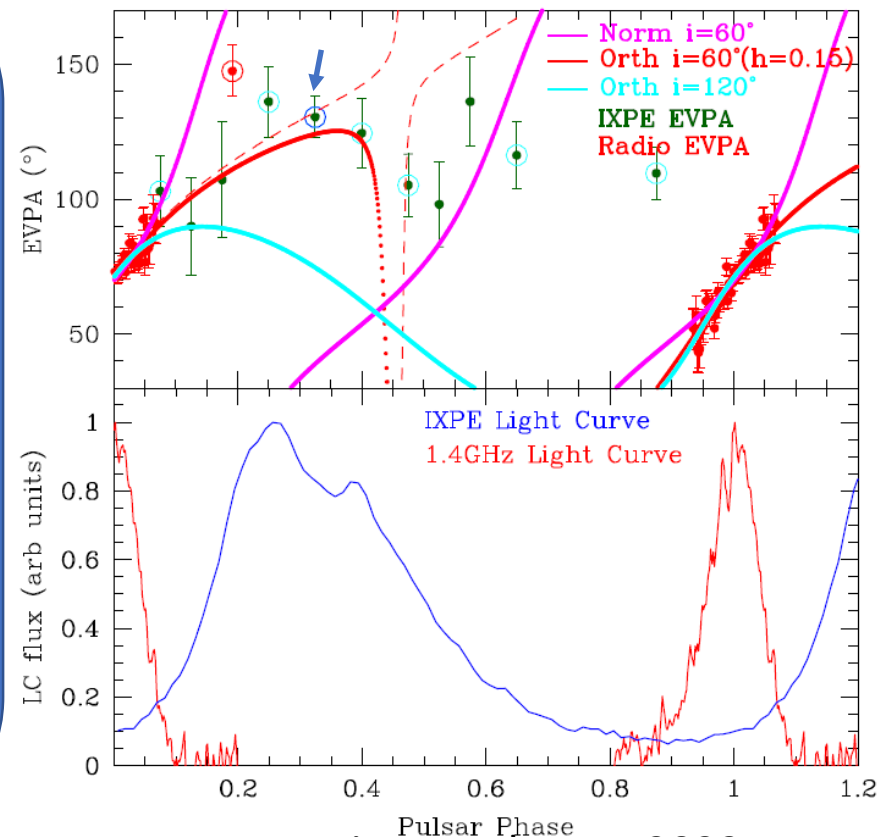
Crab PSR:

- Polarization is > 3-sigma significant in the central bin of P1
- Total pulse signal is negligible
- Consistency with optical data is marginal. It sweep faster in X-ray than in optical.

MSH 15-52 PSR:

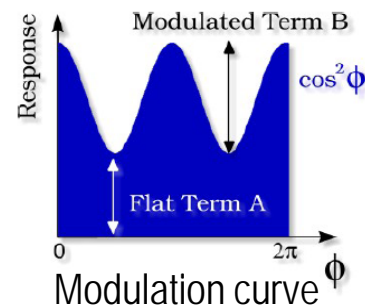
- Only the central bin of the peak has been detected with > 3-sigma (17.5 %)
- Other bins low PD 10-20 % 2-3-sigma

PSR B1509-58 (MSH 15-52 PSR)



Romani, R. et al., ApJ, 2023

Fit function: $\mathcal{M}(\phi) = A + B \cos^2(\phi - \phi_0)$



Modulation: $\frac{\mathcal{M}_{\max} - \mathcal{M}_{\min}}{\mathcal{M}_{\max} + \mathcal{M}_{\min}} = \frac{B}{B + 2A}$

Polarization: $\frac{1}{\mu} \frac{B}{B + 2A}$ μ is the modulation factor, i.e. the modulation for 100% polarized radiation

Or by using Stokes Parameters

$$S(\varphi) = I + U \sin(2\varphi) + Q \cos(2\varphi)$$

$$I = \left(A + \frac{B}{2}\right) \quad U = \left(\frac{B}{2}\right) * \sin(2\varphi_0) \quad Q = \left(\frac{B}{2}\right) * \cos(2\varphi_0)$$

$$P = \frac{\sqrt{Q^2 + U^2}}{I} \quad \varphi = \frac{1}{2} \text{atan} \frac{U}{Q}$$

No V → no circular polarization with present techniques

Kislat et al. (2015) introduced the Stokes parameters from the direction of the single carrier of polarimetric observation

THE FIRST LIMIT: IN POLARIMETRY THE SENSITIVITY IS A MATTER OF PHOTONS

$$MDP = \frac{4.29}{\mu R_S} \sqrt{\frac{R_S + R_B}{T}} \quad \text{Minimum Detectable Polarization (MDP)}$$

R_S is the Source rate, R_B is the Background rate, T is the observing time
 μ is the modulation factor: the response of the polarimeter to a 100% polarized beam
 (spanning from 0 or no sensitivity, to 1 or maximum sensitivity)

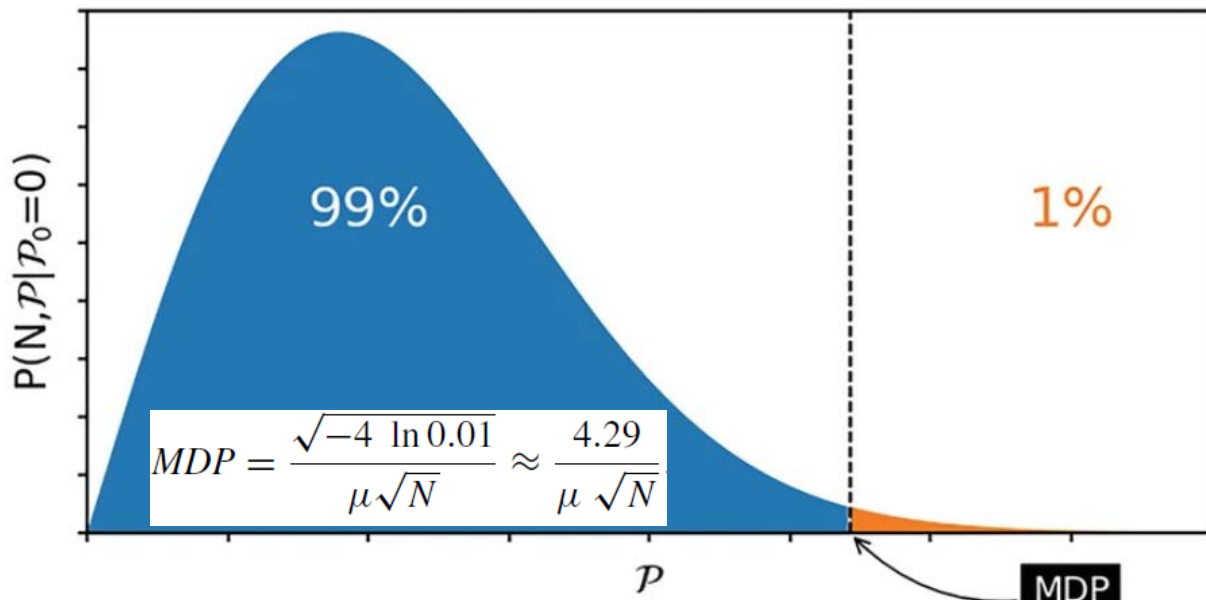
If background is negligible: $MDP = \frac{4.29}{\mu \sqrt{N_{ph}}}$

To reach MDP=1% with $\mu=0.5$: $N_{ph} = \left(\frac{4.29}{\mu MDP} \right)^2 = 736 \cdot 10^3 \text{ ph}$

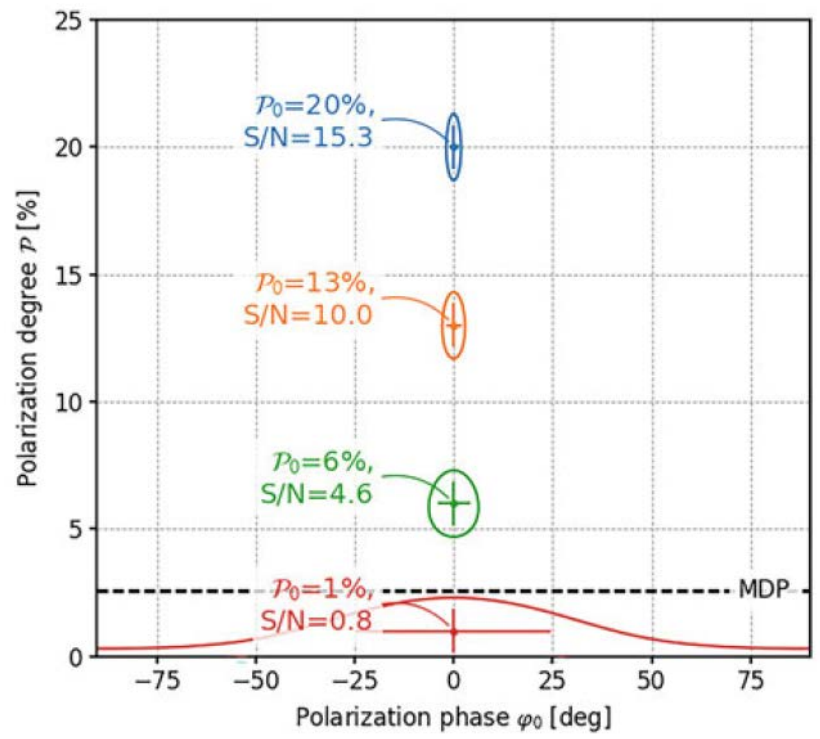
- Source detection > 10 counts
- Source spectral slope > 100 counts
- Source polarization > 100.000 counts

Caution: the MDP describes the capability of rejecting the null hypothesis (no polarization) at 99% confidence.

POLARIZATION ANALYSIS: MDP AND CONTOURS



The probability to measure a polarization P from an unpolarized source. The value of P for which this probability is 1 % or smaller is the Minimum Detectable Polarization (MDP).



Contours representing the joint probability for P.D. and P.A. at 68 % confidence level. P.D. and P.A. are covariant.

For $P < MDP$ the angle is unconstrained albeit not all the angle are equiprobable.

Muleri F., 2023

TWG 1: (Pulsar Wind Nebulae): The magnetic field is very ordered even at a large distance from the pulsar.

TWG 2: (Supernova Remnants): The magnetic field can be radially directed even in vicinity of the shock.

TWG 3: (Accreting Black Holes): The corona in hard X-ray is along the disk plane the accretion disk and the lamp-post is excluded.

TWG 4: (Accreting Neutron Stars): The rotating vector model works in X-rays. The degree of polarization is 5-6 times smaller with respect to models predictions.

TWG 5: (Magnetars): Different magnetars showed unexpectedly very different behavior on the polarization degree and angle.

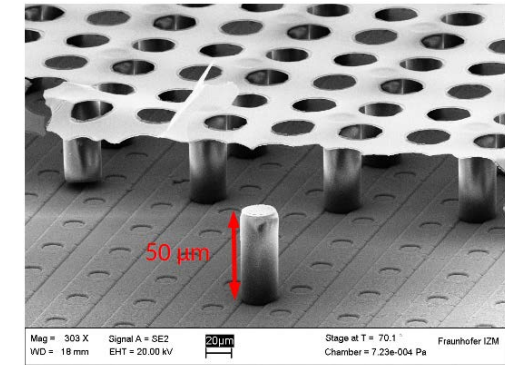
TWG 6: (Radio-Quiet AGN & SgrA clouds): Corona is sandwiching the disk. Lamp-post is excluded. Reflection confirms obscuring torus in Compton-thick AGNs. Molecular clouds points to Sgr A* as origin of their reflected emission.

TWG 7: (Blazars and Radio Galaxies): Energy stratified shock acceleration is confirmed. In X-ray fast rotation of the polarization vector with time is present in Synchrotron dominated blazars. Inverse Compton dominated blazars



TimePIX3: from MEDIPIX CERN collaboration

Timepix3: a 65K channel hybrid pixel readout chip with simultaneous ToA/ToT and sparse readout



Parameter	Value
Pixel matrix	256 x 256 = 65536 pixels (2x4 superpixels)
Pixel size	55 x 55 μm ²
Technology	CMOS 120 nm
Measurement type	<ol style="list-style-type: none"> 1. Simultaneous 10 bit TOT, 14 + 4 bit ToA 2. 14 + 4 bit ToA only 3. 14 bit integral ToT
Readout type	<ol style="list-style-type: none"> 1. Data Driven (zero-suppression) 2. Frame based (zero-suppression)
Dead time per pixel	ToT + 457 ns (pulse processing + data transfer)
Output bandwidth	Up to 5.12 Gbs (parallel 8 channels x 640 Mbps)
Maximum Counting rate	Data Driven up to 40Mhits/cm ² /s with duty cycle of 100 %
TOA precision (resolution)	1.56ns
Front End noise, minimum threshold	60 e _{rms} , 500 e ⁻

Kaminski, 2017, Lupberger 2015

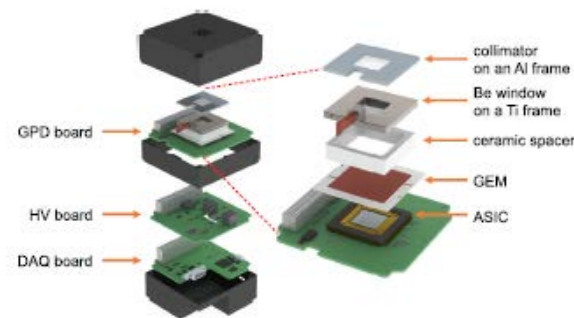
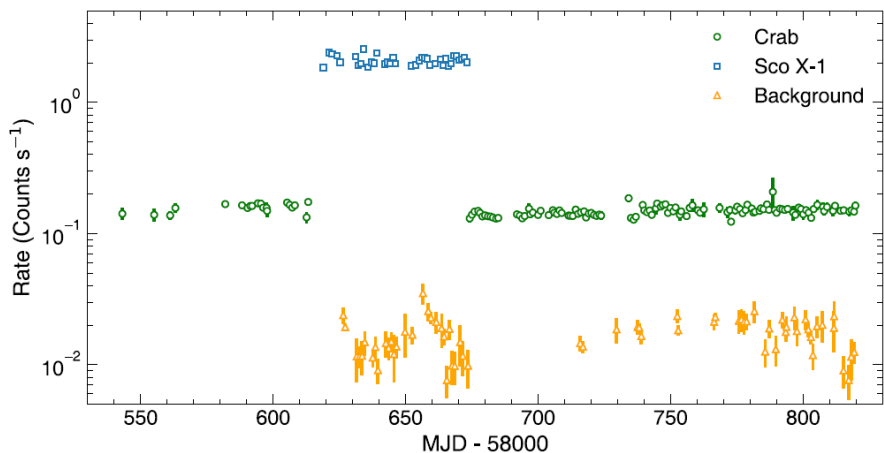
3-D imaging of the track is possible.

High rate for large optics is possible

Ongoing collaboration with
University of Bonn

A collimated experiment of X-ray polarimetry requires a large area

Li, 2021



Feng et al., 2019

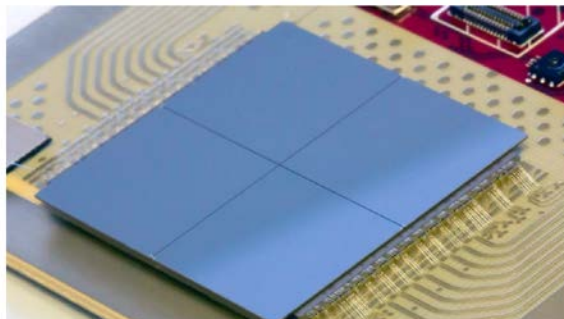
No optics!
Small Mission!
Bright Galactic Sources!

An alternative approach

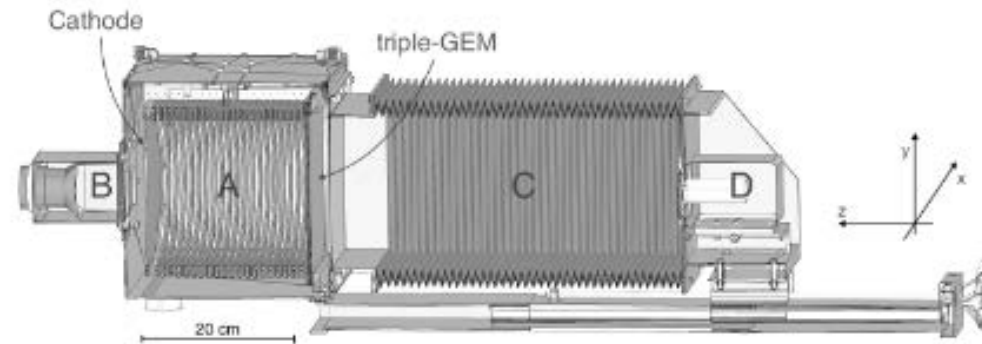
Baracchini et al., 2020, Amaro et al., 2022
 Optical photoelectron track imaging

- Background Polar Light : about 80 mCrab after discrimination, (Jiahuan Zhu 2021)
- Collimator open fraction 71 %
- Area 1000 cm²
- Crabrate = 65 c/s (2-8 keV)
- Background = 5 c/s
- MDP (1 Crab 100 000 s) = 0.5 %

Llopart et al., 2022, TimePIX 4



Timepix4v0 with 4x300 μm (256x256) edgeless Si sensor (August 2020)

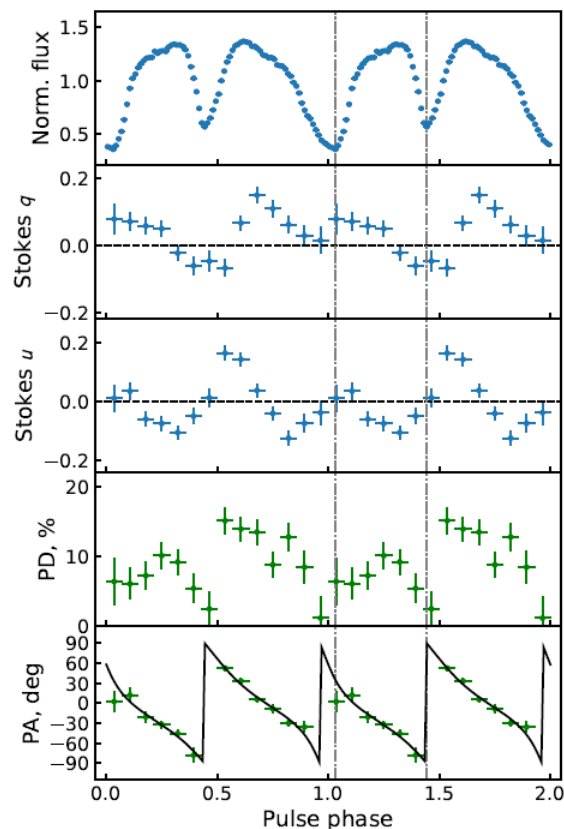


Nicely solve the problem of large collecting area !

512x448 pixels (55x55 μm²)
 Area 1 ASIC 7 cm²
 Tiling on 4 Sides
 200 ps time resolution
 140 ASICs to cover 1000 cm²

Large power required

GRO J1008-57 Tsygankov et al., 2023

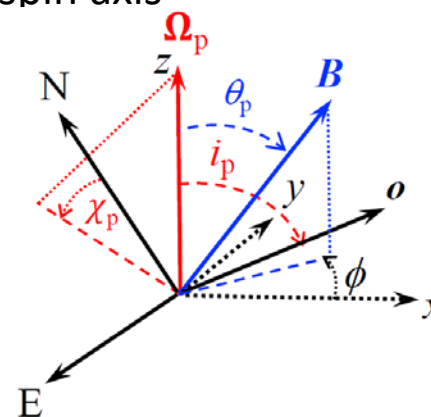


$$\tan(\text{PA} - \chi_p) = \frac{-\sin \theta \sin(\phi - \phi_0)}{\sin i_p \cos \theta - \cos i_p \sin \theta \cos(\phi - \phi_0)}$$

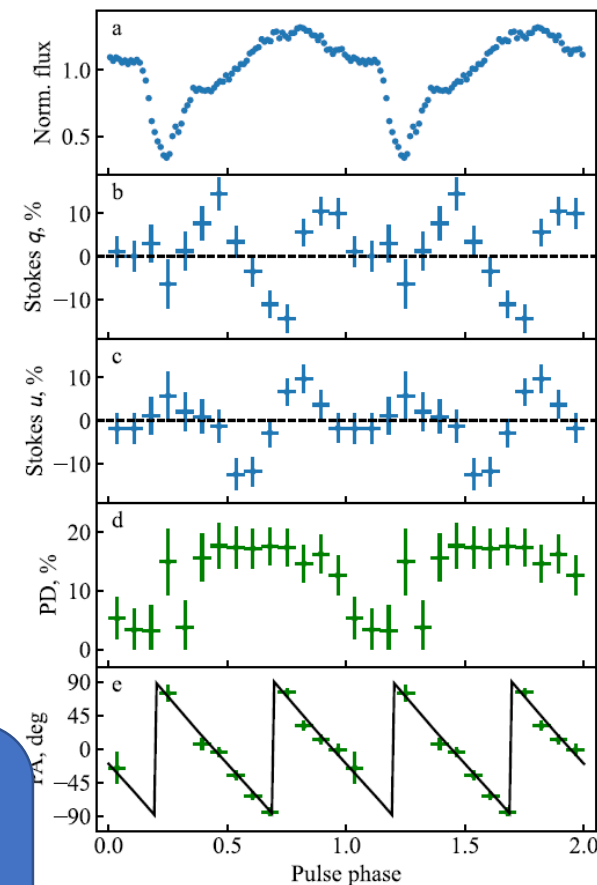
i_p is the angle between the pulsar spin and the line-of-sight, θ is the angle between the magnetic dipole and the spin axes, χ_p is the position angle of the spin axis

	GRO J1008-57	X Persei
i_p	$130^{\circ}.2 \pm 3^{\circ}.3$	$162^{\circ} \pm 12^{\circ}$
θ	$73^{\circ}.5 \pm 1^{\circ}.9$	$\approx 90^{\circ}$ ($>75^{\circ}$ 68%)
$\chi_{p,0}$	$74^{\circ}.8 \pm 4^{\circ}.2$	$70^{\circ} \pm 30^{\circ}$

$$\chi_{p,X} = \chi_{p,0} \pm 90^{\circ}$$



X Persei Mushtukov et al., 2023



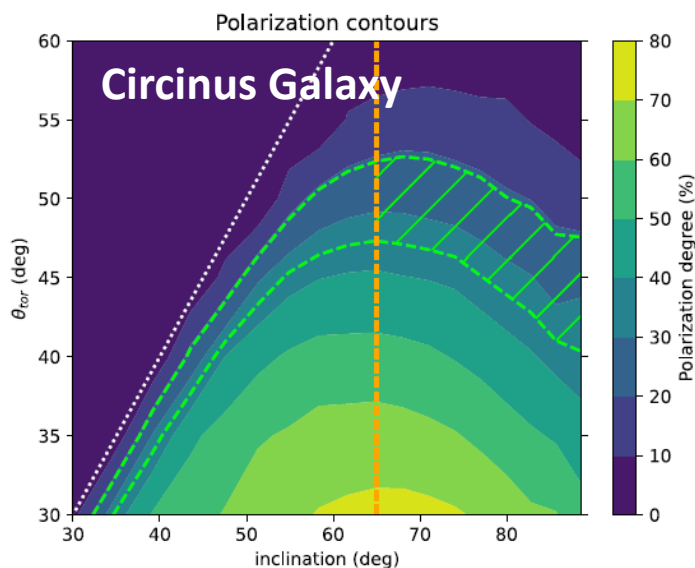
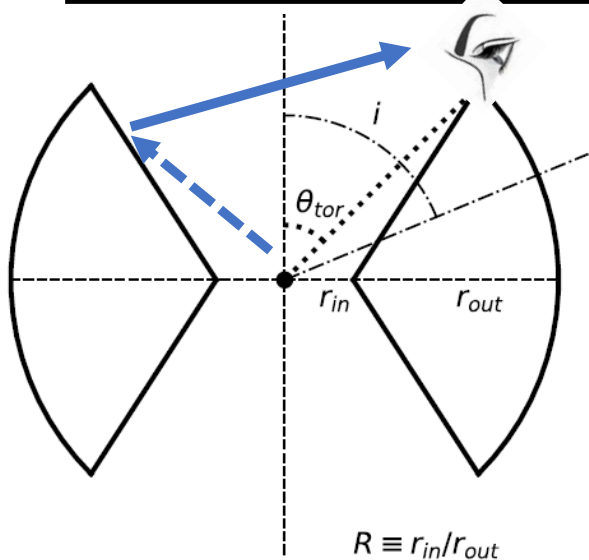
The rotating vector model showed two oblique rotator. They were in sub-critical regime

GRO J1008-57: $L \approx 10^{36}$ erg/s \ll few 10^{37} erg/s = L_{crit}

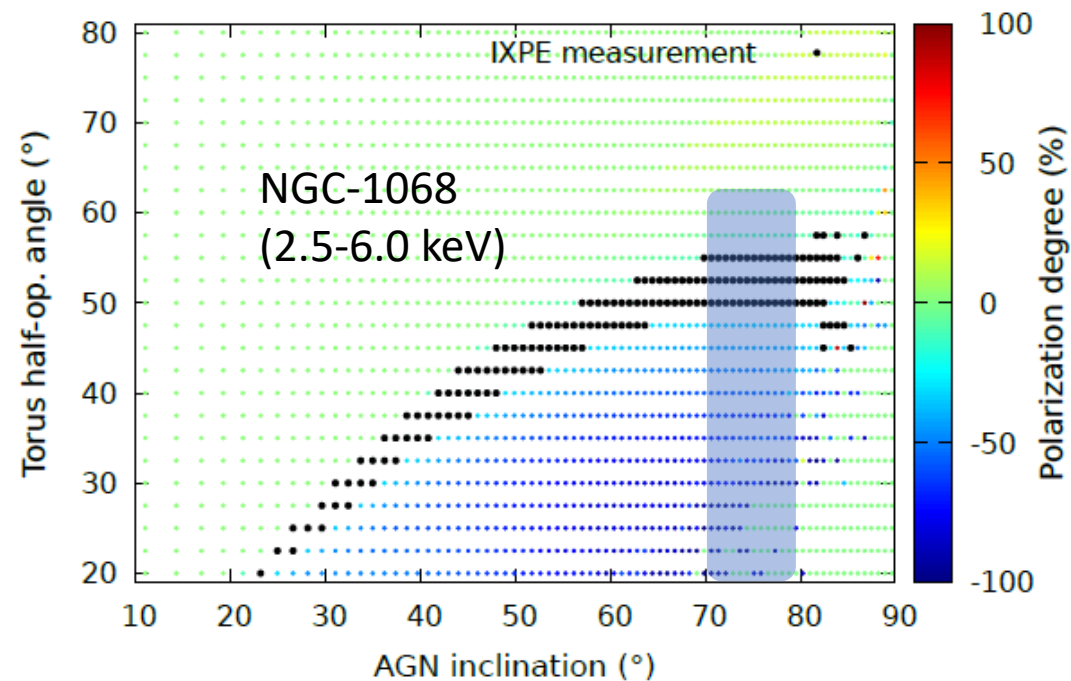
X Persei: $L \approx 5 \times 10^{34}$ erg/s \ll L_{crit} 3×10^{37}

In Subcritical regime the phase resolved PD and flux correlates

IXPE HELPS TO CONSTRAIN THE TORUS OPENING ANGLE



The orange vertical line set the lower limit to the inclination as provided by the inclination of the galaxy. The dashed lines mark the 68% confidence level region consistent with the measured polarization of the cold reflector. The hashed region mark the constraints on inclination and torus aperture.



The positive polarization is parallel to the jet, the negative polarization is perpendicular to the jet. Each colored dot represent a simulation. Black dots are consistent with IXPE polarimetry. Shaded region is the constraint from the literature on the torus inclination.

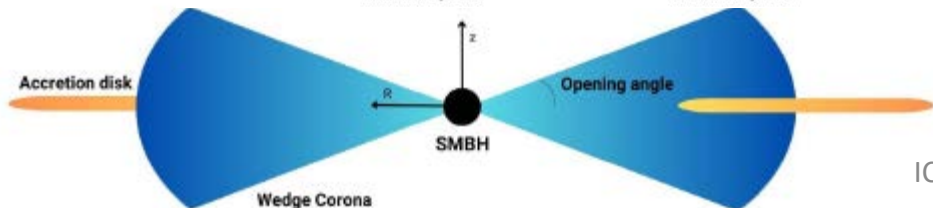
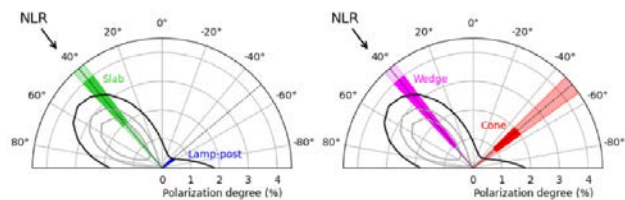
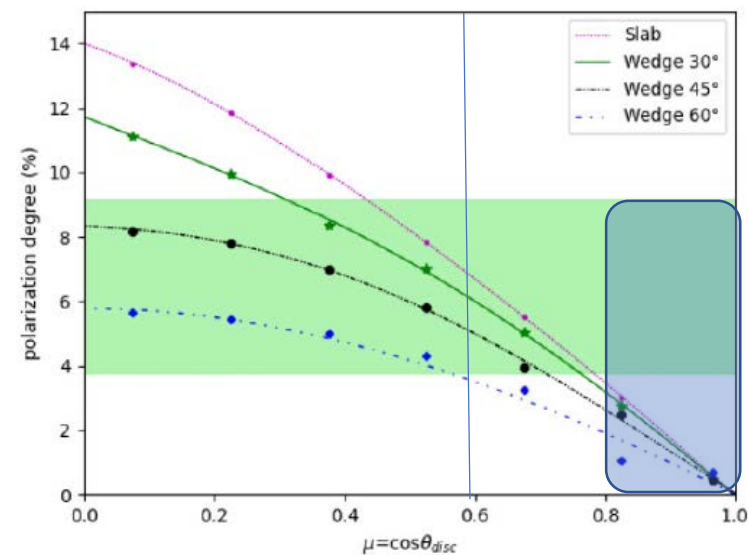
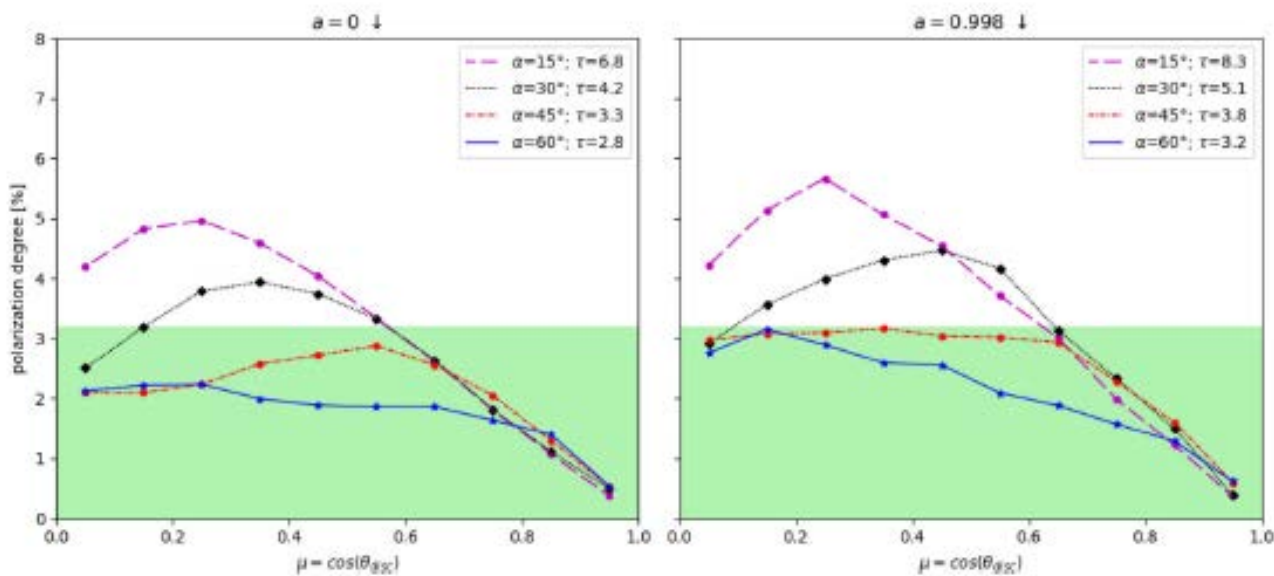
For both Circinus galaxy and NGC-1068 X-ray polarimetry constraints on the torus aperture are similar 50°-55°

IXPE helps to constrain the geometry of the corona.

MCG 05-23-16 (Tagliacozzo et al. 2023)

Simulations with MONK

NGC 4151 (Gianolli et al 2023)



For both MCG 05-23-16 and NGC 4151 Slab or Wedge geometry of the corona are consistent with the IXPE data. NGC4151 favors disk inclinations obtained by reverberation and disfavor inclination obtained by spectra



- *Model independent analysis tool and IXPE observation simulator IXPE.* Baldini L. et al. SoftwareX 2021
- *Spectro-polarimetric forwarding folding fit based on XSPEC that includes polarization phenomenological models.* (Arnaud, K. , Ast.Src.Code, 1999)

Algorithms and response matrices designed by the instrument team we engineered for the flight pipeline by the SSCD .

Two completing different software approaches provided when eventually compared consistent results.



BLACK HOLES X-RAY BINARIES SOME PUBLICATIONS:

- High Mass X-ray binaries:

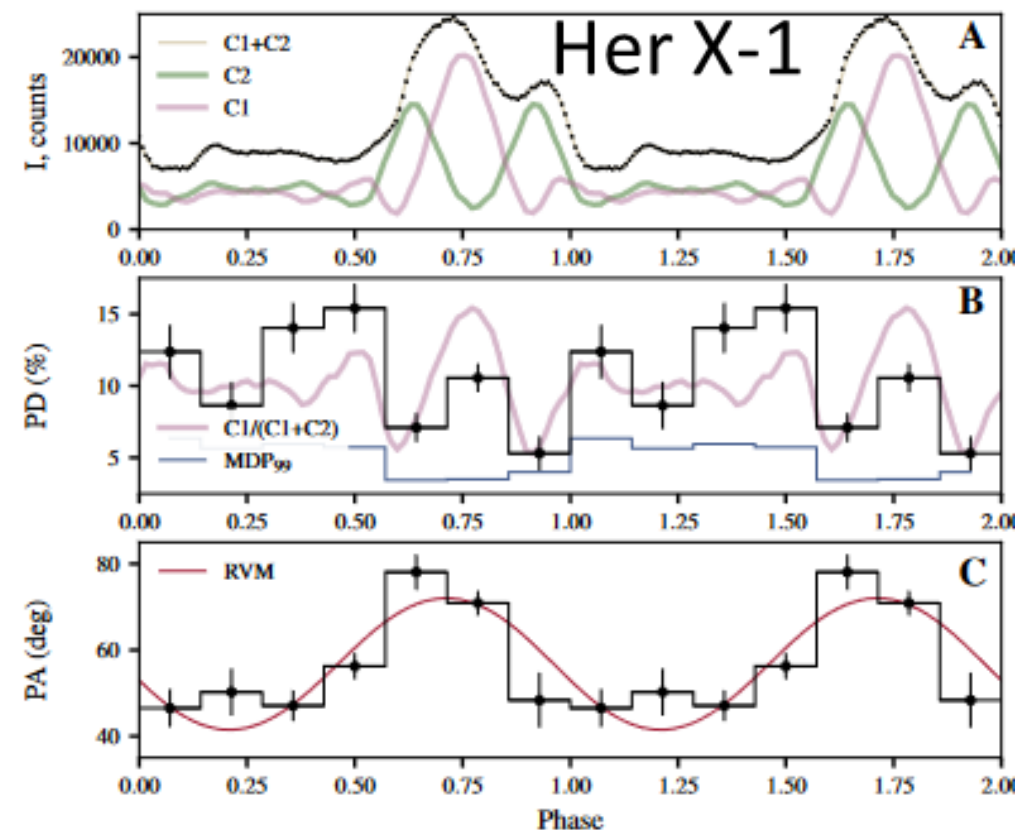
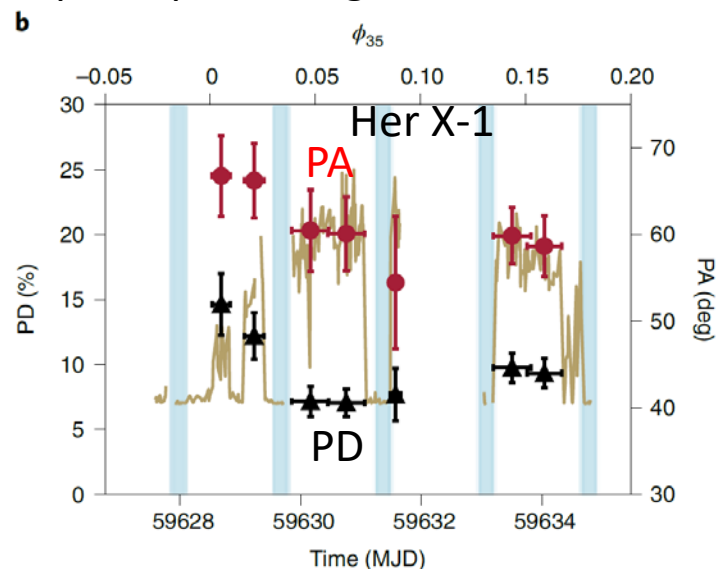
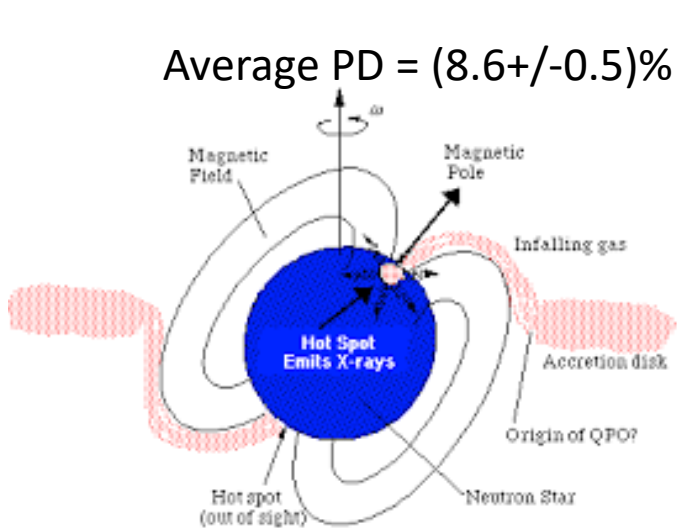
Source	Main result	Reference
LMC X-1 High Soft State	MDP ₉₉ =1.1% Standard thin disk compatible	Podgorny et al., MNRAS, 2023
LMC X-3 High Soft State	PD=(3.2+/-0.6)% PA=-42°+/-6° Low-spin (a= 0.2, a<0.7 from pol. analysis only)	Svoboda et al., ApJ, 2024

- Low Mass X-ray binaries:

Source	Goal of the study	
4U 1630-47 Steep PL/Interm.	PD = (6.8+/-0.2)% PA = 21°±0.9° PL emitting region like the disk ?	Rodriguez Cavero, N., ApJ, 2023
4U 1957+11 High Soft State	PD: (1.9+/-0.4)%; PA:-41° ±5° High spin (a> 0.96)	Marra et al., Sub A&A, 2023
SWIFT J1727 Low Hard/Inter	Disk + Corona (confirming sandwich corona)	Veledina, A. et al ApJ, 2023 Ingram, A. et al. ApJ 2024
SS 433 Eastern Lobe (1)	Synchrotron emission	Kaaret, P. et al, ApJ, 2023

ACCRETING NS – X-RAY PULSARS HER X-1

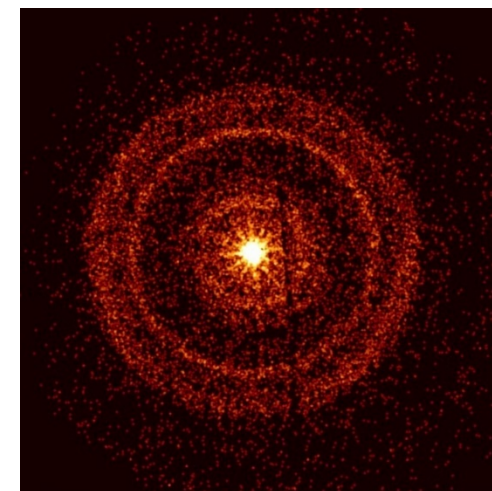
An X-ray pulsar is a binary system made of a magnetized neutron star (10^{12} G) accreting matter from a normal stellar companion. Gas is accreted from the stellar companion and is channeled by the neutron star's magnetic field on to the magnetic poles producing two or more localized X-ray hot spots.



X-ray pulsars are predicted (Meszaros et al., 1988, Caiazzo and Heyl, 2021, to be very highly polarized, because of the two different opacities while the polarization is lower than expected, but detected with very high significance in a number of sources, e.g. Her X-1 (Doroshenko et al. 2022), Cen X-3 (Tsyganov et al. 2022), Vela X-1 (Poutanen et al. 2023), GRO J1008-57 (Tsyganov et al. 2023) + ...

We did not plan to follow-up on GRBs, because of the relatively slow reaction time (2-3 days).

However, GRB 221009A (the ‘BOAT’ GRB) was so exceptional in terms of brightness, that we decided to observe it.

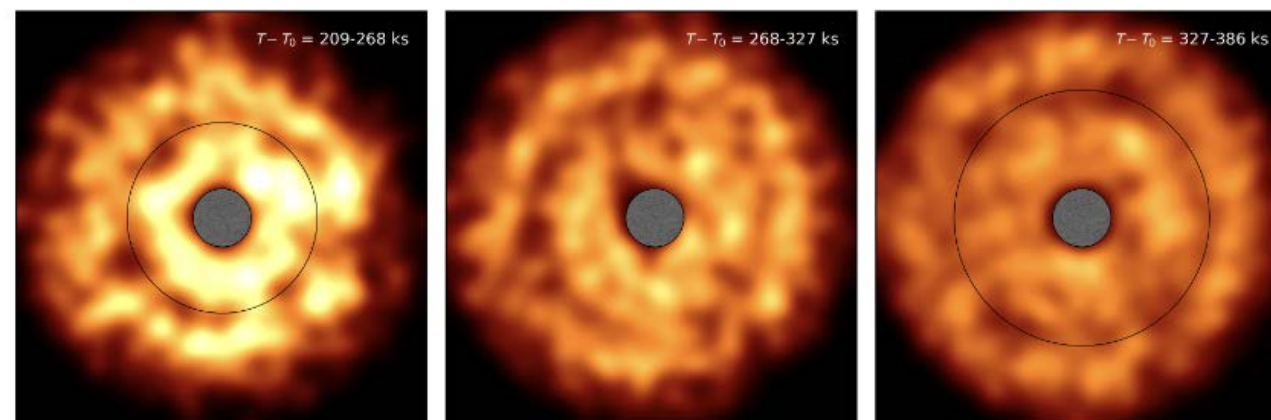


Swift/XRT image

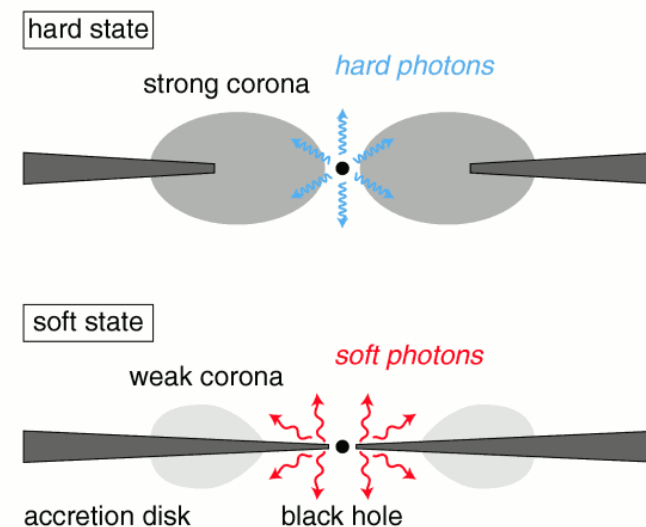
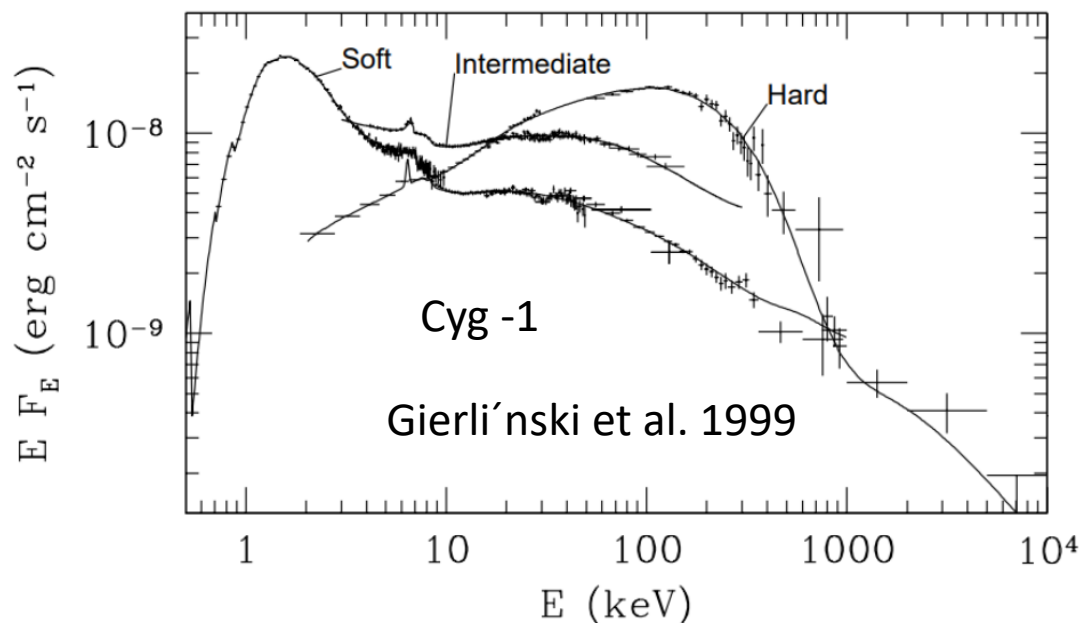
P < 13.8% (99% c.i.)

(Negro et al. 2023)

Dust rings also observed →
polarization of the prompt emission (<55%)

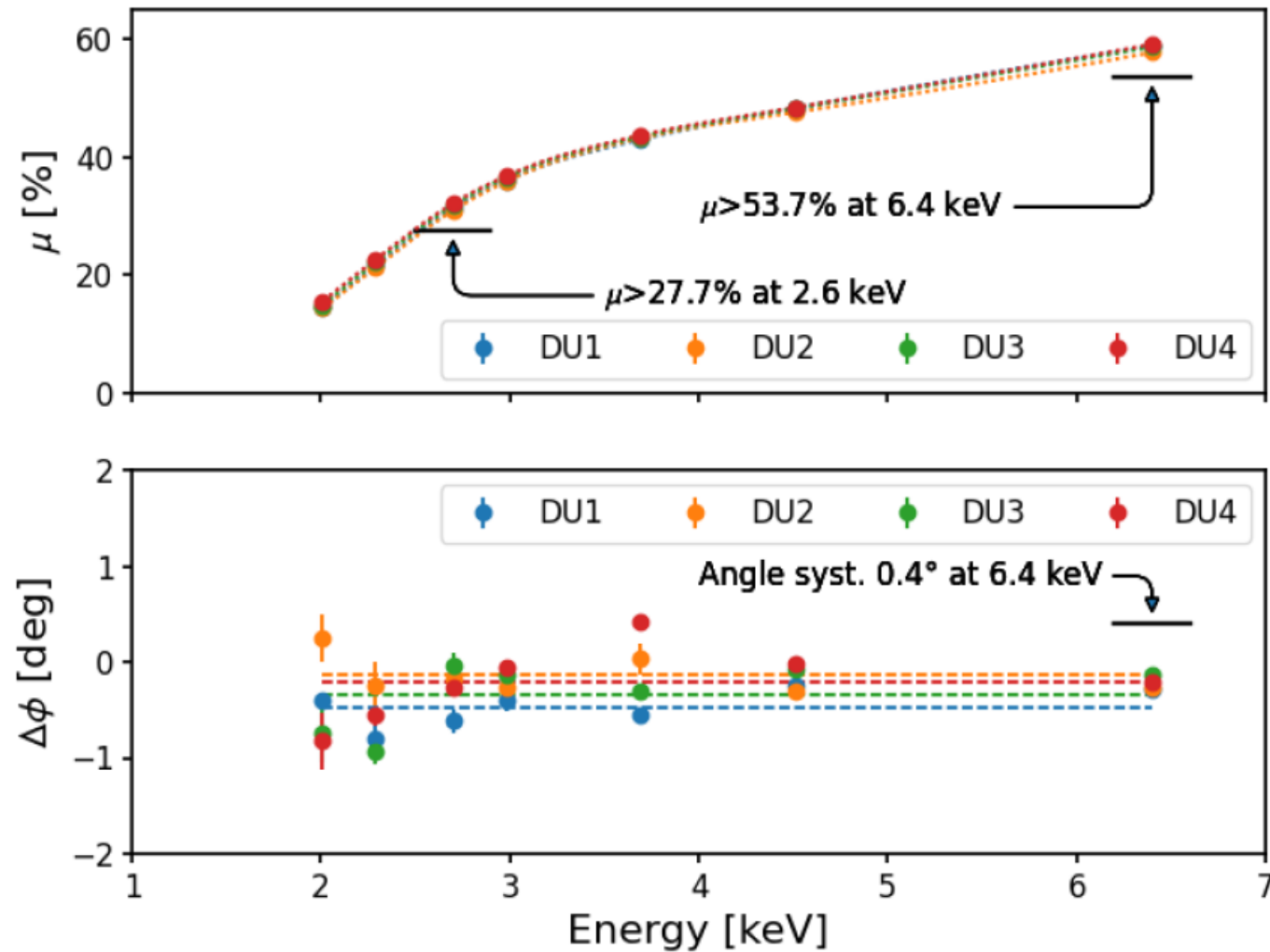


BH-BINARIES LOW-HARD/HIGH-SOFT STATE

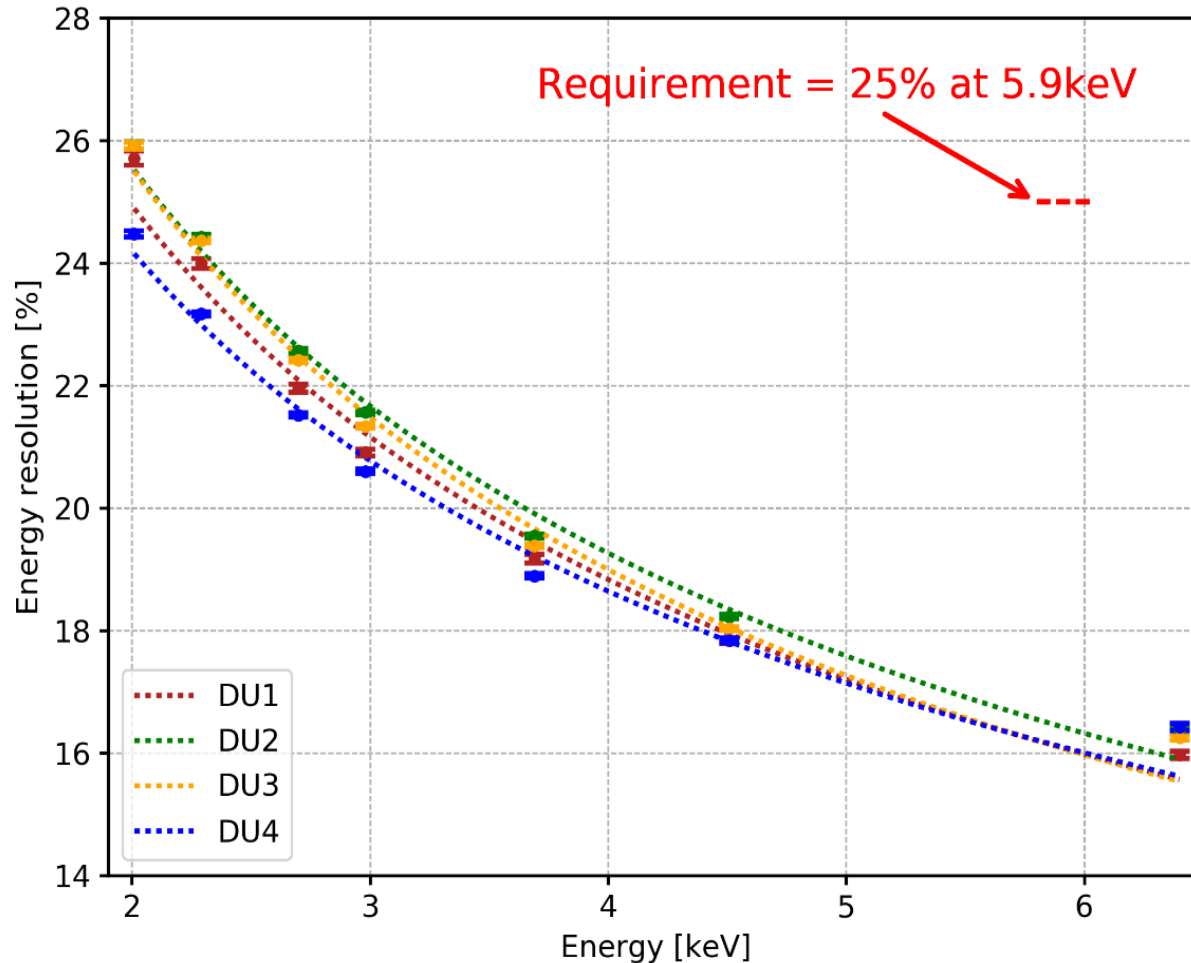


The two main states of a Black-Hole binaries are High-Soft where the X-ray emission is dominated by thermal emission of a disk surrounding the Black-Hole (multi-temperature black-body) possibly extending down to the Innermost Circular Orbit (ISCO) and Low Hard where the emission is due to Comptonized hard-X-ray photons in a hot Corona. The transition between states is an intermediate state. The transition to soft-state can be anticipated by a jet emission.

MODULATION FACTOR (FROM CALIBRATION)



ENERGY RESOLUTION

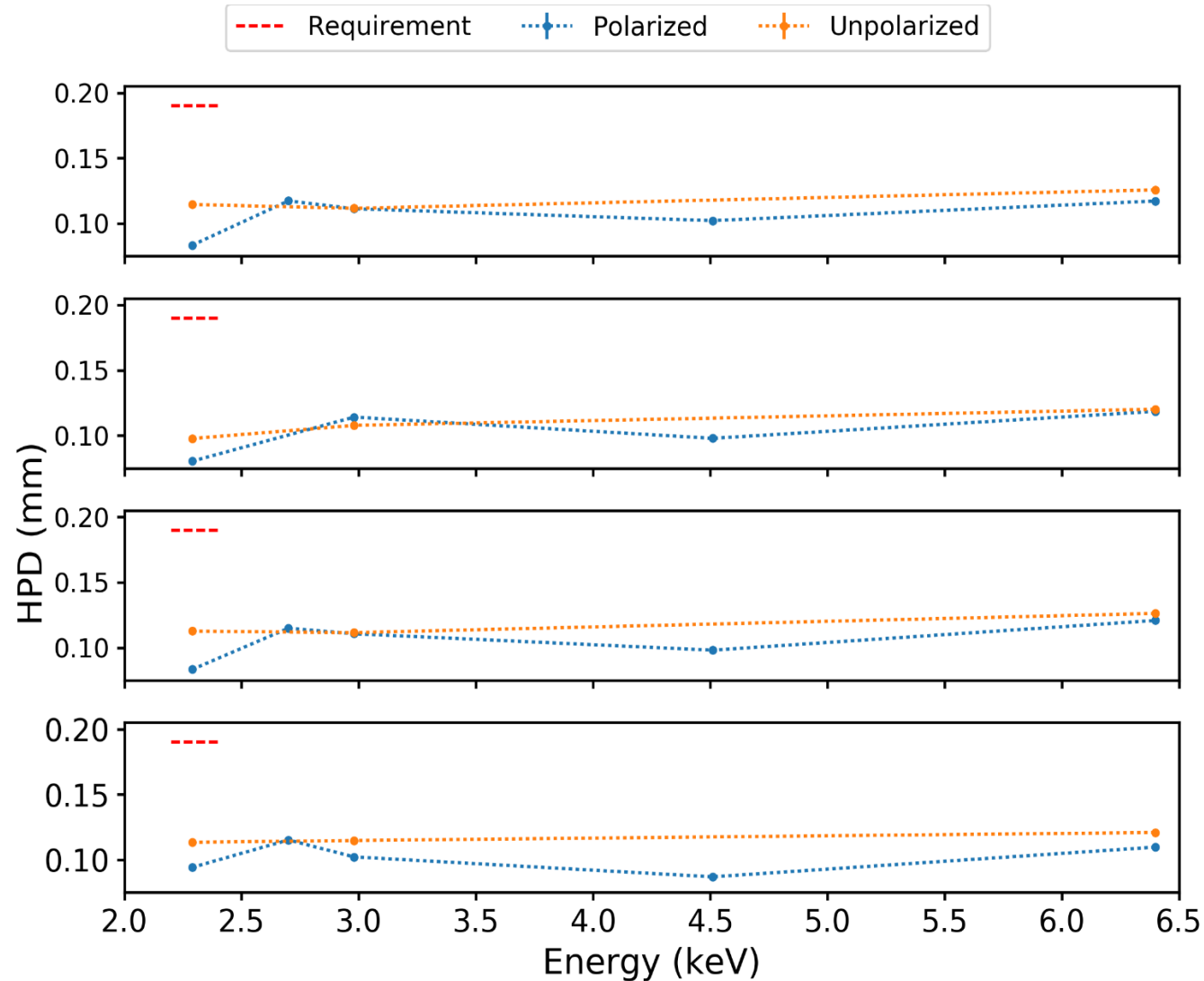


Energy calibration is much better of a typical proportional counter after gain equalization.

The gain equalization (Rankin J., et al. AJ 2023) is performed by comparing the average charge in one pixel with the one of the other pixel in the ROI.

Gain spatial maps are applied to the event energy reconstruction by the flight pipeline

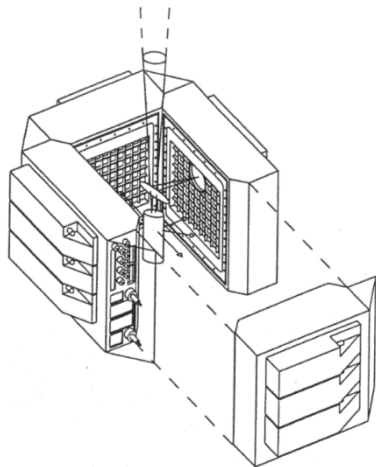
POSITION RESOLUTION OF THE DETECTOR (FROM CALIBRATION)



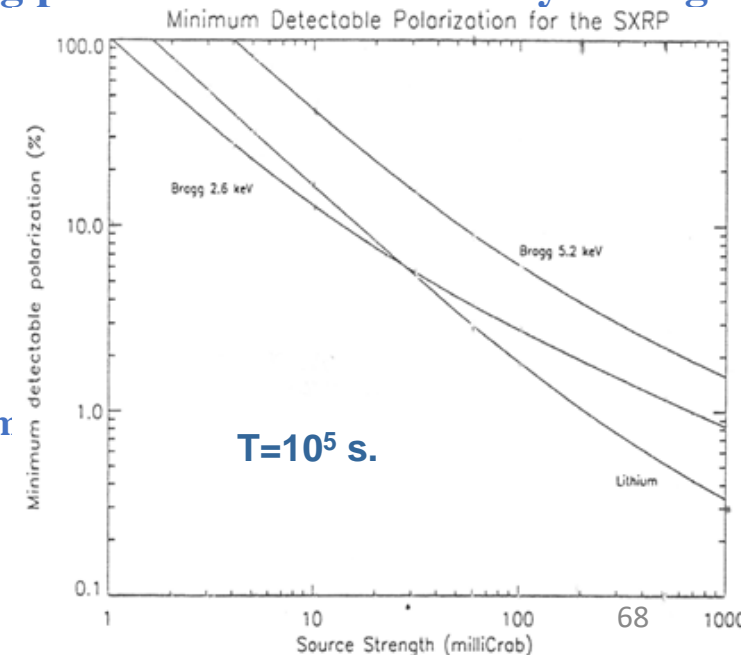
• A step forward in the sensitivity was done devising and building a polarimeter based on Bragg diffraction and Thomson scattering in the focus of a large X-ray telescope.

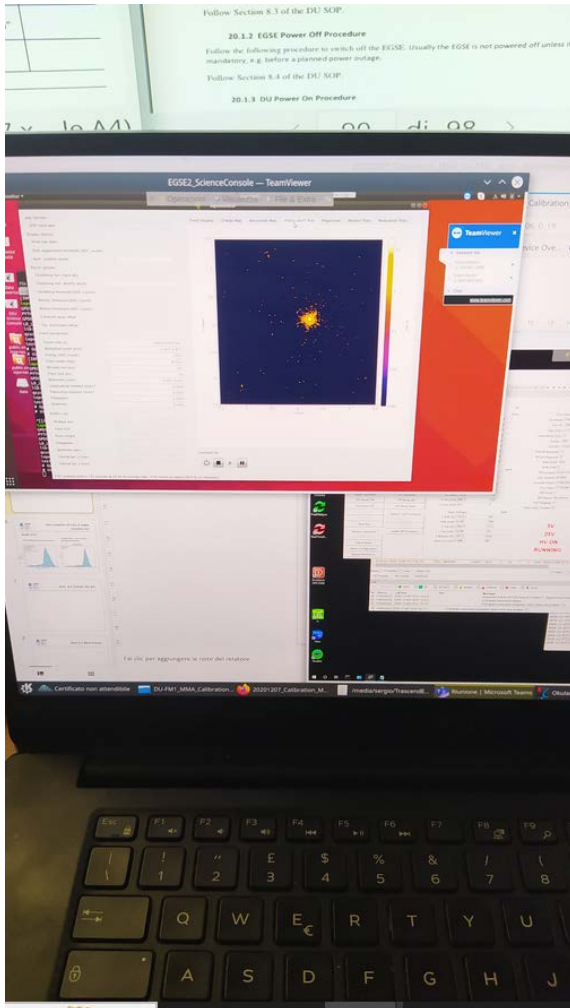
• Photons coming from the SODART telescope are diffracted by a thin mosaic graphite crystal at 2.6 keV and 5.2 keV creating a secondary focus. The photons at $E > 5$ keV that do not satisfy the Bragg condition pass through and are diffused around by a lithium scatterer. 4 position sensitive proportional counters detect simultaneously the radiation. SXRP is in rotation around the telescope axis.

• Bragg diffraction saves the images and is more sensitive at low flux, Thomson scattering provides better sensitivity at large fluxes but the image is lost.



- 4 x 100 cm² imaging proportional counter
- Composite window thickness :
 - 150 μm for Thomson scattered photons
 - 50 μm for Bragg diffracted photons, $\phi = 3.3$ cm)
- Graphite mosaic cristal (50 μm thick)
- Lithium scatterer 7 cm long and $\phi = 3$ cm encapsulated in 150 μm thick beryllium case
- Rotary motor for the ensemble detector/analyser at 1 rpm





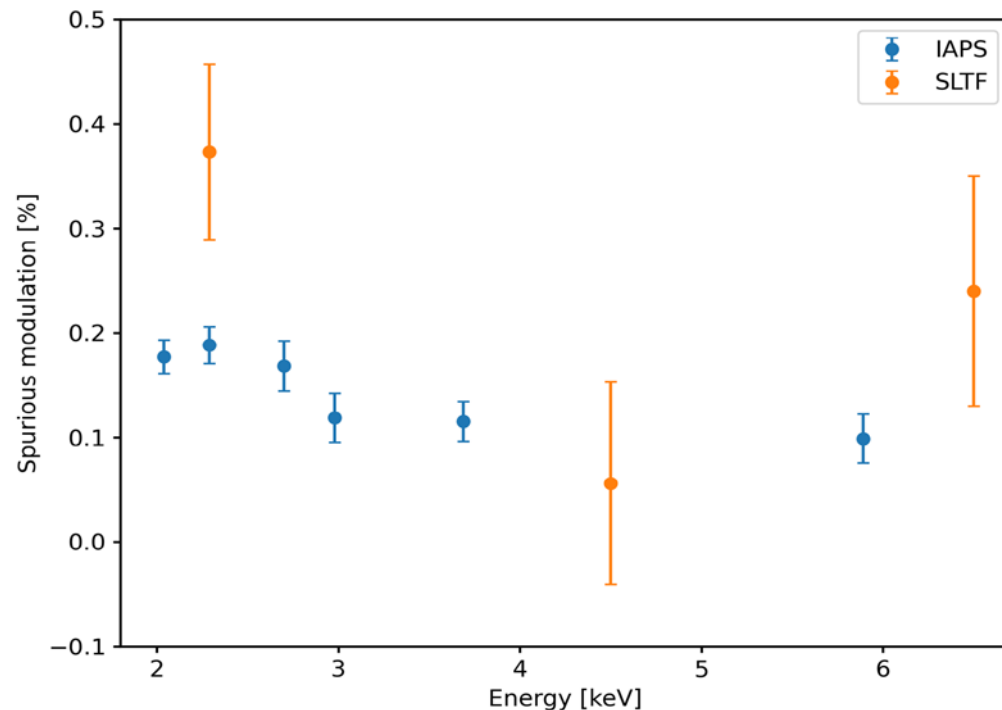
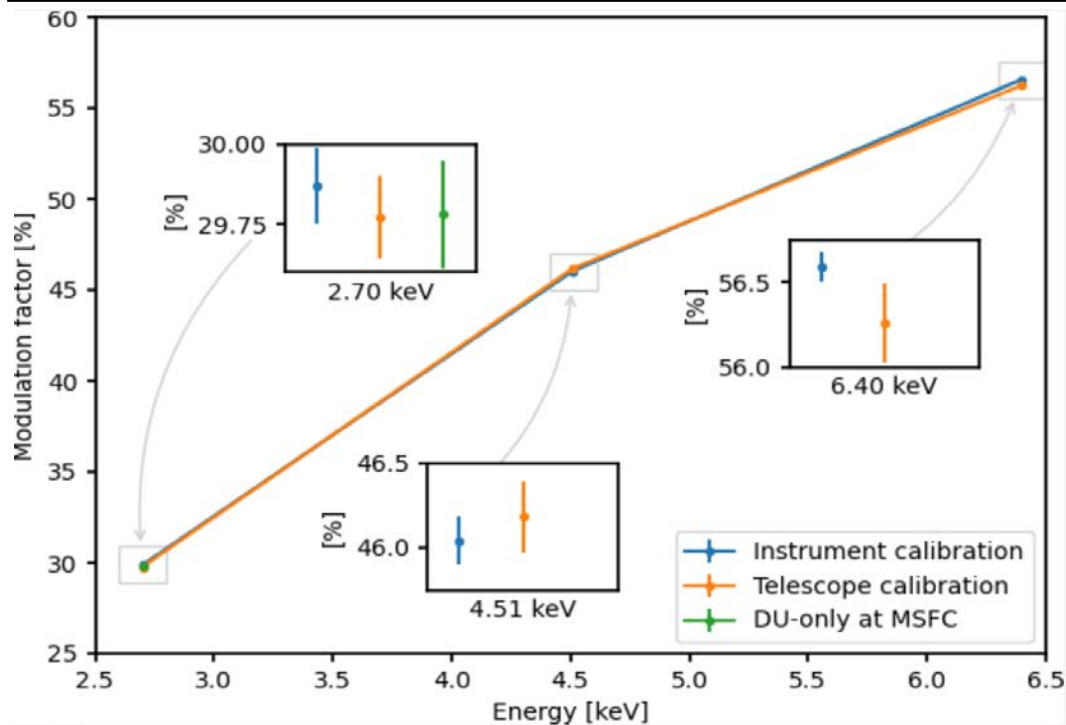
Telescope calibration were performed with a Mirror unit spare and a Detector Unit Spare to validate the separate calibration

A link for active monitoring the command was set-up for remote check and commanding.

INAF-IAPS team worked following the working hours of NASA-MSFC so up to very late at night.

Calibrations lasted about two weeks (working days).

The Stray Light facility at MSFC was adapted for the telescope calibration following the experience of the two calibration equipment built at INAF-IAPS for Calibration of prototypes and Calibration of 4 flight detector Units.



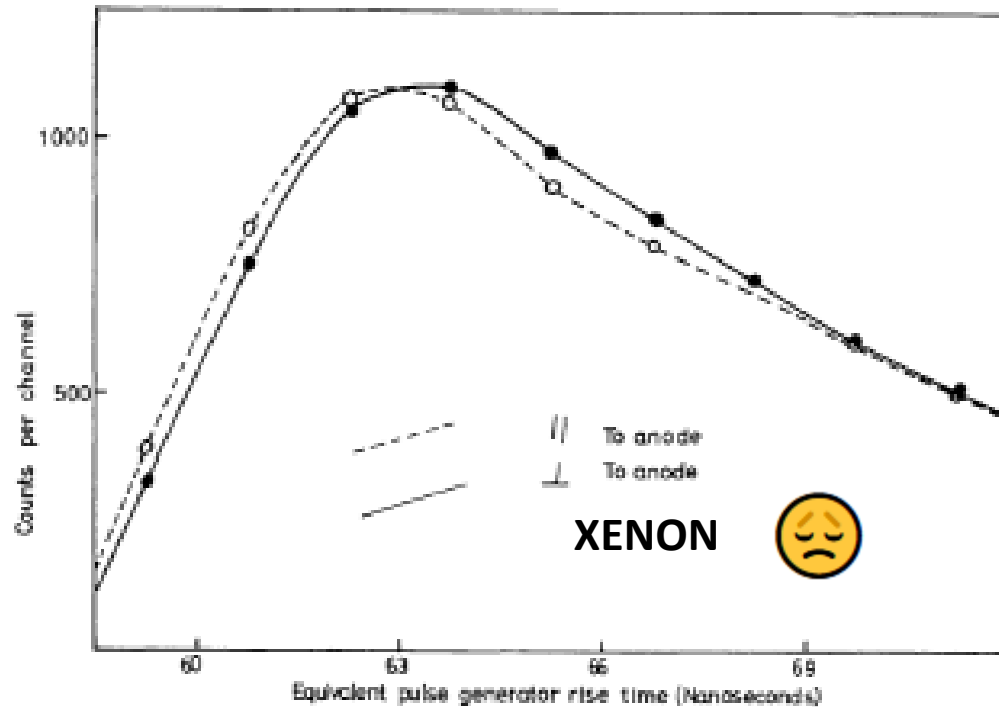
Adapted by Fabiani, S. presentation at ASI

As expected by first principles the presence of the optics does not alter the polarization: modulation factor @MSFC were the same as @ IAPS. The same for the spurious modulation

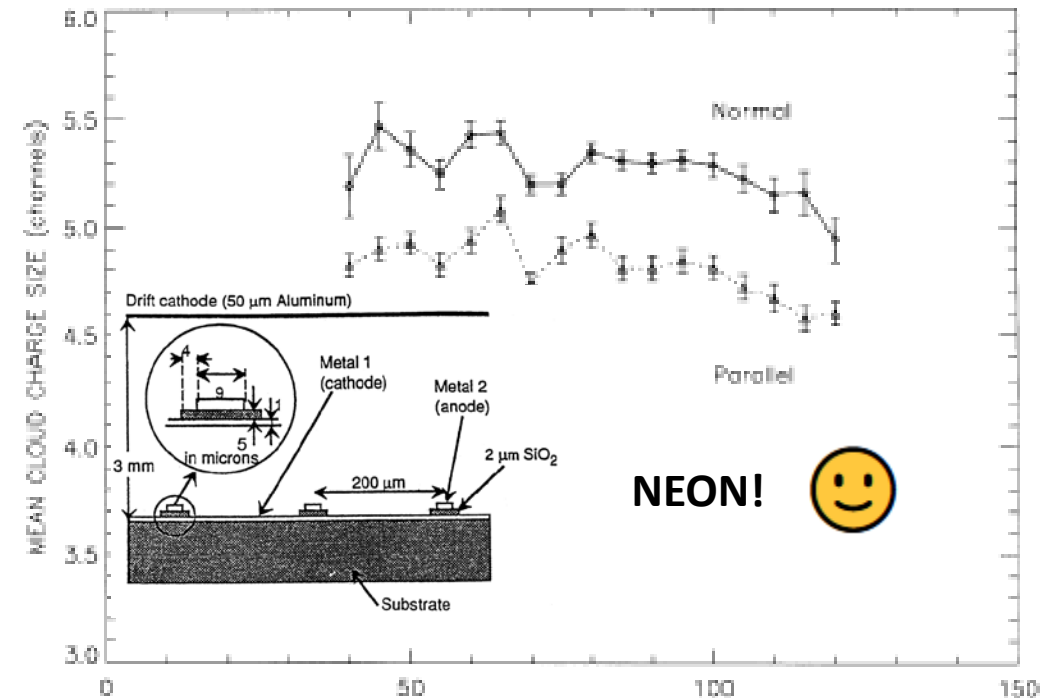
1-D PHOTOELECTRIC POLARIMETER

- CCD (Tsunemi et al., 1992, Holland 1995, Kotthaus, 1998) Edge effect polarimeter (Range is .short in Silicon)
- Gas Imager (Austin et al. 1990, La Monaca et al., 1998, Sakurai 2004) High energy/Cumberson device

Sanford , Cruise & Culhane 1970



Soffitta P. et al., 1995, 2001



We soon pointed into a low-Z gas mixture (neon) and to a highly segmented gas detector having as a goal an imaging focal plane experiment.

By the way IXPE won the 2024 Bruno Rossi Prize of HEAD:



High Energy Astrophysics Division

The 2024 Prize Winner: Martin Weisskopf, Paolo Soffitta, and the IXPE team

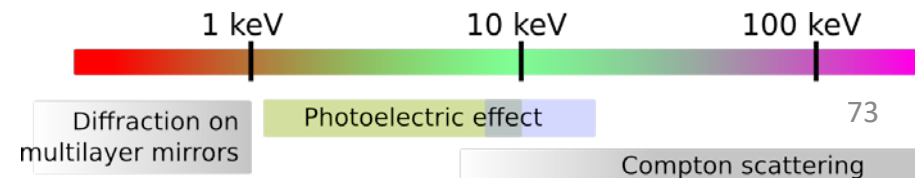
The 2024 Bruno Rossi Prize has been awarded to Dr. Martin Weisskopf, Dr. Paolo Soffitta, and the IXPE team for their development of the Imaging X-ray Polarimetry Explorer whose novel measurements advance our understanding of particle acceleration and emission from astrophysical shocks, black holes and neutron stars. Please see the [press release](#) for more information.

Winter Meetings

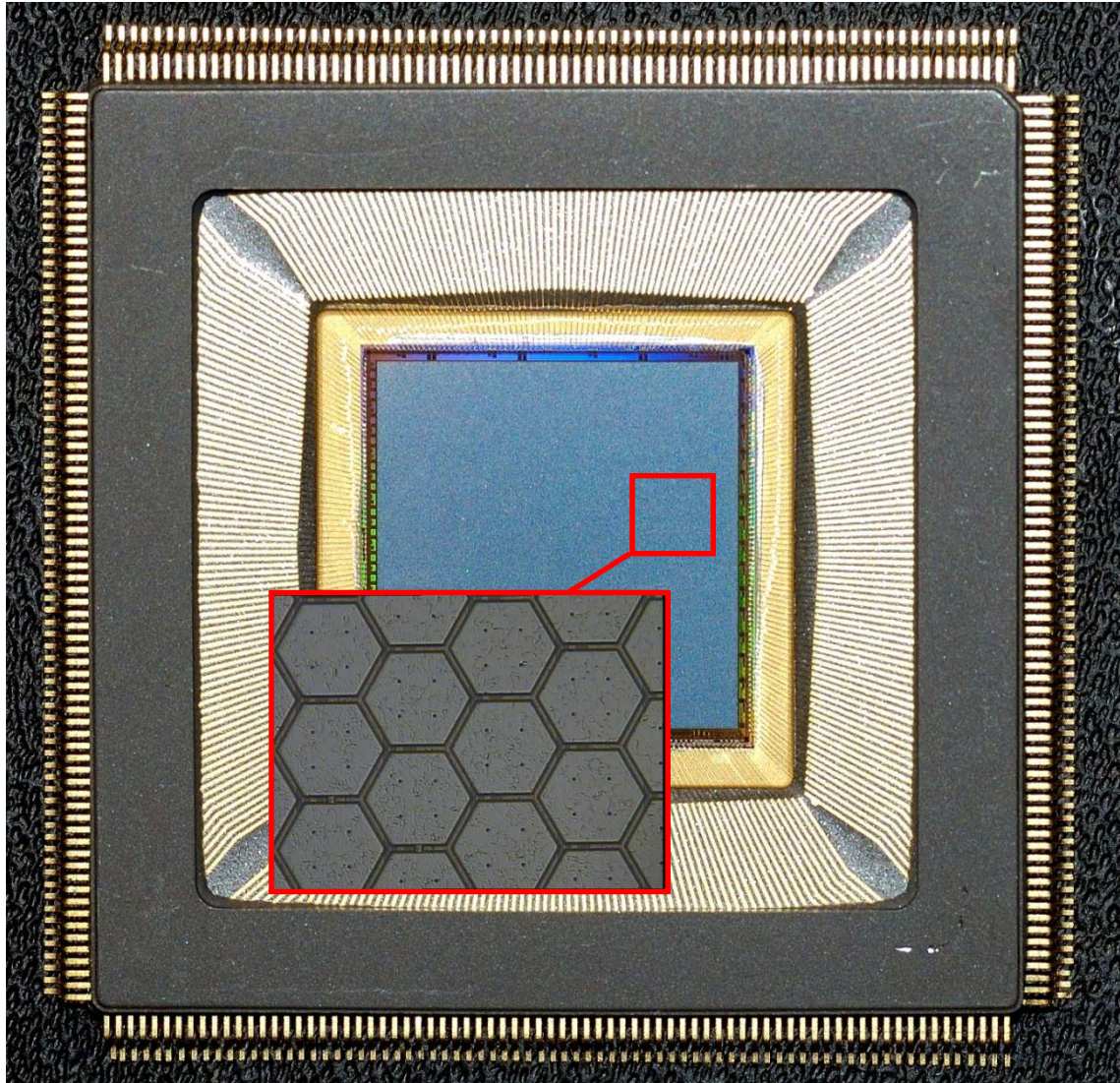
- 245th AAS Meeting: 12–16 January 2025, Gaylord National Resort & Convention Center, National Harbor, MD

WHY POLARIMETRY IN THE CLASSICAL X-RAY ENERGY BAND

Scientific goal	Sources	< 1keV	1-10	> 10keV
Acceleration phenomena	PWN	yes (but absorption)	yes	yes
	SNR	no	yes	yes
	Jet (Microquasars)	yes (but absorption)	yes	yes
	Jet (Blazars)	yes	yes	yes
Emission in strong magnetic fields	WD	yes (but absorption)	yes	difficult
	AMS	no	yes	yes
	X-ray pulsator	difficult	yes (no cyclotron?)	yes
	Magnetar	yes (better)	yes	no
Scattering in aspherical geometries	Corona in XRB & AGNs	difficult	yes	yes (difficult)
	X-ray reflection nebulae	no	yes (long exposure)	yes
Fundamental Physics	QED (magnetar)	yes (better)	yes	no
	GR (BH)	no	yes	no
	QG (Blazars)	difficult	yes	yes
	Axions (Blazars, Clusters)	yes ?	yes	difficult



ASIC FEATURES 105600 PIXELS 50 MM PITCH



- Peaking time: 3-10 μs , externally adjustable;
- Full-scale linear range: 30000 electrons;
- Pixel noise: 50 electrons ENC;
- Read-out mode: asynchronous or synchronous;
- Trigger mode: internal, external or self-trigger;
- Read-out clock: up to 10MHz;
- Self-trigger threshold: 2200 electrons (10% FS);
- Frame rate: up to 10 kHz in self-trigger mode (event window);
- Parallel analog output buffers: 1, 8 or 16;
- Access to pixel content: direct (single pixel) or serial (8-16 clusters, full matrix, region of interest);
- Fill fraction (ratio of metal area to active area): 92%

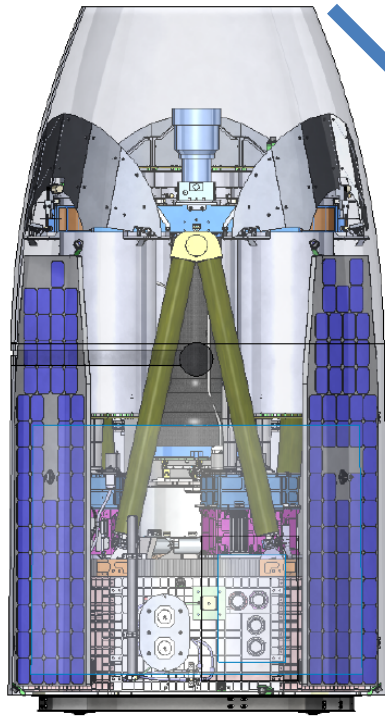
The chip is self-triggered and low noise. The top layer is the collection plane. The bottom 4 layers are a complete analogue chain for each pixel with **preamplifier/shaper/sample and hold** and serial readout.

It **defines the sub-frame that surrounds the track**. The dead time, downloading an average of 1000 pixels is 100 time lower, than for $1\text{E}5$ pixels.



IXPE
Imaging
X-Ray
Polarimetry
Explorer

FALCON 9 LAUNCHER VS PEGASUS XL LAUNCHER



IXPE in the Pegasus XL fairing.

Required in proposal and phase A and phase B

Stowed Views

Pegasus XL
Fairing
Envelope

Falcon 9
Fairing
Envelope

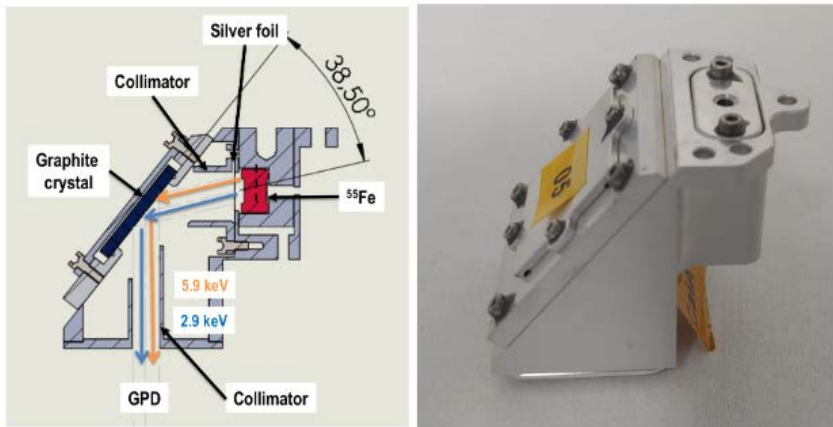
IXPE
Observatory

Separation
Plane

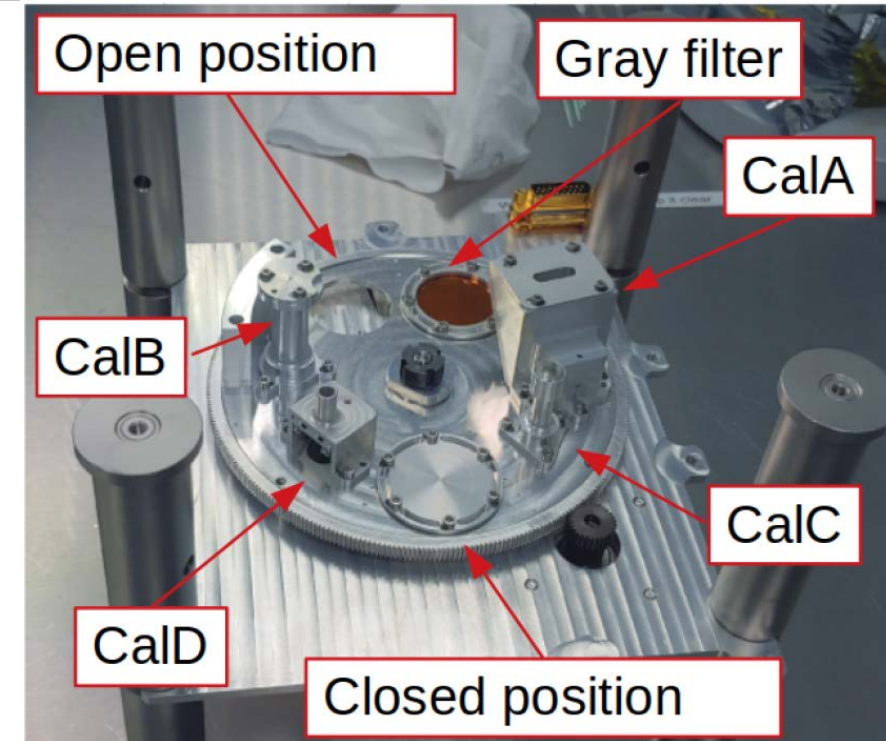
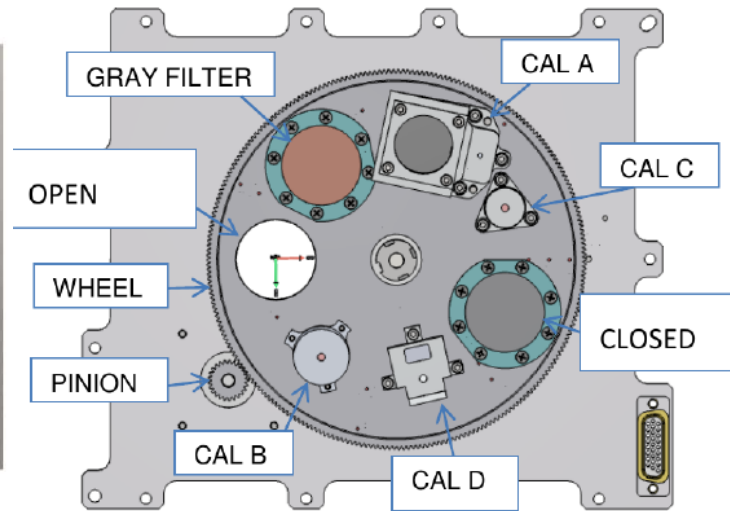


On July 8, 2019, NASA announced that Space-X of Hawthorne, California will provide launch services for IXPE.

FILTER Calibration Wheel Assembly (In-flight calibration)



Flight Polarized X-ray sources



Ferrazzoli et al., 2020

⁵⁵Fe-powered calibration sources:

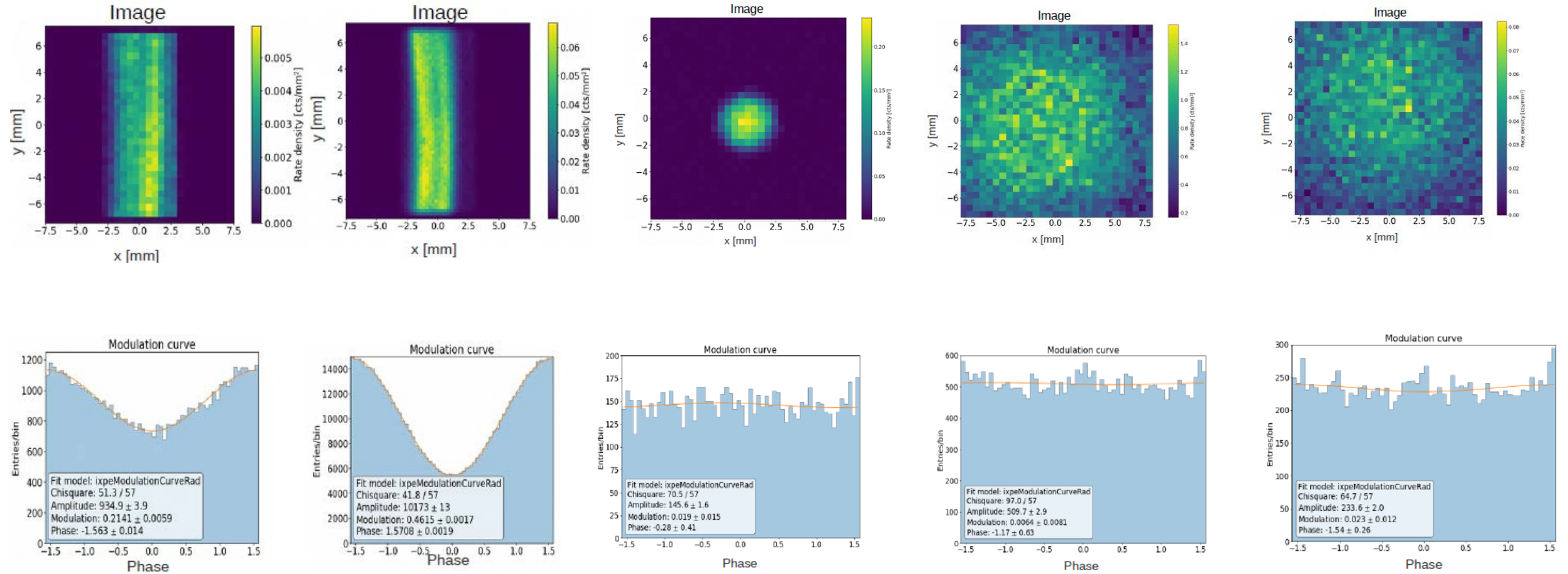
Cal A – Bragg-reflected polarized 2.98-keV (Ag-L α fluorescence) and 5.89-keV (Mn-K α)

Cal B – unpolarized 5.89-keV spot

Cal C – unpolarized 5.89-keV flood

Cal D – unpolarized 1.74-keV (Si-K α fluorescence) flood

IMAGES AND MODULATION FACTORS OF THE CALIBRATION SOURCES



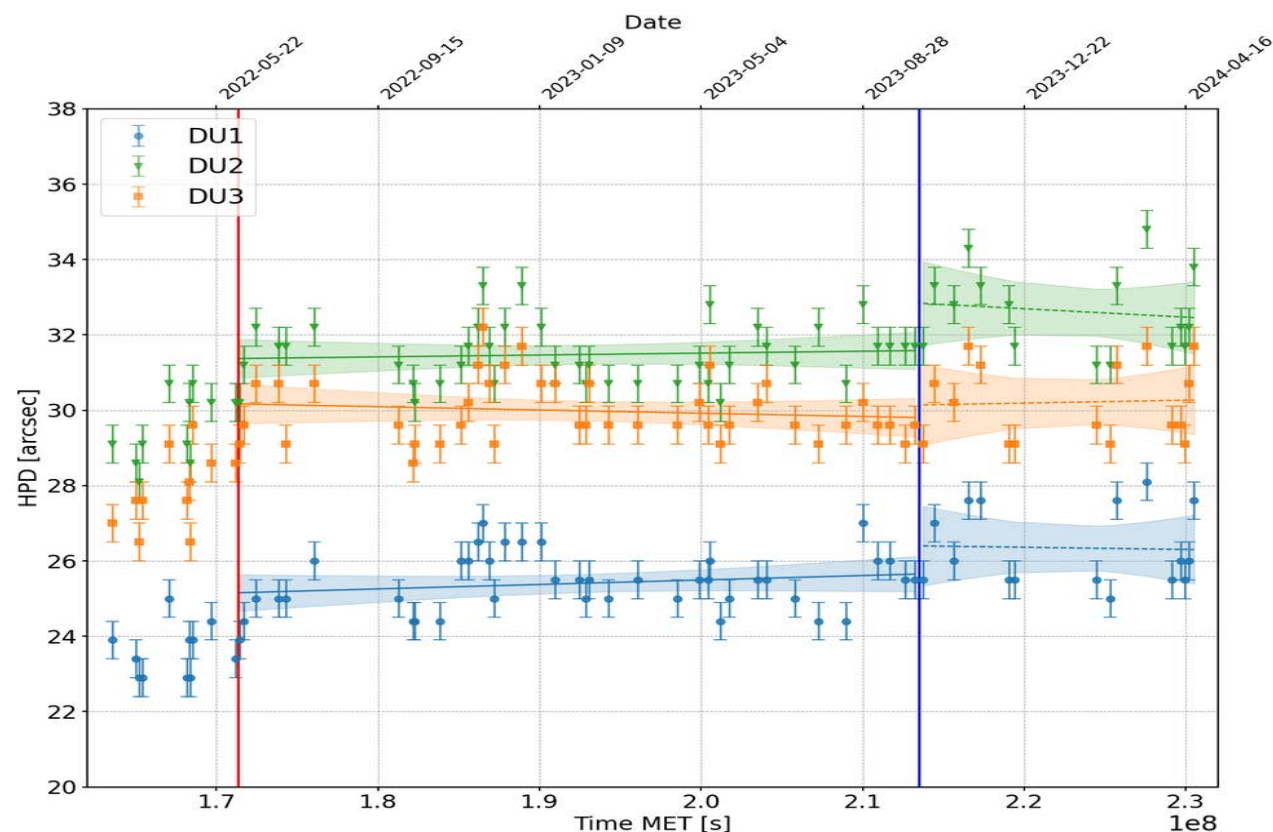
3.0 keV Cal A Pols

5.9 keV Cal A Pol

5.9 keV Cal B

5.9 keV Cal C

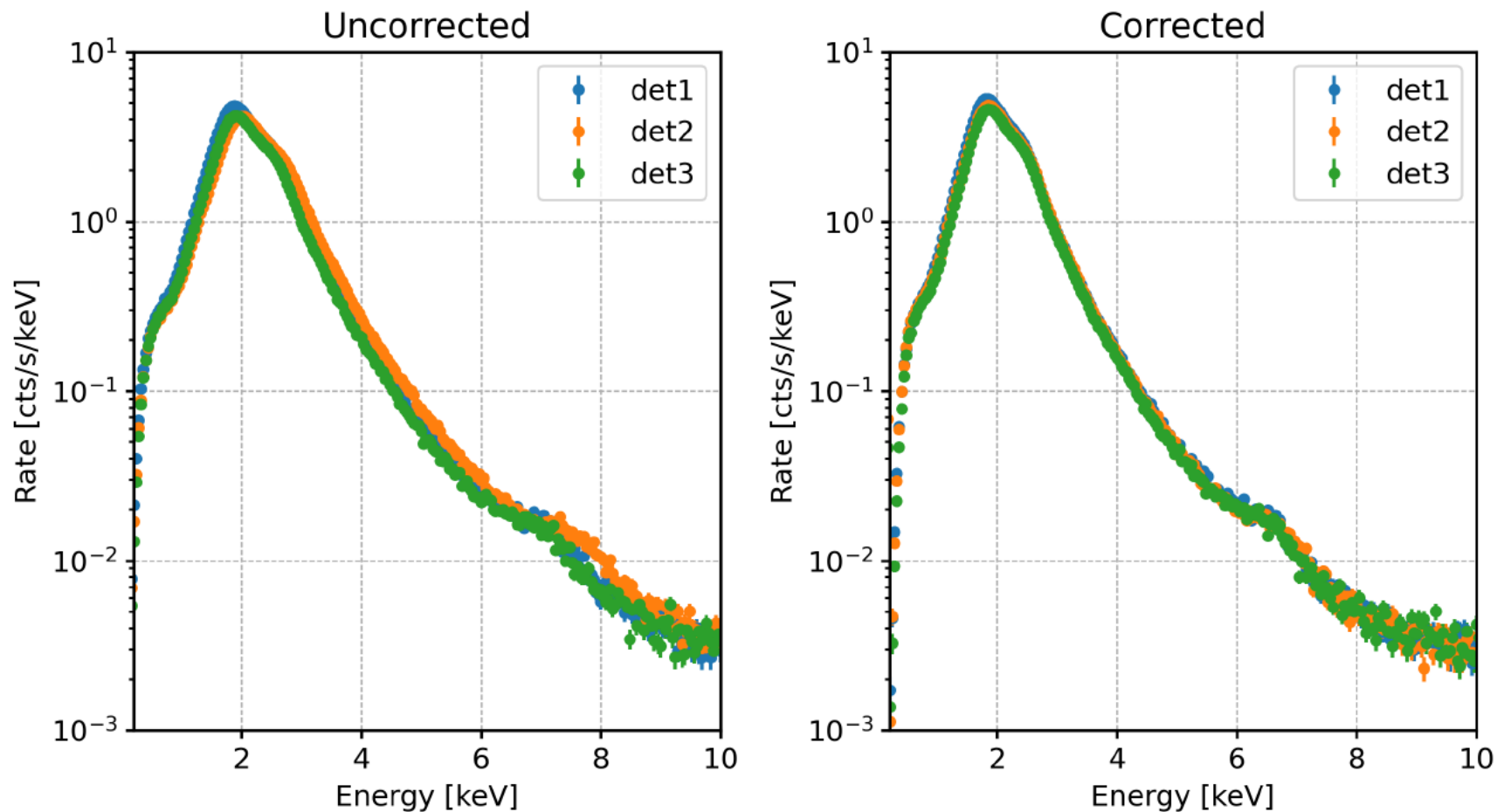
1.7 keV Cal D



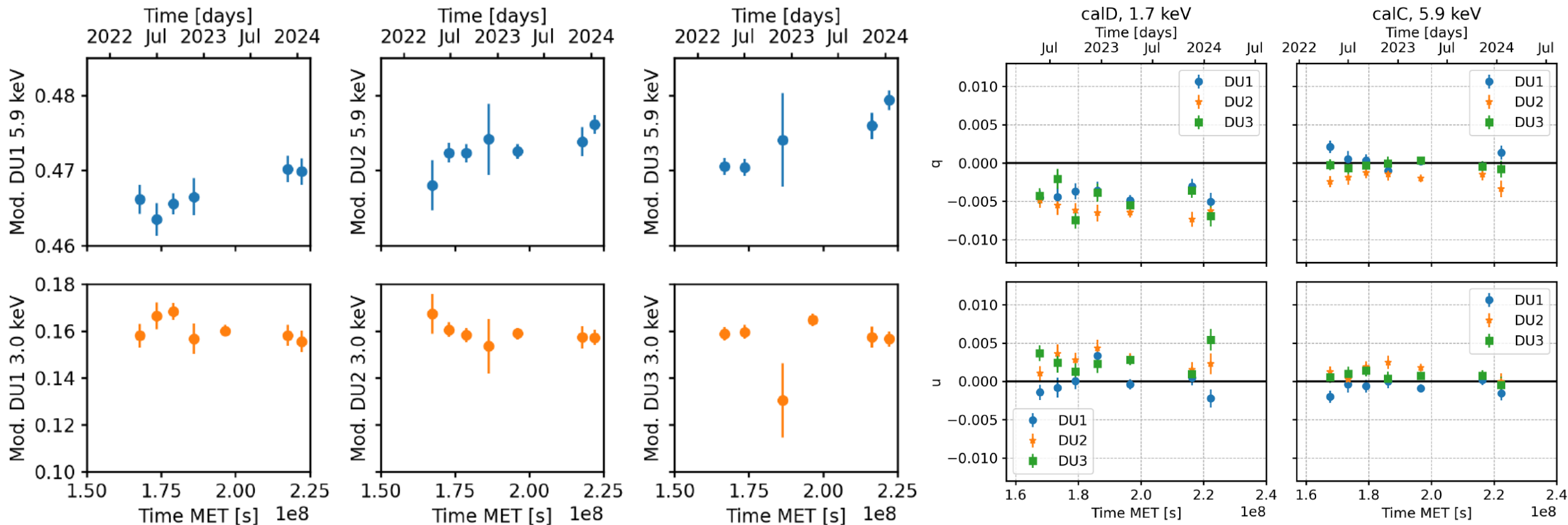
John Rankin et al., 2024 in preparation

The in-flight performance of the detector + mirror systems are in line with the expectation. The HEW is indeed dominated first by the quality of the optics, then by the inclined penetration effects finally much less by the position resolution of the detector.

WE FIRSTLY APPLIED THE CALIBRATION TO CAS-A SPECTRUM



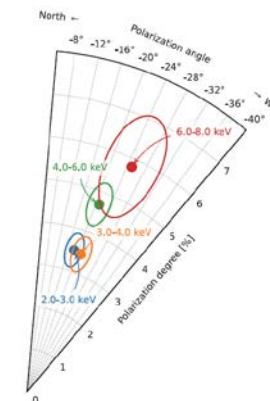
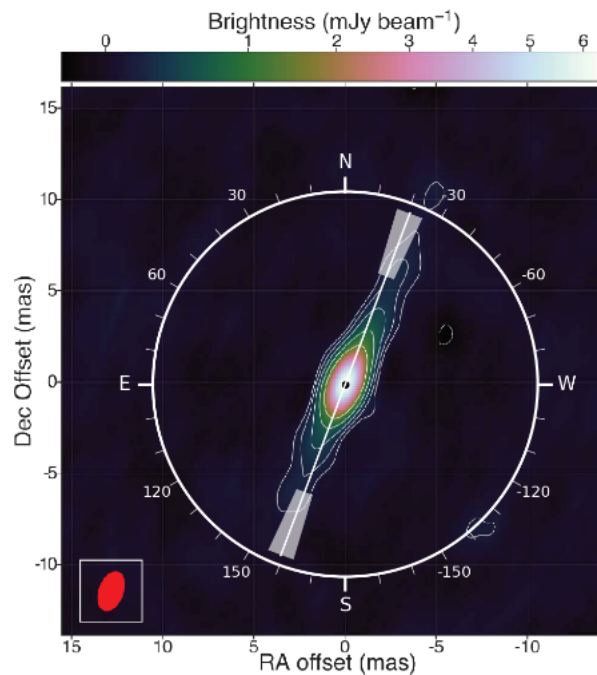
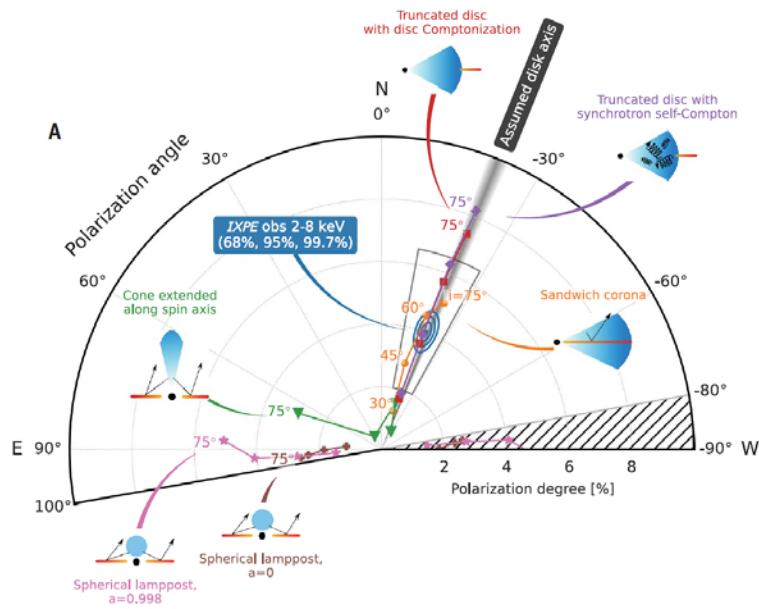
MODULATION FACTOR AND SPURIOUS MODULATION CHECK



Modulation factor as expected slightly rises (0.25-0.5%/yr)
 Spurious modulation (before the event-by-event-correction) stay constant&small

HIGH MASS BH XRB: CYG X-1 OBSERVED HARD AND SOFT STATE

Krawczynski, H. et al, Science 2022



68 % CL

Low hard state.
 $PD = (4.01 \pm 0.20) \%$
 $PA = (-20.7 \pm 1.4)^\circ$
 $i = 28^\circ$

- The polarization angle is parallel to the jet axis implying: (1a) the corona is sandwiched to the disk or (1b) an external cold truncated standard disk + an internal region corona optically thin geometrically thick. (2) the jet is launched perpendicularly to the inner flow.
- The polarization degree is larger than expected for the inclination angle implying that the disk may be warped.
- Results are consistent with low significance OSO-8 measurement.

Cyg X-1 was observed in soft state: $P = 1.99\% \pm 0.13\%$ and polarization angle still parallel to the radio jet.

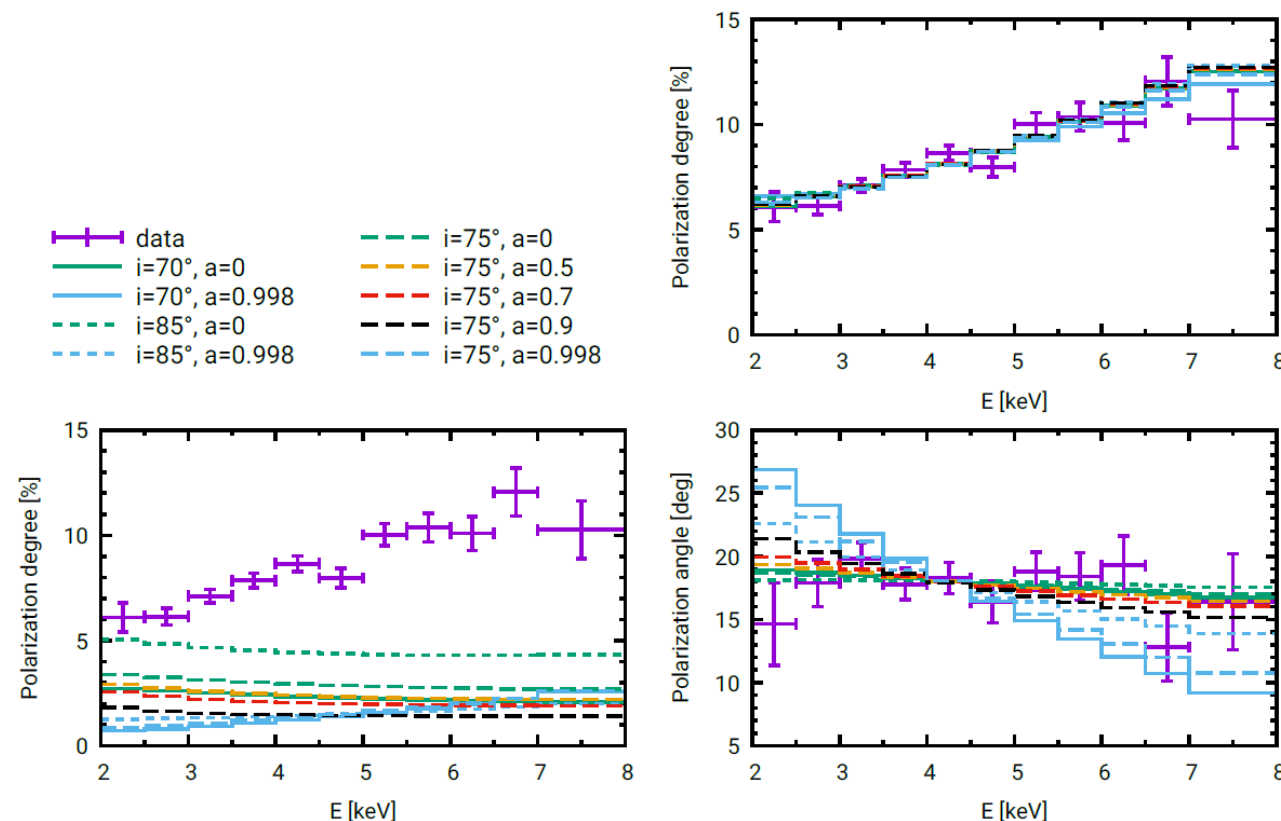
(Dovčiak, 2023, Steiner et al., 2024).

4U 1630 was observed in High Soft State during an Ouburst by a ToO.

- Orbital inclination may be 65° (absence of eclipse but dips)
- 2-8 keV energy band dominated by the disk (Corona < 2 %)
- Strong absorption line -> disk-wind
- Unresolved radio image

- The standard disk model Novikov –Thorne (geometrically thin + Chandrasekhar atmosphere) does not explain the data.
- Data are explained by a model consisting of a thin disk with an outflowing, partially-ionized atmosphere for low and intermediate spins.

Ratheesh, A., et al., ApJ, 2024

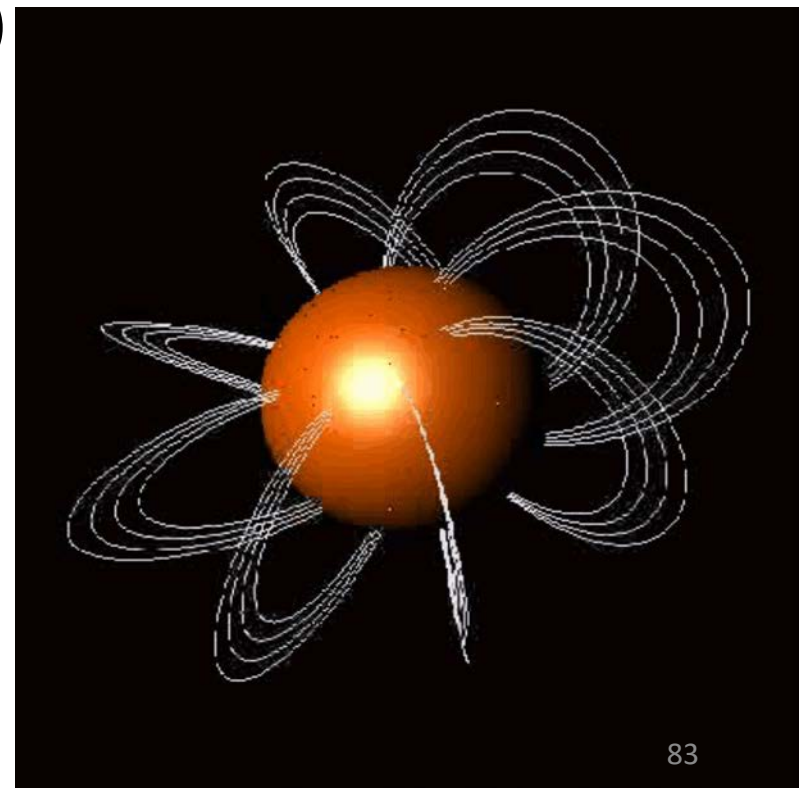


■ Anomalous X-ray Pulsars and Soft-gamma ray repeaters

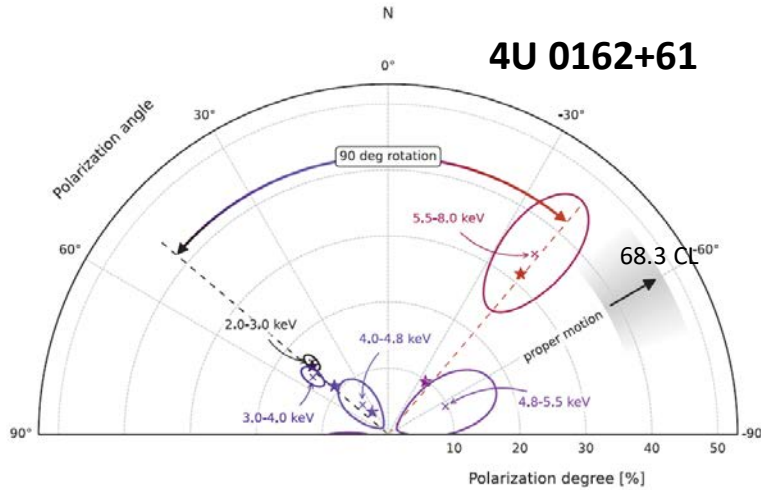
- $P \approx 2 - 12 \text{ s}$ $\dot{P} \approx 10^{-14} - 10^{-10} \text{ s s}^{-1}$
- $B_{sd} \approx 10^{14} - 10^{15} \text{ G}$
- $L_{X,persist} \approx 10^{35} - 10^{36} \text{ erg s}^{-1}$ (typically $> \dot{E}_{rot} = 10^{33} - 10^{34}$)
- Bursting activity (short bursts – intermediate/giant flares)
- Enhanced activity in transient sources (outbursts)
- Two components (thermal and PL) spectra

- **Powered by their own magnetic energy**

A twisted magnetic field is coupled to flowing charged particles which upscatters (power law) the radiation emitted from the neutron star surface (Thermal)

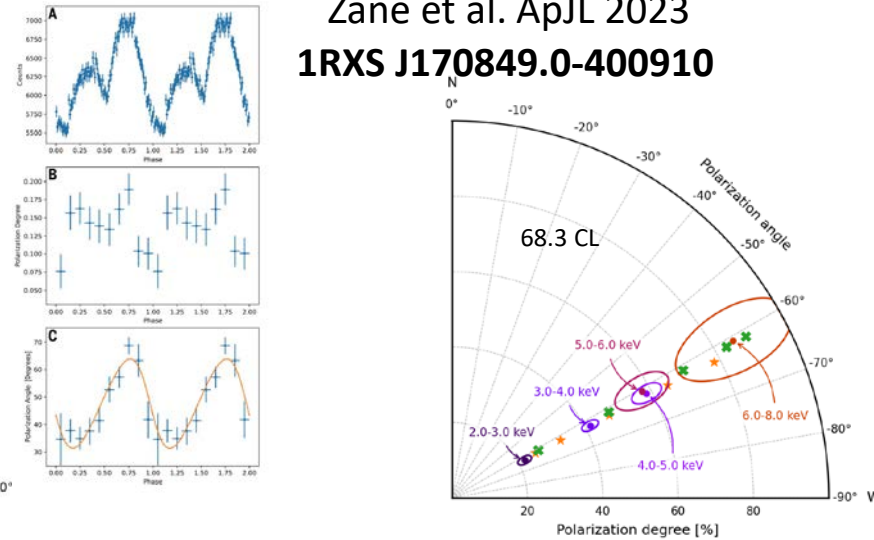


Taverna et al., Science 2022



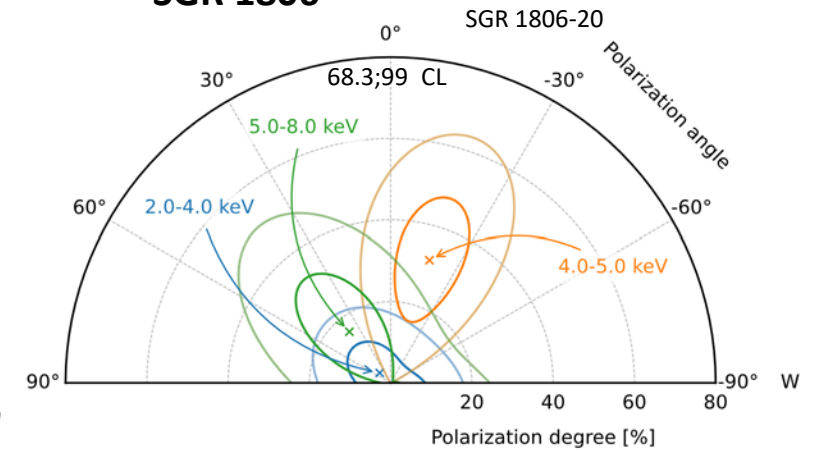
Equatorial belt condensed surface (low energy-O mode). Resonant Compton Scattering at high energy (X-model)

Zane et al. ApJL 2023
1RXS J170849.0-400910



Condensed surface region (low-P) plus hot regions with on-top an atmosphere (high P)

Turolla et al., ApJ 2023
SGR 1806

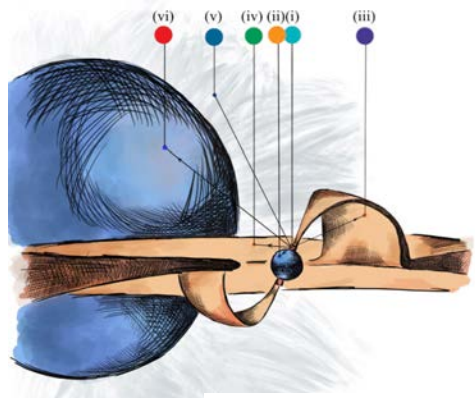


Only upper limits. Hint of behavior similar to 4U 0162+61

The magnetars observed by IXPE have very different polarization dependence with energy may be due to the fact that the atmosphere have different pattern for each one. 1E 2259+586 was also observed (Heyl et al., 2024) showing a polarization of about 20 % and an even different pattern of emission region by using the rotating vector model.

The long searched vacuum polarization and birefringence is not definitively proved because the emitting area is rather small. To eventually prove this QED effect we need small pulsed fraction and high polarization degree detected.

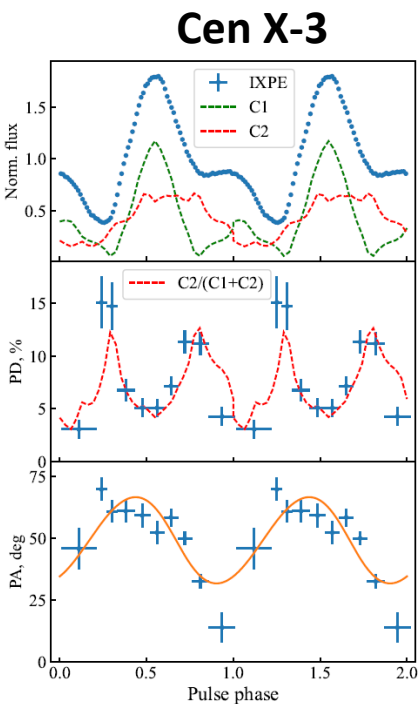
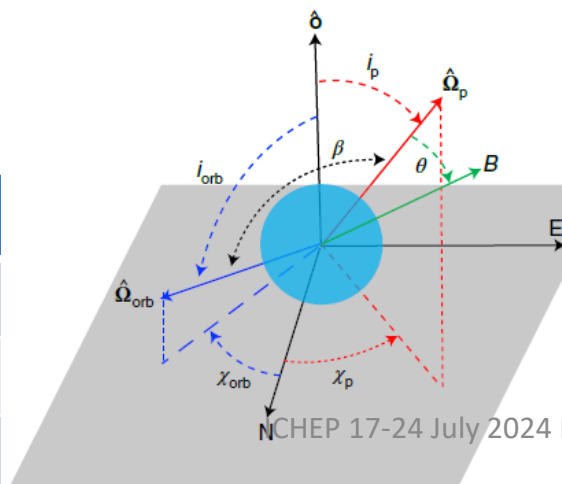
CEN X-3 AND HER X-1 DISENTANGLING THE GEOMETRY



- Intrinsic polarization from the hotspot
- Reflection from the NS surface
- Reflection from the accretion curtain
- Reflection from the accretion disk
- Scattering by the stellar wind
- Reflection from the optical companion

$$\tan(\text{PA} - \chi_p) = \frac{-\sin \theta \sin(\phi - \phi_0)}{\sin i_p \cos \theta - \cos i_p \sin \theta \cos(\phi - \phi_0)}$$

Rotating Vector model applies to the X-ray binary pulsar

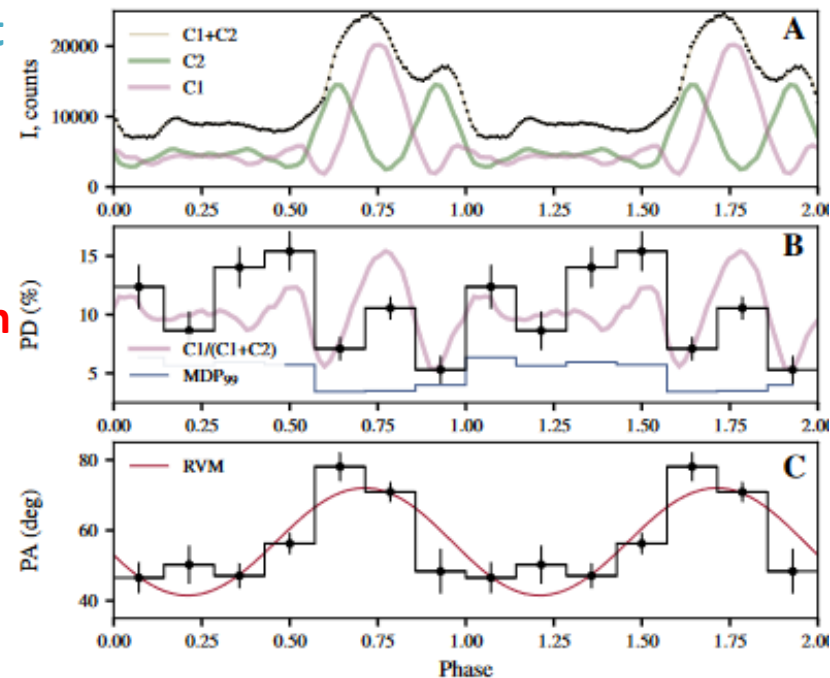


Tsygankov et al 2022

Rotating Vector Model

Magnetic obliquity	$\Theta = 16.4(\pm 1.3)^\circ$
Inclination	$i_p = 70^\circ.2$
Position angle	$\chi_p = (49.2 \pm 1.1)^\circ$

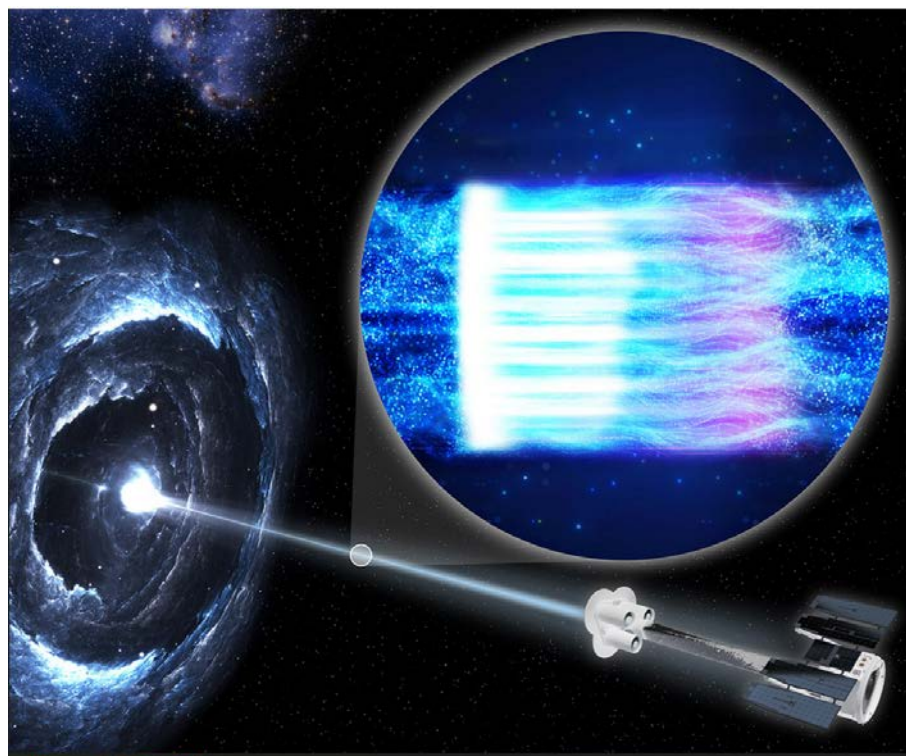
Her X-1



Doroshenko et al., 2022

Table 1 | Orbital and pulsar geometrical parameters of Her X-1

$\chi_{p,*}$	θ	i_p	$\chi_{orb,*}$	i_{orb}
deg	deg	deg	deg	deg
56.9 ± 1.6	12.1 ± 3.7	Eq. (2)	28.9 ± 5.9	100.4 ± 4.9



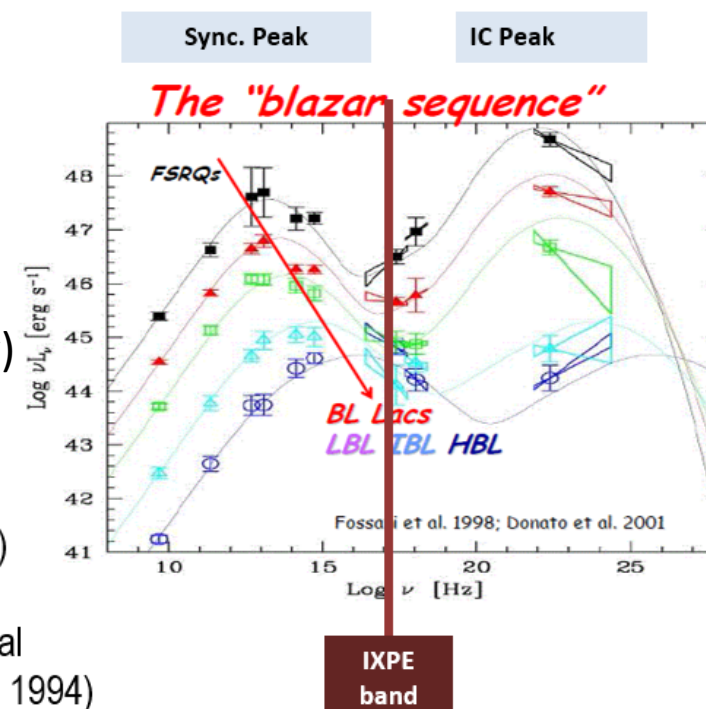
Synchrotron-dominated (with X-ray)

Blazars, multi- λ polarimetry probes **the structure** of the jet and of its **magnetic field**

Inverse Compton dominated (with X-ray)

Blazars, multi- λ polarimetry observations can determine:

- **the composition of the jet** (hadronic vs. leptonic, Zhang & Botcher, 2013)
- **the origin of the seed photons** Synchrotron-Self Compton (SSC) or External Compton (EC) (Celotti & Matt, 1994; Poutanen 1994)



A blazar is an active galactic nucleus (AGN) with a relativistic jet directed closely towards the observer. Relativistic beaming from the jet makes blazars appear much brighter than they would be if the jet were pointed in a direction away from Earth.

Liodakis et al., Nature 2022

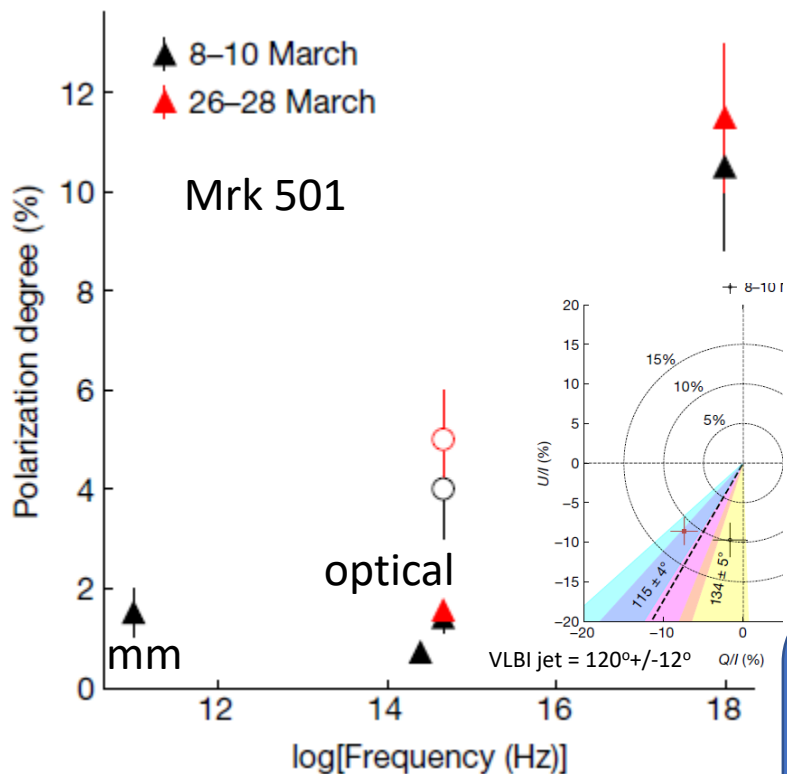


Table 1 | Summary of model properties

Model	Multiwavelength polarization	X-ray polarization variability ^a	X-ray polarization angle
Single zone	Constant ^b	Slow	Any
Multizone	Mildly chromatic	High	Any
Energy stratified (shock)	Strongly chromatic	Slow	Along the jet axis
Magnetic reconnection (kink instability)	Constant	Moderate	Perpendicular to the jet axis
Observed	Strongly chromatic	Slow	Along the jet axis

First, we find an increasing Π towards higher frequencies. Second, we do not find significant variability during the 2–3-day-long IXPE observations, and finally, we find a rough alignment of ψ with the jet axis from radio to X-rays. Therefore, a shock-accelerated, energy-stratified electron population model satisfies all our multiwavelength polarization observations.

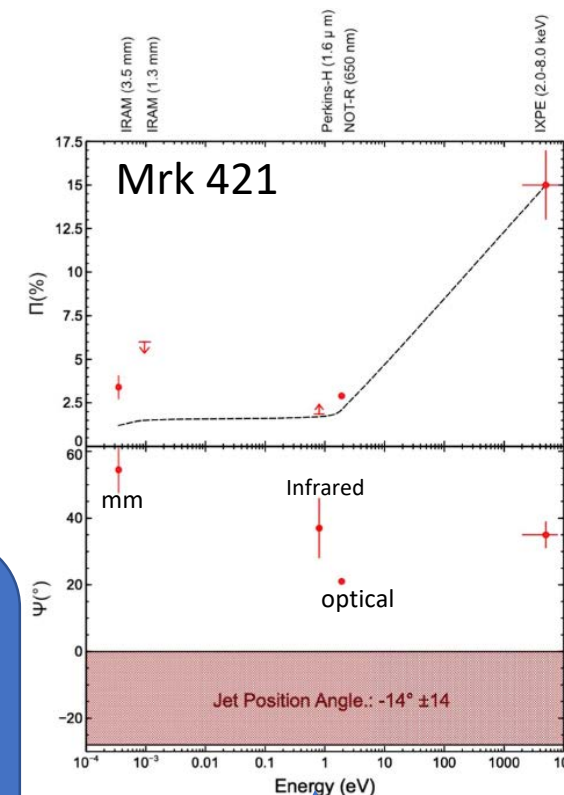
^aSlow variability, a few days to a week; moderate variability, days; high variability, less than 1 day.

^bThere is a slight dependence on the slope of the emission spectrum.

Synchrotron dominated blazars show a polarization in X-rays which is 3-5 times larger than in optical, infrared and mm.

The most probable jet acceleration mechanism is energy stratified shock.

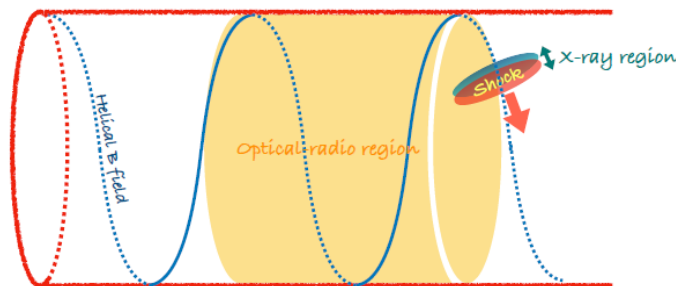
Di Gesu, L. et al. ApJL, 2022



P.A. not coincident with the jet direction

MRK 421: X-RAY POLARIZATION ANGLE ROTATION

- During X-ray rotation millimeter-wave, infrared and optical polarization angle didn't vary substantially.
- Rotation in optical light is few-few tens of degree/day
- PD_x was roughly constant and higher wrt Optical, Infrared and Radio
- At GeV was in a quiescent state



A model may explain the observed rotation is a shock propagating along the helical magnetic field down the jet.

Note: PG1553+113 showed a rotation in optical and infrared but no in X-ray

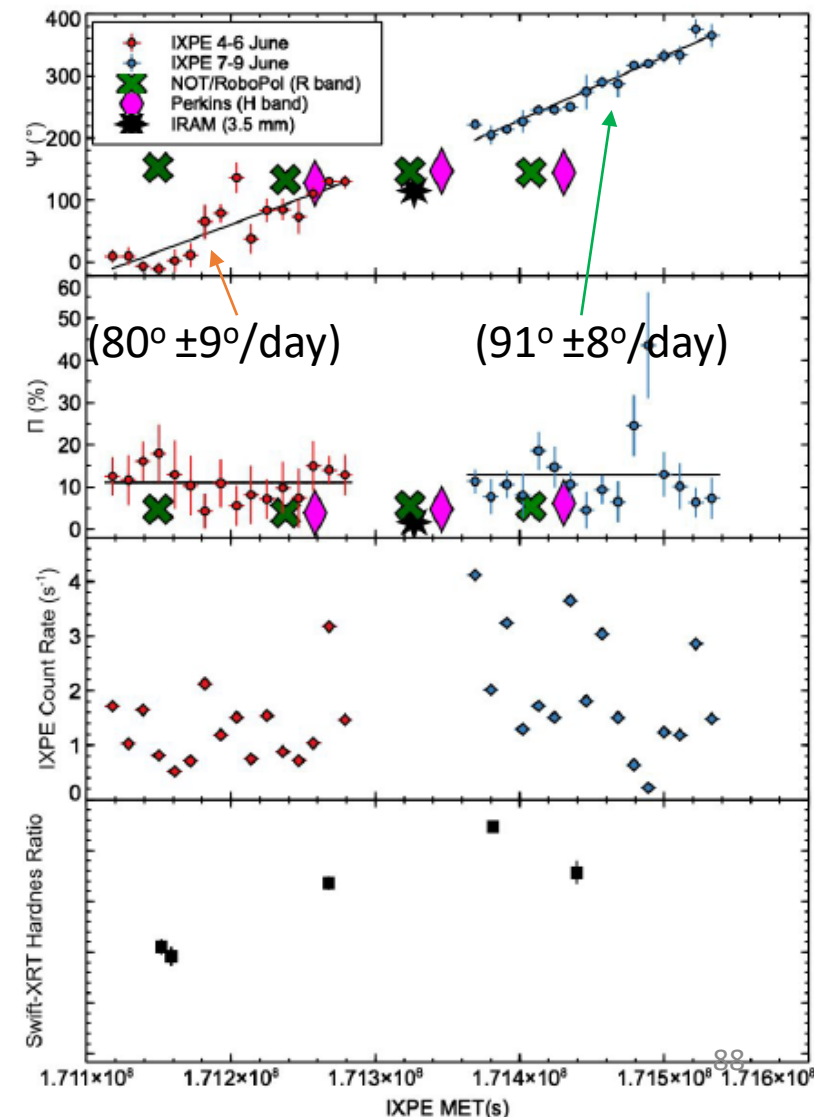


Table 1. Contemporaneous multiwavelength polarization properties of HSPs.

Source	X-ray		Optical & IR ^a		Radio ^a	
	II(%)	$\psi(^{\circ})$	II(%)	$\psi(^{\circ})$	II(%)	$\psi(^{\circ})$
Mrk 501 I ¹	10 ± 2	134 ± 5	4 ± 1	119 ± 9	1.5 ± 0.5	152 ± 10
Mrk 501 II ¹	11 ± 2	115 ± 4	5 ± 1	117 ± 3	–	–
Mrk 421 I ²	15 ± 2	35 ± 4	2.9 ± 0.5	32 ± 5	3.4 ± 0.4	55 ± 2
Mrk 421 II ³	10 ± 1	Rotation	4.4 ± 0.4	140 ± 6	2.4 ± 0.1	139 ± 8
Mrk 421 III ³	10 ± 1	Rotation	5.4 ± 0.4	145 ± 1	–	–
Mrk 421 IV ⁴	14 ± 1	107 ± 3	4.6 ± 1.3	206 ± 9	1.8 ± 0.1	167 ± 4
1ES1959+650 I ⁵	8 ± 2	123 ± 8	4.5 ± 0.2	159 ± 1	–	–
1ES1959+650 II ⁵	<5	–	4.7 ± 0.6	151 ± 19	<1.6	–
PG1553+113 ⁶	10 ± 2	86 ± 8	4.2 ± 0.5	Rotation	2.6 ± 0.7	133 ± 7
1ES0229+200 ⁷	18 ± 3	25 ± 5	3.2 ± 0.7	–5 ± 9	<7	–

^{1–8} Results compiled from the following references: [57–63]; ^a median polarization properties during the IXPE observation. Especially for optical and IR polarization, only corrected polarization values, accounting for the dilution of polarization by unpolarized starlight from the host galaxy, were considered for calculation; ^b at the lowest radio frequency (4.85 GHz).

Kim et al., 2024

X-ray polarization of HBL are comparable higher than at longer wavelength

Notably Mrk 421 was found rotating in X-rays and not in longer wavelength while PG1553 was rotating in longer wavelength but not in X-rays

3C273, 3C 279, 3C 454.3, S6 0716+714 only upper limits 9-38 %

Table 1. Summary of IXPE Observations

Source	Instrument	Observation ID	MJD range	Exposure (ks) ^a	Π_x ^b
3C 273	IXPE	01005901	59732.37 - 59734.45	95.28	< 9.0%
3C 279	IXPE	01005701	59743.02 - 59748.85	264.42	< 12.7%
3C 454.3	IXPE	01005401	59730.19 - 59732.34	98.12	< 28%
S5 0716+714	IXPE	01005301	59669.43 - 59674.80	358.68	< 26%

^a Average of exposures for the three detector units.

^b 99% confidence limits using the unbinned, event-based likelihood method (§ 2.1).

Marshall, H. et al. in Astro-ph, 2024 ApJ accepted

An intermediate Blazar BL Lac in outburst showed significant polarization (22 %) but X-rays moved into the synchrotron peak!. Peirson, L. et al., ApJL 2023

The IXPE baseline program ended on February 2024.

NASA on 6 June 2023 approved an extension of IXPE until September 2025.

The next NASA senior review for mission is foreseen in 2025.

GO 1 program is at the present time from February 24 to January 2025

GO 2 (from January 2025 to September 2025) call ends 29 August 2024

**Data are public (except special case) one week after the end of the observation
Analysis software (HEASARC-XSPEC and Collaboration software) are public**

IXPE is working great. In proposing don't be shy to ask large observing time

IXPE is not a Swift like mission

- Time for a TOO is not earlier than about 3 working days after the proposal
- GRB 221009A was indeed a special case TOO was requested on 10-10-2022 at 16:48 UTC and started on 10-11-2023 at 23:34:28 UTC
- We expect to trigger about one TOO per months.
- After a ToO started, the object that was in the long term planning is somewhat 'lost' and there is some discretion if it will be recovered later in the schedule

TOO (32 requested between new and pre selected 15 sources observed)

- Cyg X-1 (TWG 3)
- 4U 1630-472 (TWG 3)
- XTE 1701-46 (TWG 4)
- GRB 221009A No TWG
- EXO 2030 + 375 (TWG 4)
- Cyg X-3 (TWG 3)
- LS V + 44 17 (TWG 4)
- 4U 1630-47 (TWG 3)
- Swift J0243.6+6124 (TWG 4)
- 1ES 1959+650 (TWG 7)
- Swift J1727.8-1613 x 2 (TWG 3) multiple times
- GX 339-4 (BH, pre assigned)
- SRGA J144459.2-604207 (AMS, pre assigned)
- Swift J151857.0-572147 (BH)
- Cyg X-3 & Cyg X-1 (XL-Calibur simultaneous)

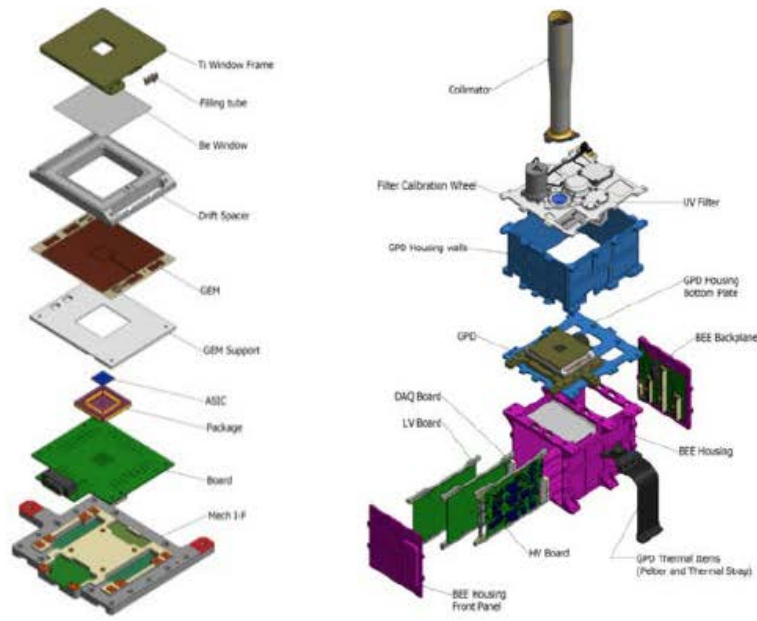
Mission	Allowed Sun Angle (deg)
HST	60-180 (+/-30 deg)
IXPE	65-115 (+/-25deg)
NICER	45-180
NuSTAR	43-180
SWIFT	47-180
XMM	70-110 (+/-20deg)

From HEASARC tools website

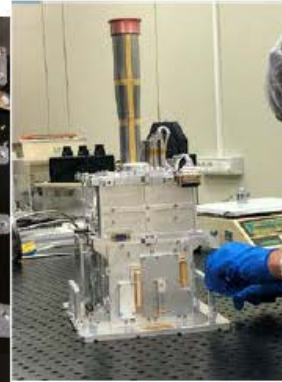
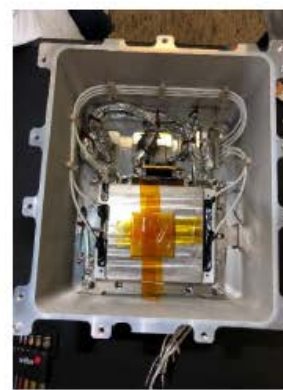
IXPE Allowed Sun Angle now increased up to +/- 34 deg

Before Pandemic!

INFN-TEAM ASSEMBLY & TEST OF THE DUS



- DU mechanical housing design and procurement.
- DU thermal design and parts procurement
- Stray-light collimator design & procurement
- DU alignment system (collab. with MSFC & Ball & INAF)
- BEE electronics design and procurement
- BEE DAQ firmware, BEE software
- BEE Test



4 Flight Detector Units - AIVT (including environmental tests)
 1. Engineering Model DU (for BEE performance development)
 2. Qualification Model DU (Thermal and Structural models)

INAF: FLIGHT POLARIZED & UNPOLARIZED SOURCES: DESIGN, CONSTRUCTION & TEST

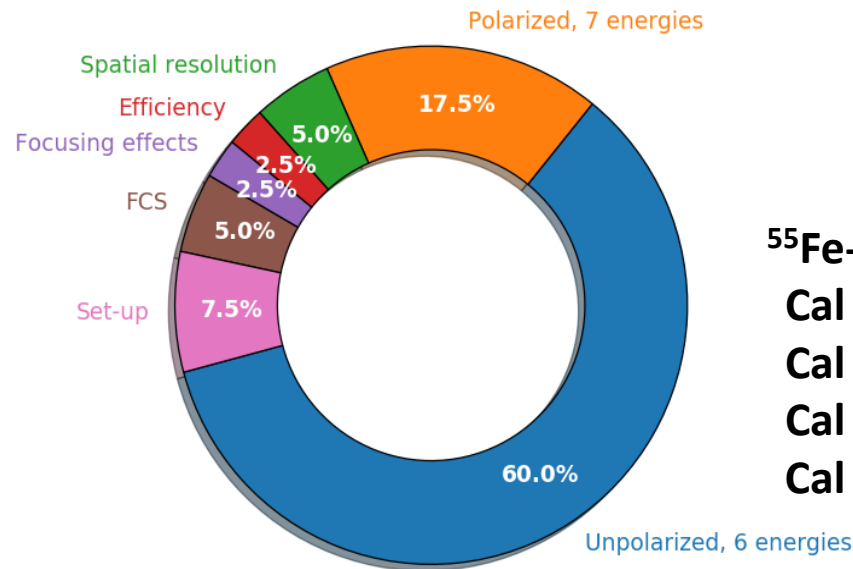
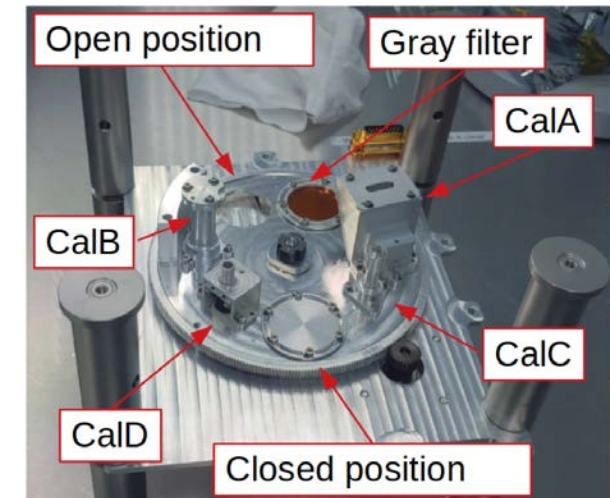


DURING PANDEMIC!

CALIBRATION OF 3 FLIGHT DUS + 1 DU SPARE, INSTRUMENT AIV&T

- Calibration of DU have been carried out in Italy at INAF-IAPS, before Instrument integration and delivery to USA
- 40 days for each DU (3 flight + 1 spare units)
 - Up to 24/7 data acquisition
- First unit started calibration on 26th July, DU-FM2 started on 6th Sep 2019, DU3 on 23 Oct. 2019, DU 4 on 16 Dec. 2019
- 60% of time dedicated to characterization of the response to unpolarized radiation at 6 energies
- 17.5% of time dedicated to measurements of modulation factor at 7 energies
- Remaining time to calibrate other parameters of interest
- Energy calibration and dead-time are by-product of previous measurements

Ferrazzoli R. et al., JATIS 2021



⁵⁵Fe-powered calibration sources:
 Cal A – polarized 2.98-keV and 5.89-keV
 Cal B – unpolarized 5.89-keV spot
 Cal C – unpolarized 5.89-keV flood
 Cal D – unpolarized 1.74-keV

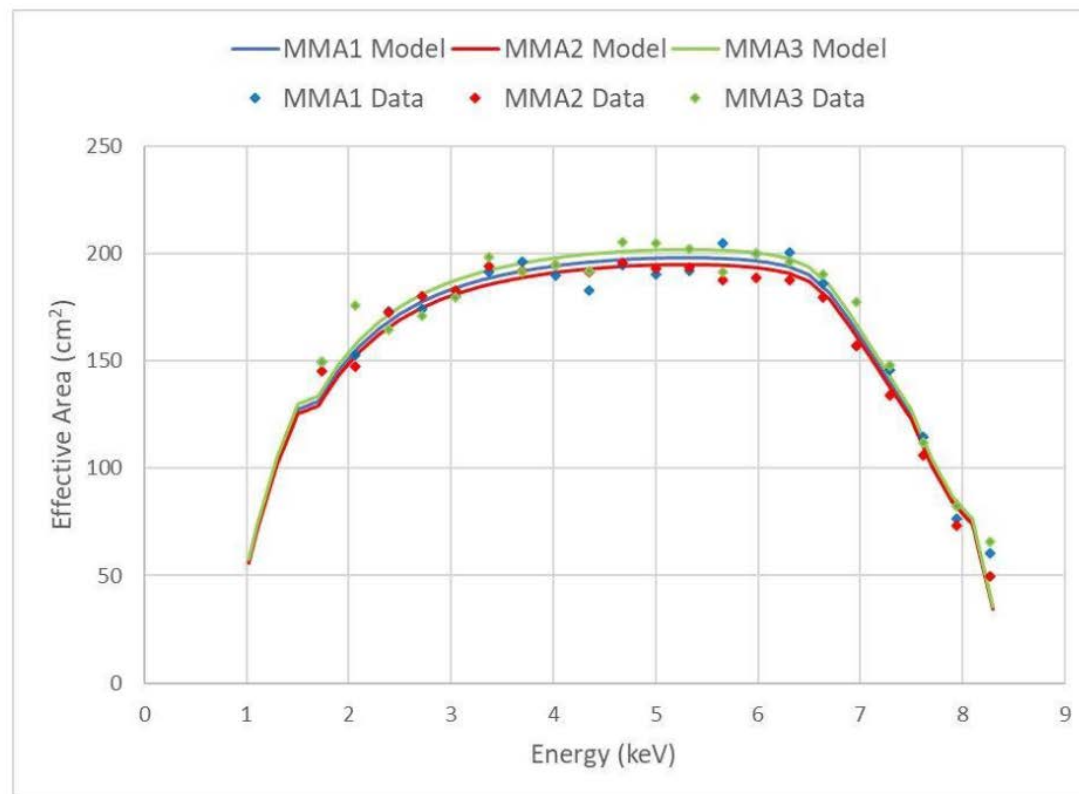
ICHEP 17-24 July 2024 Prague
 Muleri F. et al., Astr. Phys, 2022

Parameter	Value
Sensitive area	15 mm x 15 mm (13 x 13 arcmin)
Fill gas and composition	DME @ 0.8 bar
Detector window	50-um thick beryllium
Absorption and drift region depth	10 mm
GEM (gas electron multiplier)	copper-plated 50-pm liquid-crystal polymer
GEM hole pitch	50 um triangular lattice
Number ASIC readout pixels	300 x 352
ASIC pixelated anode	Hexagonal @ 50-pm pitch
Spatial resolution (FWHM)	< 120 um (6.4 arcsec) @ 2 keV
Energy resolution (FWHM)	1.0 keV @ 6.4 keV (scaling as sqrt(E))
Useful energy range	2 - 8 keV

MIRROR MODULE ASSEMBLY PROPERTIES

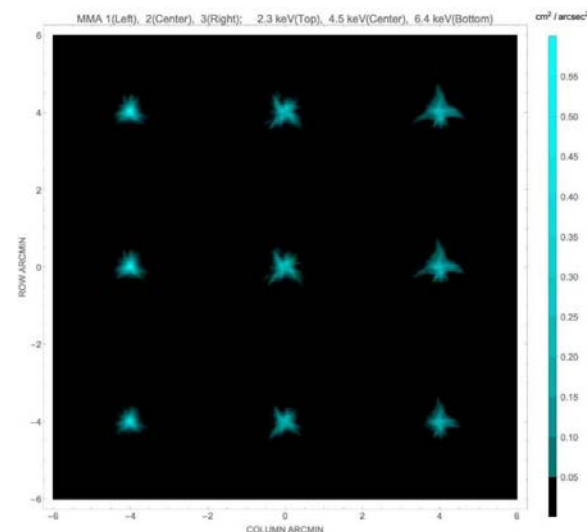
Property	Value
Number of modules	3
Mirror shells per module	24
Inner, outer shell diameter	162, 272 mm
Total shell length	600 mm
Inner, outer shell thickness	180, 250 μm
Shell material	Nickel cobalt alloy
Effective area per module	163 cm^2 (2.3 keV) ~ 192 cm^2 (3-6 keV)
Angular resolution	< 30 arcsec HPD
Detector limited FOV	12.9 arcmin
Focal length	4 m
Mass (3 assemblies)	93.12 kg

18 July 2024

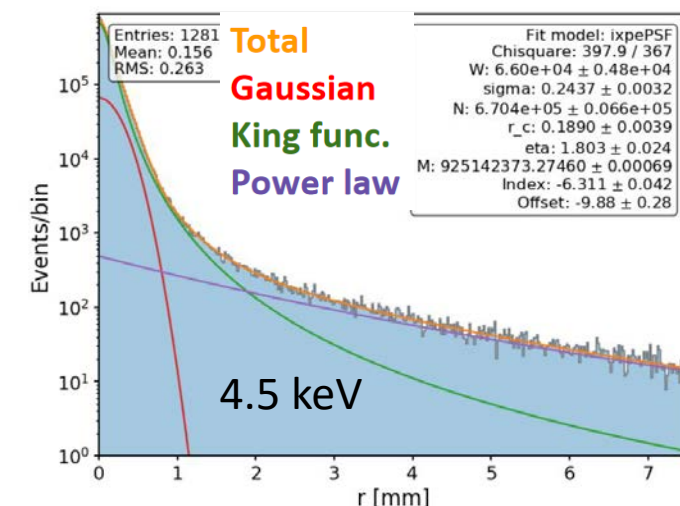


MMA	#1	#2	#3
6.4 keV	18.9"	24.8"	24.2"
4.5 keV	18.9"	25.0"	26.9"
2.3 keV	18.7"	24.5"	26.7"

Values in the table are half-power diameters (HPDs) for the individual MMAs alone.



Point Spread Function (Mirror+Detector)



Based upon X-ray calibration, analysis, and on-orbit performance the telescope performance is = 30" HPD (25" HPD for Telescope 1)

The presence of a power-law component in the Point Spread Function requires background subtraction be done only for dim sources not to subtract source photons (see Di Marco, A. et al., ApJ 2023)

Science Advisory Team (chaired by Giorgio Matt and Roger Romani)

Coordinates science activities required for planning, analyzing, interpreting, and reporting IXPE observations
Organized into seven Topical Working Groups

- **TWG1 Pulsar Wind Nebulae**, led by *Niccolò Bucciantini (INAF-Arcetri)*

Obtain polarimetric imaging to constrain the magnetic-field geometry of the nebula and the phase-dependent polarization of the pulsar

- **TWG2 Supernova Remnants**, led by *Pat Slane (CfA)*

Obtain spectral polarimetric imaging of Supernova Remnants (SNR) to constrain the magnetic-field structure of the X-ray emitting regions

- **TWG3 Accreting Black Holes**, led by *Michal Dovčiak (CAS-ASU)*

Obtain spectral polarimetry of microquasars to constrain the value of the black-hole spin parameter (if in soft state), or constrain the geometry of the corona (if in hard state)

- **TWG4 Accreting Neutron Stars**, led by *Juri Poutanen (Turku)*

Obtain phase-dependent polarimetry of accreting X-ray pulsars (high-magnetic-field binaries) to constrain models and geometries for the pulsing emission. Obtain polarimetry of non pulsating accreting NS to constrain the geometry of the system

- **TWG5 Magnetars**, led by *Roberto Turolla (Uni Padua)*

Obtain phase-dependent polarimetry of magnetars to constrain the effects of vacuum polarization (birefringence in a strong magnetic field)

- **TWG6 Radio-Quiet AGN & Sgr A**, led by *Frédéric Marin (Strasbourg)*

Obtain polarimetry of RQ AGN to constrain the geometry of the emitting regions

- **TWG7 Blazars & Radio Galaxies**, led by *Alan Marscher (Boston U)*

Obtain polarimetry of Blazars and RG to study jet emission

PHOTOELECTRIC EFFECT TO MEASURE POLARIZATION OF X-RAYS

